Microfluidic devices for heterogeneous assays

By Arash Dodge

Sensors, Actuators and Microsystems Laboratory

Institute of Microtechnology, University of Neuchâtel, Switzerland

PhD dissertation performed under supervision of:

Dr. Elisabeth Verpoorte

Prof. Nico F. de Rooij

This work is dedicated to

my mother,

my father

and my brother

The road goes ever on and on

Down from the door where it began

Now far ahead the road is gone

And I must follow if I can

Pursuing it with eager feet

Until it joins some larger way

Where many paths and errands meet

Whither then? I cannot say…

J.R.R. Tolkien

IMPRIMATUR POUR LA THESE

Microfluidic devices for heterogeneous assays

de M. Arash DODGE

UNIVERSITE DE NEUCHATEL

FACULTE DES SCIENCES

La Faculté des sciences de l'Université de Neuchâtel sur le rapport des membres du jury,

Mme E. Verpoorte,
MM. N. de Rooij (directeur de thèse),
R. Neier, G. Turcatti (Coinsins) et
G. Desmet (Bruxelles B)

autorise l'impression de la présente thèse.

Neuchâtel, le 21 février 2003

Le doyen:

F. Zwahlen

ABSTRACT

Microfluidics is a recent field of research involving manipulation of fluids in micrometer sized channels. The basic idea behind this topic is to miniaturize fluidic analysis systems in order to perform (bio-) chemical analyses and reactions on a very small scale. Some of the main advantages of chip-based methods are to increase speed of analysis, reduce sample and reagent volumes used for synthesis or analyses, and achieve better control over chemistry and reaction conditions. One of the applications of interest is the realization of heterogeneous assays on microfluidic chips. Biochemical assays where probe molecules are bound to a solid substrate, and sample molecules diffuse from the sample matrix towards the surface in order to react, can take many hours in order to achieve a detectable measurement. Macroscopic flowing systems have already been used in order to actively bring samples to react with detection surfaces, but their low surface-to-volume ratios still limit this approach. Microfluidic devices, having high surface-to-volume ratios and better fluidic control than their macroscopic peers, have already been proven to enhance some of the advantages of the existing macroscopic techniques. This thesis presents different microfluidic devices enabling studies involving heterogeneous assays. The first assay type is a heterogeneous immunological assay performed in three different devices using electro-osmosis as a pumping mechanism. The second assay consists in solid-phase hybridization of single DNA strands in a temperature-controlled

microdevice in order to perform thermal dehybridization of DNA double-strands. Pressure-driven flow was used to pump solutions in this case. Since temperature control is essential for certain biochemical reactions, novel techniques of control and calibration were achieved.

Table of Contents

1 INTRODUCTION

Since the early ‘80s, advances in the fields of molecular biology and genetics have revolutionized the way new medical treatments are being developed. The possibility of synthesizing monoclonal antibodies has improved specificity of immunoassays, so that disease diagnoses can be performed with more robust methods. The recent completion of the first draft of the human genome will increase our understanding of genetically-related diseases and disorders, and lead to treatments at a molecular level, specific to each individual.

In order to perform the required analyses for detecting eventual abnormalities or illnesses in a patient, different methods can be employed. For viral infections or blood-related pathologies, immunoassays can be performed in order to determine what type of foreign body is affecting a person’s immunological defenses. This can be performed either in a homogeneous system, meaning that sample and detection molecules are in the liquid phase, or in a heterogenous system, where one of the molecules involved is bound to a solid substrate. In the latter case, preconcentration of target molecules is possible, for increased sensitivity of the analysis. For genetic diseases, DNA analysis can be performed in order to know if a patient possesses a mutation in a specific gene which could explain an existing illness or even predict the appearance of a disease beforehand.

There are different methods of analysis for determination of DNA-related malfunction. One method is to analyze the DNA of an individual by performing a gel-phase electrophoretic separation of fragments formed from the DNA in question. Differences in fragment lengths obtained from the patient's DNA and a healthy reference indicate either the presence or possibility of illness in the future. Another method is to introduce many different, known, single-stranded DNA sequences bound onto particles or in gels into microtiter-plate reaction wells. The human DNA sample is then hybridized with these different sequences, and, by seeing in which well the sample reacts, one can determine the sequence of the DNA sample. Immunoassays and DNA analysis therefore are both characterized by some form of interaction of the analyte with a specifically modified solid phase to perform clinical diagnostic tests. This makes it possible to preconcentrate analytes onto a surface and therefore enhances sensitivity of detection. Another seemingly trivial but non-negligible aspect of being able to immobilize molecules onto a surface is that it is easier to locate molecules bound to a surface than to search for them in a given volume of liquid sample.

A fundamental point that DNA analyses and immunoassays have in common is that they both possess an enormous selectivity. Each molecule has a certain spatial configuration and charge distribution for which there exists a very specific complementary structure. For example, an antigen will possess a certain "key" region on its geometry which perfectly fits into its complementary antibody which contains the appropriate "lock" region. A single strand of DNA will have a certain sequence of bases which can only perfectly hybridize with its complementary strand.

This thesis primarily concentrates on the integration of these types of heterogeneous assays on chip, in order to perform DNA and immunological analyses in ways which promote speed and control of reactions by using microfluidics. Since most bio-chemical reactions are temperature-dependent, temperature control and calibration inside biochemical microreaction devices is also addressed in this manuscript. New original methods for heating, cooling and determining temperature inside a microfluidic device are described. One of these temperature control methods is used for performing an on-chip DNA heterogeneous analysis.

1.1 Heterogeneous assays: general aspects

The principle of a heterogeneous assay is to use probe molecules bound to a solid substrate in order to detect target molecules in a given sample. When a liquid sample is brought into contact with the surface-bound probe molecules, target molecules migrate towards the walls by diffusion. In most cases, target molecules are found in low concentrations, if they are at all present in sample. These will eventually make their way to the wall and react with the probe molecules. Different detection methods can be used, such as fluorescence, radiolabeling and absorbance. The use of evanescent waveguides to detect the difference in signal as the evanescent wave reacts with molecules at the surface of the reactor walls is also possible. The advantage of using a solid support is the effect of sample molecule concentration occurring at the surface, therefore increasing sensitivity of the analysis by lowering limits of detection.

Figure 1.1 shows a schematic describing the general principle of a heterogeneous assay. The solid support could be for example the walls of a microtiter well or a chromatography column. Probe molecules could be antibodies targeting for antigens, or

single strands of DNA probing for complementary strands of a human sample to determine a sequence. Probe molecules, be they DNA or antibodies, can be bound covalently or non-covalently to the substrate by using intermediate anchoring molecules. These may be silanes, or other molecules which can enhance reactions by increasing spatial freedom[1] or orienting the probe molecules in the appropriate spatial configuration for reacting with target molecules[2, 3].

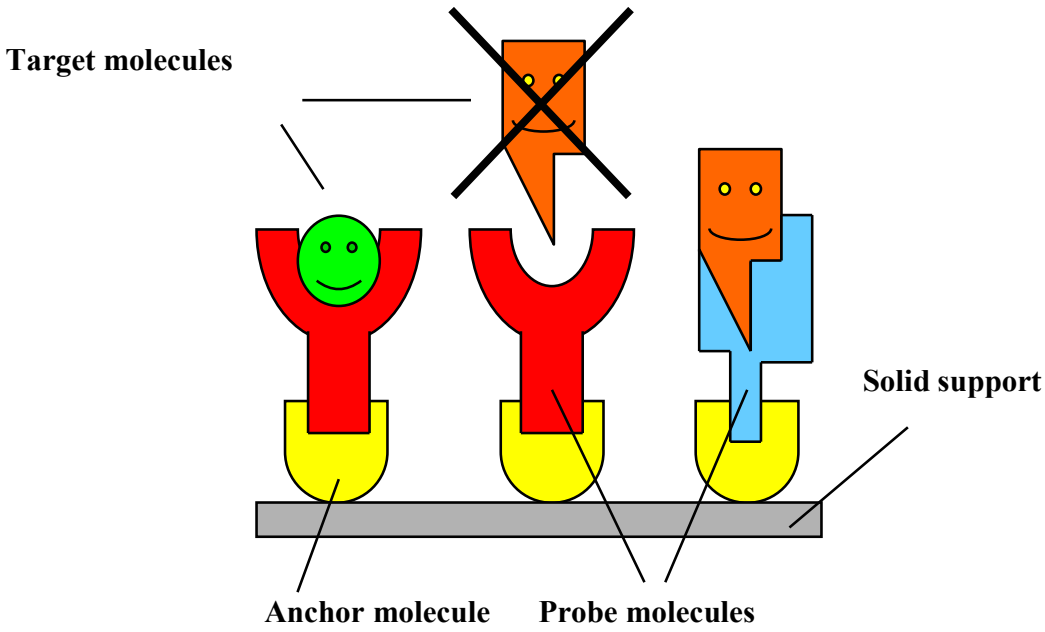

Figure 1.1: Heterogeneous assay principle

1.1.1 Heterogeneous immunoassay

There are two main methods of performing a heterogeneous immunoassay. The first method is called a competitive assay, and is shown in Figure 1.2. A known antibody is bound to a solid support. A known number of labeled antigen molecules, or tracer molecules, are added to the sample. A general rule for this type of assay is that the number of available binding sites is less than the combined number of antigen and tracer

molecules. If the target antigen (analyte) is present in sample, the tracer molecules will compete with the target molecules for the limited number of available binding sites.

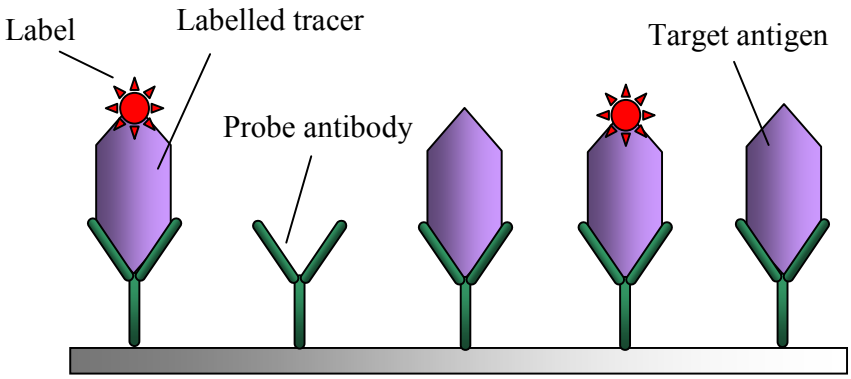

Figure 1.2: Competitive assay.

Therefore, if there is no target antigen in the sample, all sites will be occupied by tracer molecules and signal will be at a maximum. If target antigen is present in the sample, it will occupy a certain number of available sites and thus signal intensity will decrease. The signal will be directly related to the concentration of antigen present in solution.

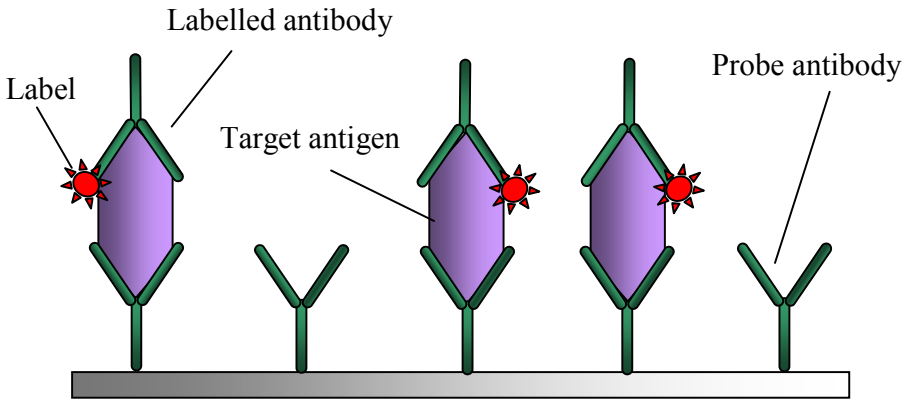

Figure 1.3: Immunometric assay.

The second method is an immunometric assay known as a “sandwich” assay, shown in Figure 1.3. First, an antibody is bound to the surface. The sample antigen is then allowed

to react with the antibody-coated reactor walls or solid phase. In order to reveal if there was any antigen in the sample, a third layer of labeled antibody also specific for the antigen is incubated in the chamber. If antigen is present in the sample, the labeled antibody will bind to the antigen layer and a signal will be detected. If no antigen is present, then no signal is observed. If the number of available binding sites is much greater than the targets in the sample, then it is possible to obtain the concentration of antigen in solution. Since this type of assay uses two antibodies, they offer better specificity than competitive assays, because cross-reacting substances which can interfere in competitive assays do not bind to both the capture and the detection antibodies[4].

1.1.2 DNA analysis by hybridization

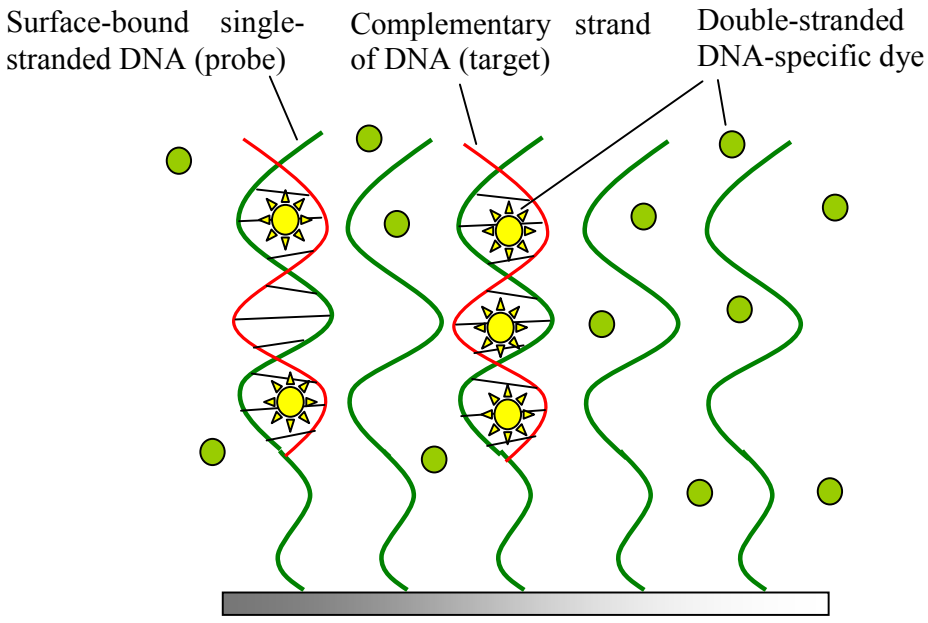

Figure 1.4: Heterogeneous DNA hybridization. Detection performed via double-stranded DNA-specific dyes.

Heterogeneous DNA analysis is performed by binding single-stranded DNA molecules whose sequences are known onto a solid substrate, and then allowing for hybridization

with the sample DNA in solution, as shown in Figure 1.4. Detection in this case uses dyes which only fluoresce in the presence of a double strand of DNA. If hybridization occurred, double strands of DNA are present and the dye will fluoresce. If not, no signal is detected.

1.1.3 Performing heterogeneous assays: Transport aspects

In conventional systems, assays are performed with many different probe molecules bound inside many separate reactors, and sample containing the target molecule to be analyzed is pipetted into the different wells. Molecules are often left to react without stirring, which means that transport of sample molecules to the reactor walls strictly depends on diffusion. Large molecules such as DNA or antibodies move very slowly via this passive means of transportation, and reactions can take from many minutes to several hours. The Einstein-Smoluchowski equation relates the time a molecule takes to travel a certain distance via diffusion[5]:

$$d_{diff} = (2Dt)^{1/2} \qquad (1.1)$$

where d_{diff} = diffused distance

t = time of diffusion

D = diffusion coefficient

Immunoglobulin G (IgG), a large protein (150 kDa) and of interest in this study, has a D of 4×10^{-7} cm^2/s. In a conventional microtiter well, distances that molecules need to travel to interact with the wall are on the order of mm. For IgG to diffuse 1 mm would require about 3 hours and 30 minutes. Therefore, in order to reduce the time molecules have to diffuse in order to find the reactor walls, one can reduce the diffusion distances

by shrinking reaction chamber dimensions. By creating micrometer-size chambers via microtechnology, one can increase speed of analysis from hours to minutes. This is one of the main driving motivations for integrating various biochemical reactions in the microfluidic format, such as immunoassays[6-9], DNA analysis[10-14] or enzymatic digestion[15]. Beads or gels may also be used to increase available surface area relative to the sample volume, thereby improving reaction times. Beads have been used in microfluidic devices for immunoassays[16] and DNA analysis[17].

A disadvantage of these types of analyses is that they require a lot of fluid handling. This is usually implemented by pipetting the different reagents robotically with an automated pipetter, with rinsing steps in between each reaction. Volumes of reagents are in the order of several microliters, which can be expensive, whereas in microfluidic systems volumes are reduced to the nano- to picoliter range. Also, integration of the different fluid-handling steps can be achieved within a microfluidic device. This combines increased versatility and simplicity of fluid handling with lower volumes, which could be a route to faster and cheaper analysis with a higher degree of precision. Other advantages include integration of extraction of molecules of interest from the sample matrix (sample pretreatment)[18], but this will not be treated within the framework of this thesis.

In summary, microfluidic systems have the potential to enhance speed and precision of reactions, while simplifying fluid handling and lowering reagent consumption.

1.2 Surface modification

In macroscopic systems, surface modification protocols for immobilization of probe molecules to reactor walls prior to analysis are long, since again, surface reactions

depend on diffusion-based motion. Treatments consist of entirely immersing microtiter wells or other support substrates into liquids or gases, and waiting for long periods of time to insure that sufficient reaction has occurred. Often, an initial layer or coating of tethering or anchoring molecules must be formed. Only then are probe molecules pipetted into the different wells and left to react for sometimes hours for immobilization on the first layer to occur. Densities of reagents at the surface are difficult to optimize to obtain the situation where spatial freedom of molecules may better enhance binding with target molecules in DNA analysis[1]. This may be accomplished by optimizing the chemistry used to condition the surface. Parameters such as concentrations of conditioning reagents in solution and reagent composition will determine the spacing between surface binding sites. In a microfluidic system, where flowing systems can precisely control replenishment of reagent solutions to a surface, an additional degree of freedom is available. Flowing a conditioning reagent over a surface at higher flowrates or for longer times will create denser surface layers (until saturation of the surface). This gives additional control on surface conditioning, independent of the chemistry used.

The different surface treatments used in this study are based either on covalent or non-covalent binding of probe molecules to a silanized glass surface. A schematic of the different strategies used for the immunoassay and DNA analysis performed is presented in Figure 1.5. A two-molecule chemical model was chosen for proof of concept for realizing an immunoassay on chip, as depicted in Figure 1.5a. This Protein A-rabbit Immunoglobulin G model was chosen because it has been reported to be a good system for testing binding assays. A glass chamber was treated with chlorodimethyloctadecylsilane (CDMODS), a silane which covalently binds to the SiOH

groups of the glass surface using the chemistry described in Figure 1.6a. This silane contains a long alkyl chain to which the chosen probe molecule, Protein A (PA), likes to stick in a non-specific way. This is a non-covalent bonding method which does not orient the probe molecule in any specific spatial configuration. PA contains 4 binding sites for the chosen target molecule, rabbit immunoglobulin G (rIgG), whose availability depends on how the PA molecule has randomly been sorbed onto the silanized surface. Generally, a maximum of two rIgG will bind to any given PA[19]. PA-rIgG bonds are weak in comparison to true IgG antibody-antigen bonds. It is possible to disrupt them, using a glycine/HCl buffer.

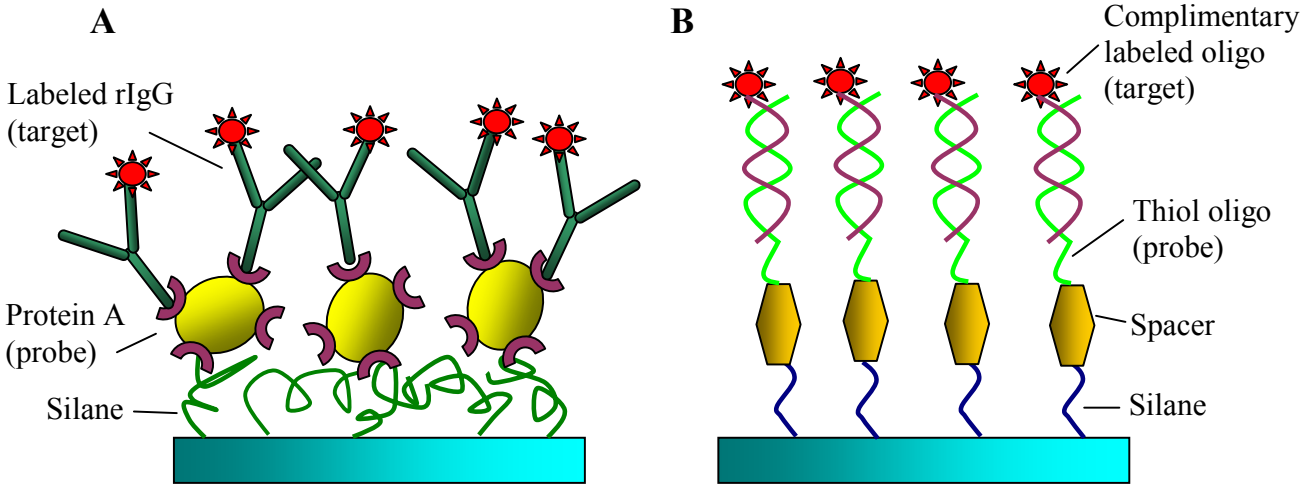

Figure 1.5: Different binding strategies. a) for immunoassay b) for DNA analysis.

For DNA analysis, the method used produced a chemically more robust layer, because covalent bonds were formed between the different molecules, as depicted in Figure 1.6b. This leads to somewhat more uniform orientation of the molecules in the bound layer. A glass chamber was treated with (3-aminopropyl) aminotriethoxysilane (ATS), a different silane which also covalently binds to the SiOH groups of the glass surface but in a more oriented fashion[20, 21]. The chemistry is illustrated in Figure 1.6b. After silanization, a

spacer molecule demonstrated to enhance hybridization, cross-linker m-maleimidobenzoyl-N-hydroxysulfosuccinimidyl ester (sulfo-MBS), was covalently bound to the silane via the succinimidyl ester group of the spacer.

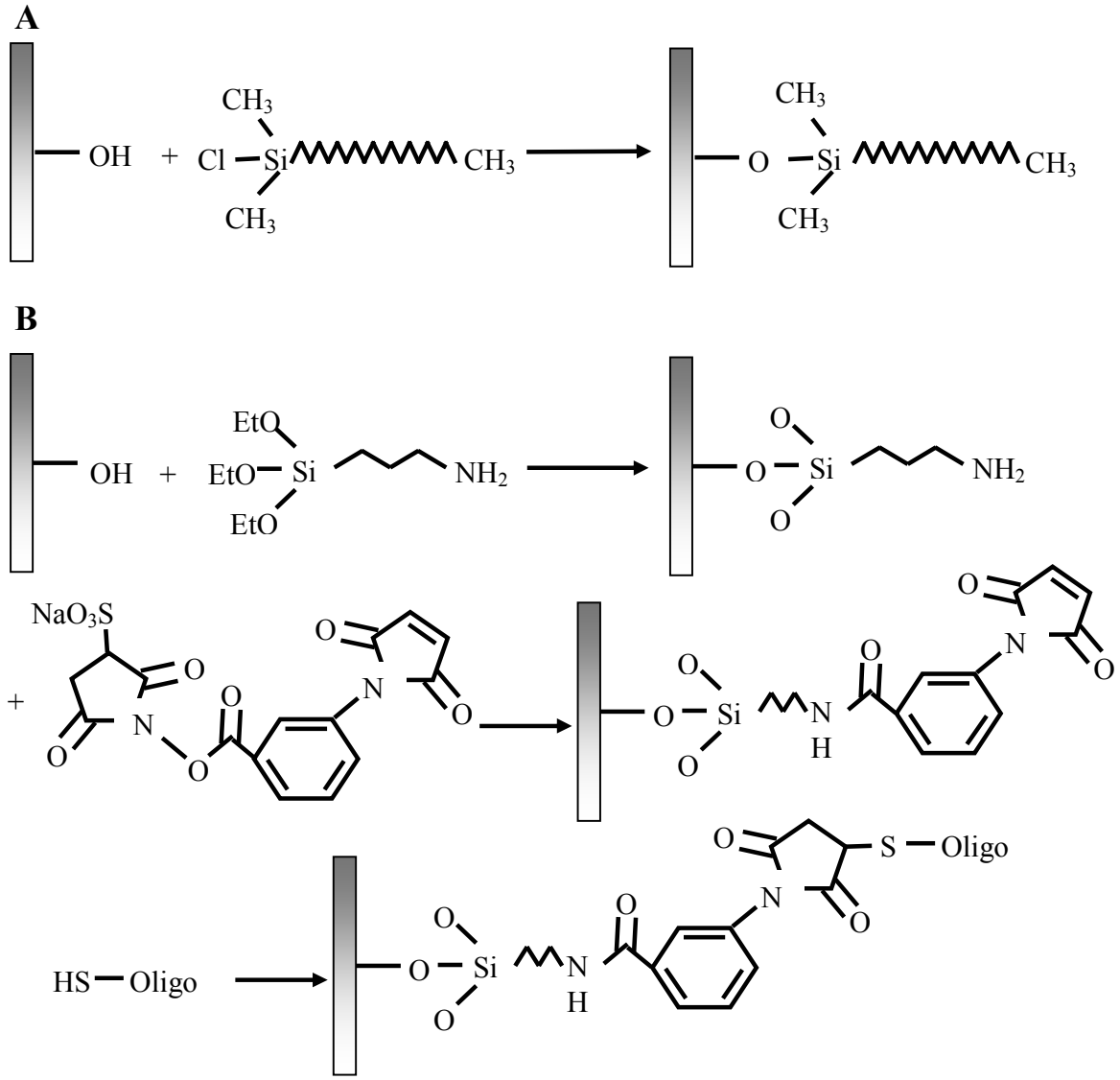

Figure 1.6: Surface chemistry a) for immunoassay b) for DNA analysis. Two SiO bonds appear to be dangling in the b) schematic. This is because it is unclear whether they also bind to the surface or remain free.

The probe DNA oligomer possessed a 5'-thiol end which was covalently bound to the maleimido-group of the spacer. During analysis, the target complementary oligonucleotide was hybridized to the thiol oligomer.

1.3 Detecting bio-molecules

In most methods for quantification of bio-chemical events, detection schemes using fluorescent or radioactive labels are used to determine whether a binding event has occurred or not. There exist different techniques to label bio-molecules in order to locate them and see if a reaction took place. Fluorescence detection is a popular method because of its sensitivity. The most common coupling reaction between dyes and bio-molecules takes place between the active group of the dye and a primary amino group of the biomolecule. A common reactive group is the N-hydroxysuccinimide (NHS) group. It is often used in conjunction with dyes like Cy5, to bind dye covalently to a protein. The chemical schematic of NHS-Cy5 binding to an amine group is given in Figure 1.7. This was the chemistry used to label rIgG antibodies with Cy5 in these studies.

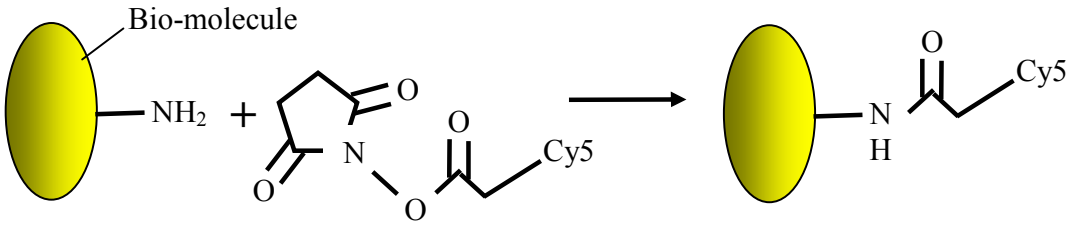

Figure 1.7: Chemical binding of Cy5 to amine group.

Since the recognition elements of the bio-molecules often contain amine groups, the labeling reaction time should not be too long in order to avoid labels attaching to these

groups. This is because the presence of dye molecules in these regions could alter bio-molecular functionality, and inhibit recognition ability.

1.4 Temperature control in biochemical reactions

A very different aspect of heterogeneous assays that needs to be controlled is temperature. Most human-related biological reactions such as antigen-antibody binding are optimal close to 37 °C, which is the average body temperature of a human being. Other species of mammal have similar body temperatures. Performing assays at these temperatures, then, can enhance reaction speed. In DNA heterogeneous analysis, hybridization of probe molecules to complementary strands is also performed at temperatures higher than room temperature to increase specificity (stringency) of reactions occurring. This is because heat discourages weaker non-specific binding (NSB), thereby reducing undesired reactions where one or more basepairs is mismatched[22, 23]. Another very important temperature-dependent process which is often used in DNA analysis is the amplification of DNA in a sample, since it is often available in relatively small quantities. This is performed via the polymerase chain reaction (PCR) described in Figure 1.8. Sample is mixed with a special buffer containing the 4 bases, C, G, A, T, and a building enzyme (usually the Taq polymerase), and thermally cycled at 3 different temperatures. The three temperatures correspond to 3 phases: denaturation, extension and annealing. During the denaturation phase, the double-stranded helix structure of DNA is first melted at 95°C in order to obtain 2 complementary single strands. The sample is then brought to 72°C during the extension phase. This temperature is optimal for the enzyme, which uses the bases in solution to make copies of the two single strands.

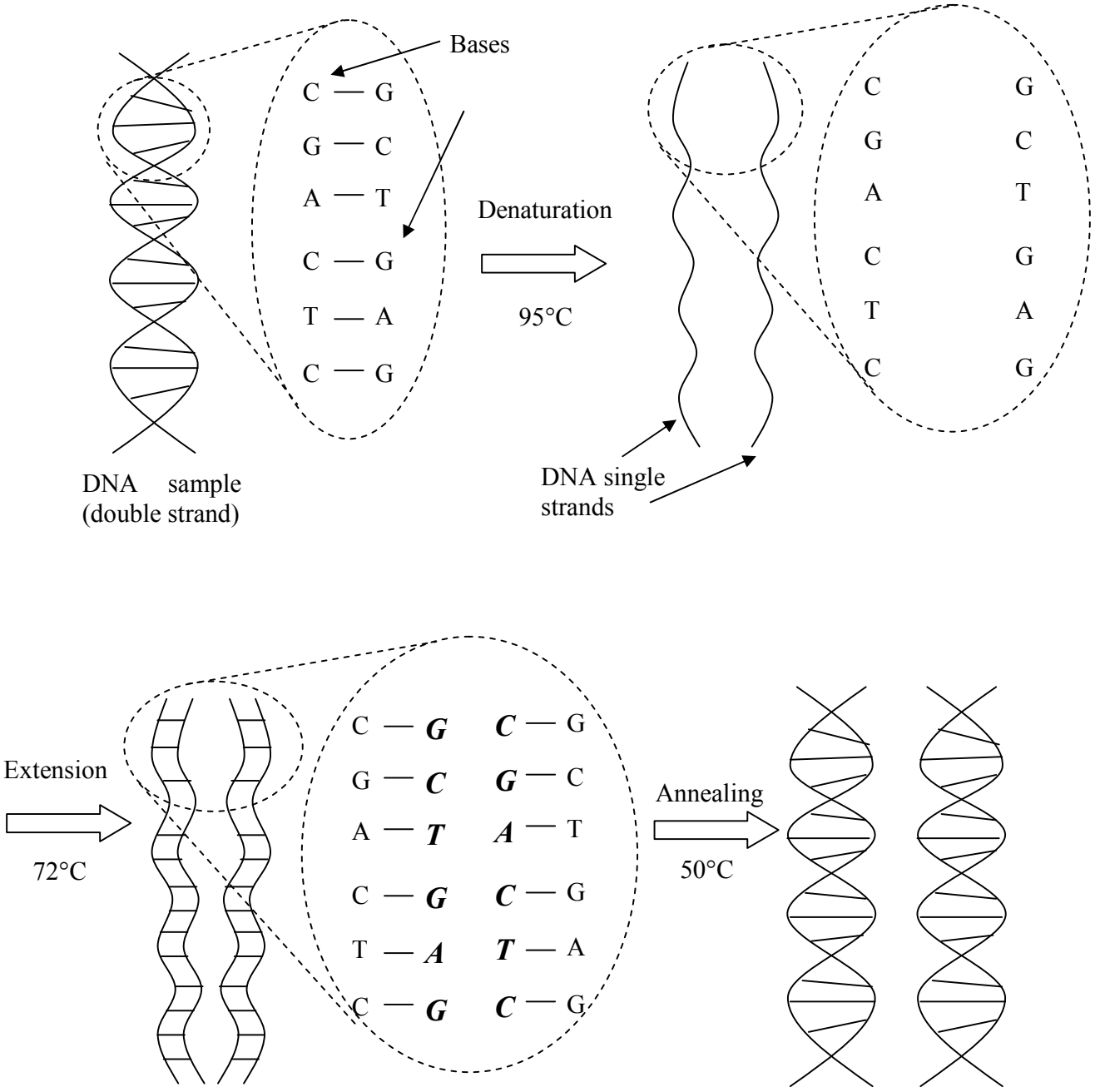

Figure 1.8: A PCR cycle.

Two full double strands of DNA are created in this way from the initial double strand DNA fragment. The third phase consists of lowering the temperature to 50°C in order to

"relax" the new double-stranded structures before performing a new cycle. Therefore by cycling n times, one should obtain 2^n copies from a single molecule of DNA[24].

Temperature therefore plays an important role in many biochemical reactions. In most systems, incubation of samples with probe molecules is performed in a reaction chamber of some kind, which is maintained at a fixed temperature. For cycling temperature during PCR, thermocycling instrumentation is available. Microtiter plates or microvials can be inserted into these instruments, which ramp temperature in a controlled fashion. The large thermal mass of most of these instruments, however, limits heating and cooling rates, and it is difficult to perform enough PCR cycles (usually in the order of 25 cycles) to obtain a measurable amount of sample in less than 1h and 30 min. In a microfluidic device, high surface-to-volume ratios can be achieved. This enhances heat transport, to and from a microchamber, which leads to faster temperature changes. Low thermal mass and high surface-to-volume ratios in microfluidic devices have already been exploited to perform PCR. For example, recent reports describe non-contact infrared-light-mediated thermocycling in which cycle times were reduced to as little as 17 sec[25], and enough DNA produced in 240 sec[26]. Temperature control can therefore be improved and temperature changes realized more rapidly in a microfluidic device.

1.5 Microfluidics, methods and means

In the previous paragraphs, we have seen that microfluidics is a route to improved speed of reaction and enhanced temperature control for performing different biochemical reactions. In this section, some general aspects of microfluidic technology relevant to this thesis will be described.

1.5.1 Technology

In this section, the different essential steps for the microfabrication of chips used in this work will be described. This is a general description of device fabrication only. Details for each specific case will be given in the relevant chapter. The process used to create micro-channels is depicted schematically in Figure 1.9. The material used primarily in our lab for the different devices is Pyrex 7740, a transparent borosilicate glass which allows good optical detection with fluorescence methods, and enables electro-osmostic pumping (vide infra). First, a 10-mm-diameter Pyrex 7740 wafer is subjected to a thorough cleaning procedure, to ensure both cleanliness and a native surface which is always the same before beginning the different fabrication processes. Cleaning starts with the wafer being dipped in electronic-grade acetone for 2 minutes, followed by a rinse with electronic-grade isopropyl alcohol for 2 minutes, and a rinse in doubly-distilled deionized (DI) water for 5 minutes. Then it is immersed in 97% fuming nitric acid for 10 minutes to remove any organic residues. It is finally rinsed in DI water and dried with nitrogen. The cleaning procedure is followed by deposition of a masking layer of polysilicon in a furnace at 570 °C. The technique commonly used to define microscale structures is called photolithography, a method which resembles photography. It involves transferring a pattern drawn on an optical mask to a photosensitive layer deposited on the substrate to be patterned. The optical mask is made of a quartz substrate bearing a pattern of transparent and opaque regions. This pattern, which contains the channel layout, is formed either in a layer of chromium deposited on the quartz substrate, or on a high-resolution transparency layer by inkjet printing. The usual minimal feature size on the chromium-quartz masks is 1 µm, while on the transparency masks it is about 7 µm.

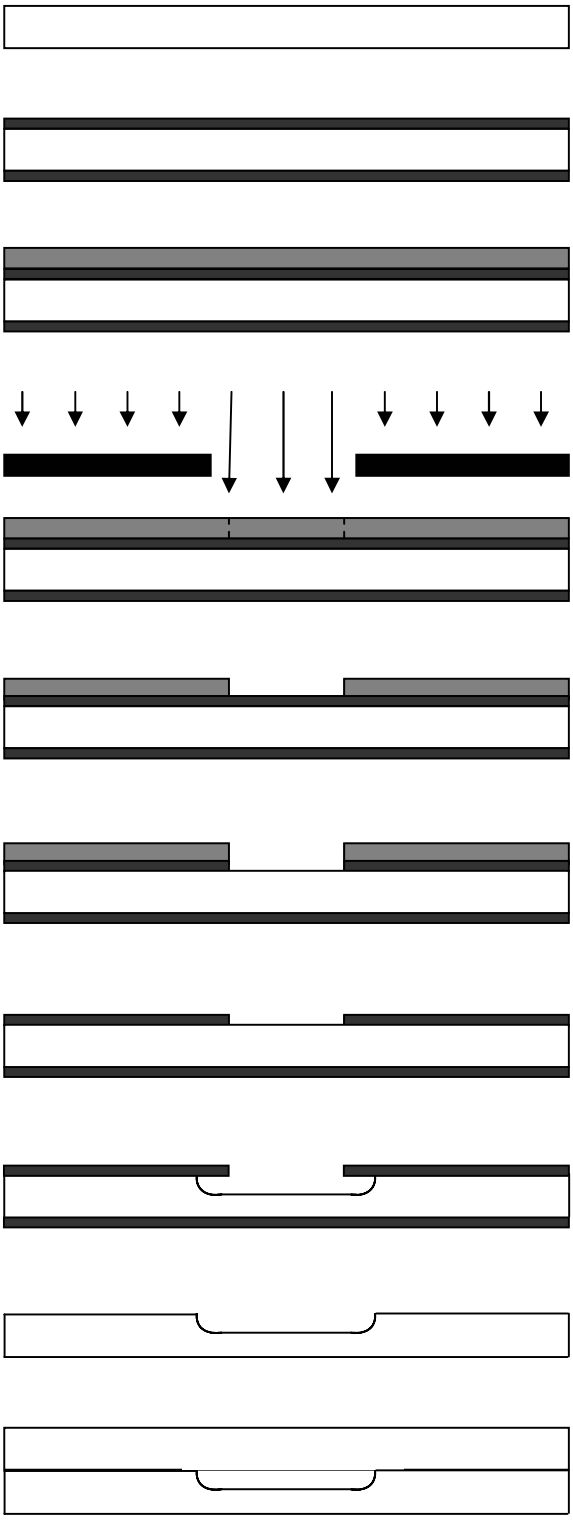

Figure 1.9 : Fabrication of a microchannel in glass.

The photosensitive layer (photoresist) is deposited on the substrate by spin-coating. A small volume of photoresist is pipetted onto the substrate, which is then spun, like a record on a record player, at certain velocities for certain lengths of time. A uniform thin layer of resist is formed in this way, its thickness depending on the spinning parameters and resist characteristics (viscosity, particle content, etc…). It is then heated to remove the solvents used to preserve the resist during storage. The resist is then exposed to UV light (λ = 365 nm) through the optical mask, thus transferring the mask pattern onto the device. It is developed using an alkaline developer solution for a certain time (just as in photography) and rinsed with DI water. Finally, the resist is heated to harden it, so that it becomes mechanically more resistant and can withstand further processing. The pattern is transferred to the polysilicon layer by using a reactive-ion etching procedure, after which the resist is removed with electronic-grade acetone for 2 minutes, rinsed with isopropanol for 2 minutes, and finally DI water for 5 minutes. The Pyrex substrate is etched by dipping it into a 50% HF bath with an etch rate of approximately 10 μm per minute. The polysilicon acts as a mask and the pattern is therefore transferred to the glass substrate. HF etching of glass is isotropic and therefore the channels will have profiles with rounded walls. It is possible to create channels with depths as shallow as 1 micrometer with this technique, since channel depth is determined by etch time. If a less concentrated HF bath is used, it is possible to create nanometer-scale channels, since the slower etch rate means longer etch times, and thus better control over depth. The polysilicon layer is then removed by dipping the wafer in a KOH bath at 60°C for 5 minutes and thoroughly rinsing in a DI-water cascade. The patterned wafer is bonded with a Pyrex coverplate with predrilled access holes. These two wafers are thoroughly cleaned prior to bonding.

The cleaning process involves first rubbing the substrates with a cleanroom-grade cloth wetted with electronic-grade acetone. A rinse in electronic-grade isopropanol is performed, followed by a rinse with DI water. The wafers are then immersed in a 97% fuming nitric acid bath for 10 minutes in order to remove any organic residues and also to hydroxylate the surface to create a maximum number of OH sites to promote bonding. Wafers are then rinsed in DI water and dried with nitrogen. After this cleaning procedure, the access holes (1.02 mm diameter) in the coverplate are aligned manually with the ends of the microchannels of the patterned wafer. They are put in an oven to perform fusion bonding by ramping the temperature up to 650°C, which is close to the annealing point of Pyrex. This creates an irreversible seal, resulting in a single piece of glass with integrated microchannels.

These various procedures are performed in a cleanroom. They are a demonstration of the power of microtechnology to create 3D micrometer-scale channels, which can then be used as reactors for enhanced biochemical reactions, as described above.

1.5.2 Pumping systems

Two different pumping mechanisms used in microfluidic devices will be described. The first is pressure-driven flow, where fluids are pumped through a system by application of a pressure to the inlet of a channel. This can be done in various ways, using a syringe pump, peristaltic pump, isocratic pump, or simply by applying a vacuum at the outlet of a microchannel. Flows induced with these pumping systems have a parabolic profile (Figure 1.10) given by Poiseuille's parabola of constant negative curvature[27]:

$$v = -\frac{dp}{dx}\frac{h^2}{2\eta}\left(1-\frac{y^2}{h^2}\right) \qquad (1.2)$$

where: v = velocity

h = channel height

η = fluid viscosity

$-\frac{dp}{dx}$ = constant pressure decrease along the channel

y = position across the channel

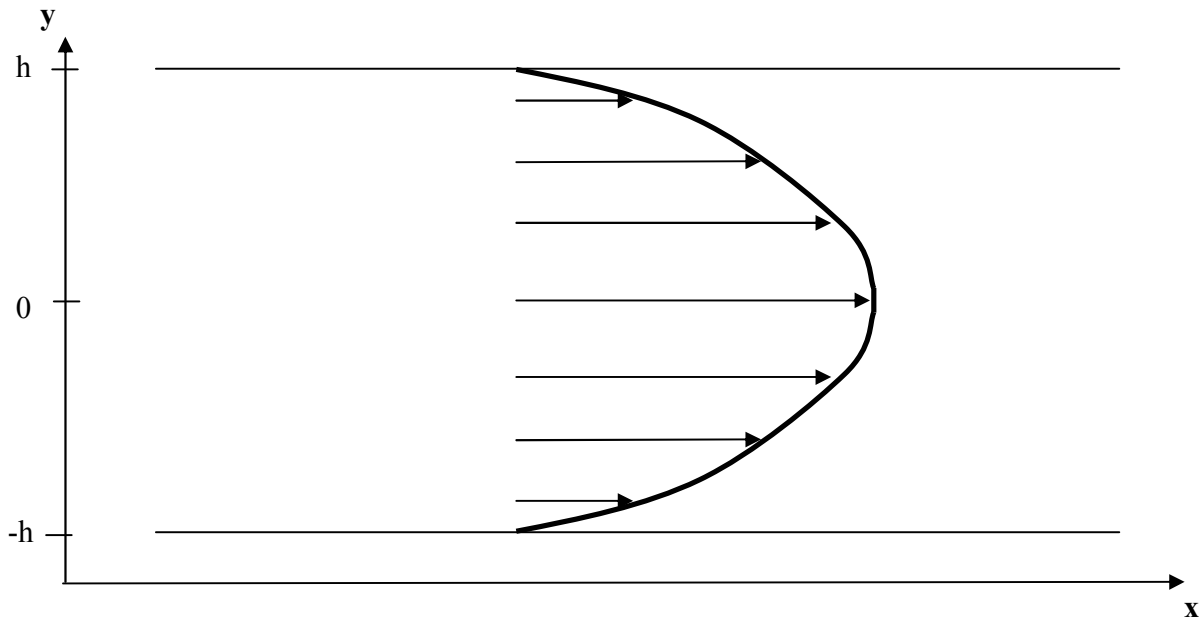

Figure 1.10: Poiseuille's parabolic flow velocity profile.

When there is a difference of pressure, ΔP, between the inlet and outlet of a channel, the flow, Q, induced in this channel can be obtained by:

$$Q = \Delta P/R \tag{1.3}$$

where R is the channel hydraulic resistance given by:

$$R = C_i \cdot \eta_i \cdot L_i / 2A_i \cdot D_i^2 \tag{1.4}$$

where: A = area of channel cross-section

D = hydraulic diameter (dependent on channel cross-section)

C = geometric constant (dependent on cross-section shape)

η = viscosity of the fluid in the channel

L = length of the channel

In the case where the channel is rectangular, with a width that is much larger than the height, the hydraulic resistance is given by [28]:

$$R = 12 \cdot \eta \cdot L/w \cdot h^3 \tag{1.5}$$

where: w = channel width

h = channel height

giving a flowrate of:

$$Q = w \cdot h^3 \cdot \Delta P/12 \cdot \eta \cdot L \tag{1.6}$$

This type of flow is often used to carry out flow injection analysis on a small scale by pushing several fluids at the same time through a microchannel system. Different reagents can be merged in a single channel and mixed with sample in this way, to convert the sample chemically into a form which is visible to the detector[29].

A different pumping system often used in glass channels is electro-osmotic pumping. The principle is illustrated in Figure 1.11. The surface of a glass channel contains SiOH sites. When a buffer solution fills such a channel, the SiOH sites will deprotonate to a certain extent, depending on the pH of the solution. The remaining O^- negative sites will attract the positive ions in solution close to the channel walls to create a double layer of ions. The layer closest to the channel walls remains immobile when an electric field is applied, while the second half of the double layer becomes mobile. In between these two layers lies what is called the plane of shear, which defines the interface between the layers of mobile and fixed ions. A potential known as the zeta potential, ζ, is created at the plane of shear. Upon application of an electric field, the positive ions in the mobile part of the double layer are accelerated to a velocity dictated by their charge-to-mass ratio. These ions will drag solvent with them, generating a movement in the surface layer which is transferred to adjacent solution layers by viscous forces. The result is the rapid establishment of bulk flow in the channel which is characterized by a flat velocity profile with little dispersion. Electro-osmotic mobility, μ_{eof}, will depend on the zeta potential and therefore the surface properties of the channel. There are two parameters which influence the zeta potential. The first is the charge density at the surface, which will yield a high zeta potential when surface charge density is high and vice versa. Charge density is a measure of the number of deprotonated SiOH sites on the glass surface, which depends on the pH of the buffer solution used. The higher the pH, the more sites will deprotonate, and the higher the EOF. At low pH, the opposite is true, and acidic buffers will yield low EOF. The second parameter that will influence the zeta potential is the distance, d_{shear}, between the glass wall and the plane of shear. This will directly depend

on the ionic strength of the buffer solution. If there are less ions in solution, the ionic strength will be lower, which will increase d_{shear}. The zeta potential can be considered as the potential created between two plates of a planar capacitance C, one plate being the negatively-charged glass wall and the other plate being the mobile layer of ions in the double layer. The relation here between capacitance charge, Q_c, and its potential becomes[30]:

$$\zeta = \frac{Q_c}{C} = \frac{Q_c \cdot d_{shear}}{\varepsilon \cdot \varepsilon_0 \cdot A} \tag{1.7}$$

where the capacitance is inversely proportional to the distance between the two plates. Therefore, the zeta potential will increase when d_{shear} increases. This implies that low concentration buffers will have higher electro-osmotic mobilities.

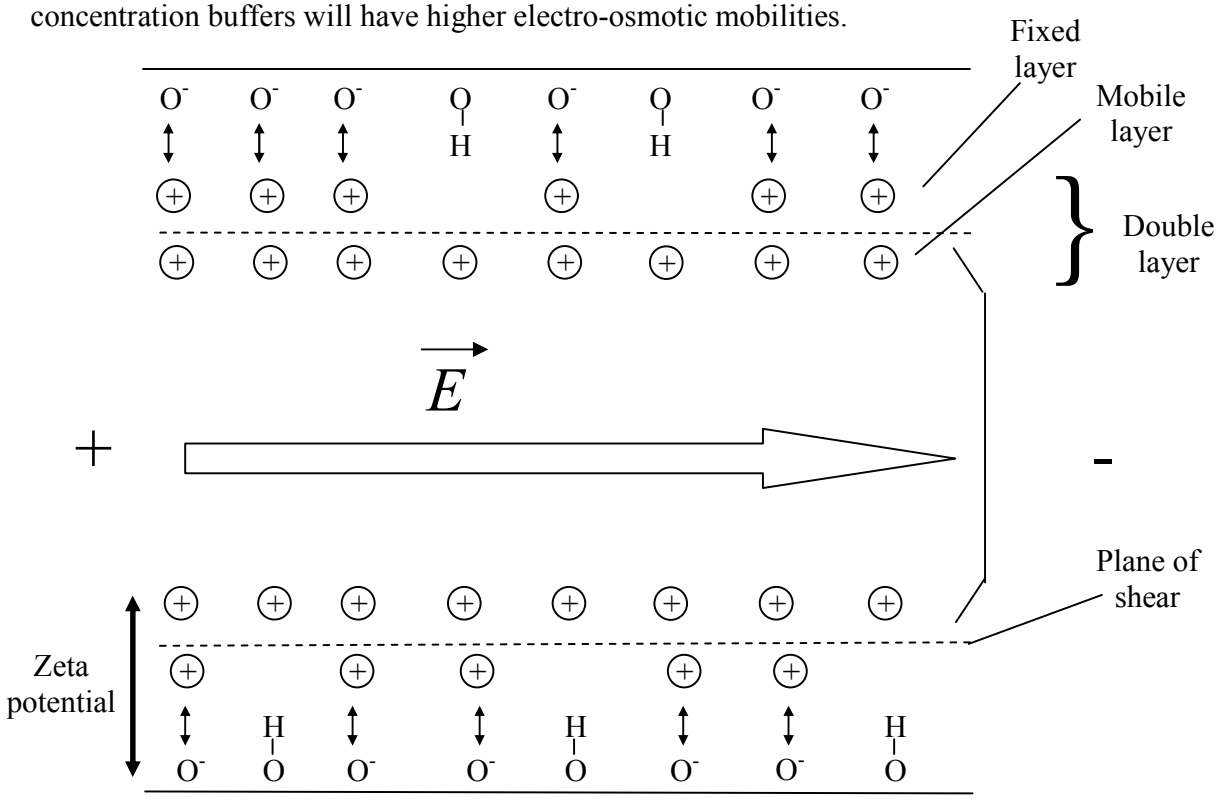

Figure 1.11: Electro-osmotic pumping

The equation describing the electro-osmotic flow (EOF) is[31]:

$$v_{eof} = \mu_{eof} E \tag{1.8}$$

where v_{eof} = electro-osmotic velocity

μ_{eof} = electro-osmotic mobility

E = applied electric field

Typical values for v_{eof} fall in the μm/s to mm/s range, for E > 100 V/cm.

The mobility of the buffer is given by:

$$\mu_{eof} = \varepsilon \zeta / 4\pi\eta \tag{1.9}$$

where η = buffer viscosity

ε = buffer dielectric constant

ζ = zeta potential, the potential at the plane of shear within the double layer

Because the electro-osmotic velocity is proportional to the electric field, it is possible to precisely control very low flowrates and therefore pump low volumes of samples throughout a system. Since the electro-osmotic mobility depends on the surface charge of a channel, the mobility can change if a surface is coated with a certain molecule. Pressure-driven flow, of course, is independent of surface charge.

If a complex network of channels is connected to a reaction chamber, it is possible to bring fluids to the chamber in a controlled fashion by simply applying an electric field

between two or more points in the system. Fluids will faithfully follow electric field lines, a feature difficult to obtain with pressure-driven flow. Figure 1.12 shows a very commonly used microfluidic element called the double-T injector [32]. It is called thus because of its geometry, which resembles two T's hooked to one another. This simple structure is used to define a precise volume of fluid. If a potential difference is applied between x and y, fluid starts to flow from the higher voltage (+) to the lower voltage (-). This is because cations are generally the charge carriers which result in EOF. The fluid follows the path essentially without creating a backpressure, which would occur if pressure-driven flow is used. Diffusion occurs in the case depicted in Figure 1.12a where flows are not controlled at w and z. Figure 1.12b shows a method to avoid diffusion occurring by simply controlling the voltages at w and z. By correctly tuning the different voltages, a "pinching" effect can be created by inducing small flows from w and z to push sample back into the double-T injector. This will create a very well-defined plug of a given sample volume, as desired.

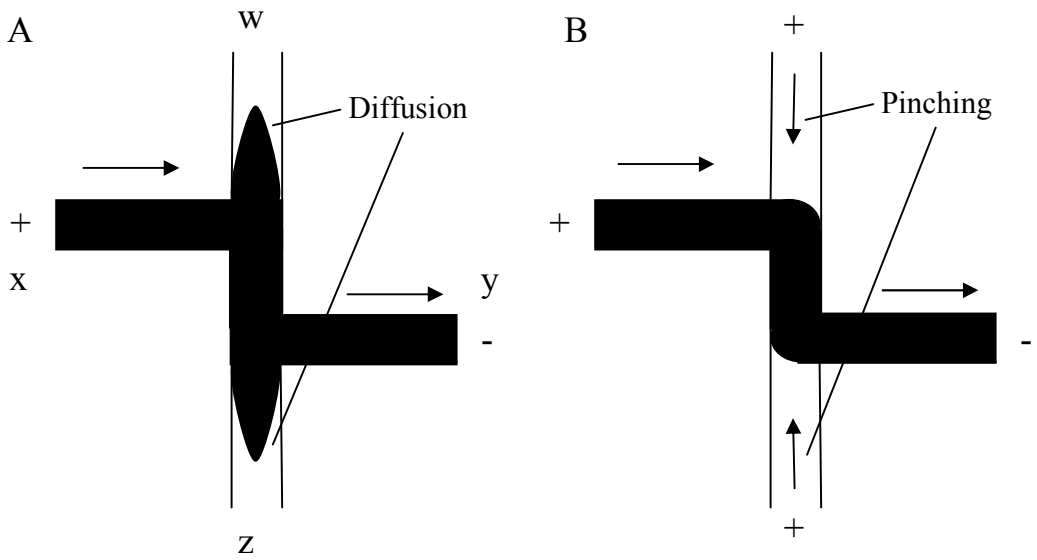

Figure 1.12: The double-T injector a) without pinching, b) with pinching.

This illustrates that even in a complex network of channels, it is possible to precisely control the different flows and volumes of fluids circulating throughout a microfluidic system with proper application of voltages. Therefore, electro-osmotic pumping is often better adapted than pressure-driven flow to cases where low sample volumes need to be transported with low dispersion. Unfortunately, EOF is difficult to use at higher buffer concentrations (usually greater than 100-150 mM), because of the high electric fields involved (hundreds of volts per centimeter). This induces high currents and Joule heating, which can heat buffer solutions up to their boiling point, with air bubbles created inside the channels as a result. Once these bubbles reach the size of the channel diameter, they cut the electric field, rendering it impossible to use electro-osmotic pumping. This is the type of problem which could arise in DNA hybridization experiments, since single strands of DNA require high salt buffer concentrations in order to hybridize.

Therefore, both pressure-driven flow and electro-osmotic flow are useful in microfluidics, this strongly depending on the application. In this thesis, electro-osmotic pumping was used for the immunoassay work, and pressure-driven flow used for the DNA hybridization experiments.

2 HETEROGENEOUS IMMUNOASSAYS ON CHIP

This chapter is adapted from:

Electrokinetically Driven Microfluidic Chips with Surface-Modified Chambers for Heterogeneous Immunoassays

A. Dodge, K. Fluri, E. Verpoorte, N.F. de Rooij, Analytical Chemistry, 73, pp 3400-3409, 2001.

A Microfluidic Chip for Multi-Step, Heterogeneous Immunological Reactions

A. Dodge, E. Verpoorte, N.F. de Rooij, Proceedings of the μTAS '2001 Conference, Monterey, CA, USA, pp.499-500, Oct. 21-25, 2001.

Multi-Inlet Chip for Electrokinetic Immunometric Heterogeneous Immunoassay

A. Dodge, X. Wang, E. Verpoorte, N.F. de Rooij, Proceedings of the Transducers'01-Eurosensors XV Conference, Munich, Germany, pp.1194-1197, June 10-14, 2001.

Valveless, Sealed Microfluidic Device for Automated Heterogeneous Immunoassay: Design and Operational Considerations

A. Dodge, K. Fluri, V. Linder, G.-L. Lettieri, J. Lichtenberg, E. Verpoorte, N.F. de Rooij, Proceedings of the μTAS '2000 Conference, Enschede, the Netherlands, pp.407-410, May 14-18, 2000.

This chapter describes how heterogeneous immunological assays can be performed in a microfluidic device. Three different prototypes have been designed, demonstrating the diversity of device functionality which can be achieved by microtechnology, but also the different constraints one should take into account while designing. A bimolecular biochemical model is used in the first device to demonstrate that binding of an analyte in solution with a protein immobilized on a microchannel wall can be detected and quantified. A device with a smaller overall size (so-called "footprint") using the same biochemical model is then described. This example shows that miniaturization does not always increase speed and precision if certain design considerations have not been taken into account. Finally, a third device designed for a sandwich-type assay is described, where a true three-layer heterogeneous immunological assay is performed for the first time in a microfluidic device.

2.1 Introduction

The ability to perform diagnostic tests in a quick and easy manner is becoming increasingly important in the medical realm, especially with recent trends towards clinical laboratory decentralization and more home testing. Immunoassays, which exploit the highly specific interaction of antibodies, produced by the immune system, with foreign molecules or antigens, are a standard tool for disease diagnosis. In established homogeneous assays, formation of the antibody-antigen complex in solution leads to a change in detector signal. Though the simplest approach from a fluidic standpoint, the number of available assays is small, since many binding events cannot be chemically configured to generate useful changes in signal. This can be compensated to some extent by including a solution-phase separation of reaction products, as has been demonstrated

by the application of capillary electrophoresis (CE) to immunoassays[6-9]. The heterogeneous immunoassay, in which one of the reactants, usually the antibody, is attached to a solid surface, continues to offer a versatile approach. In this format, the surface is incubated with sample to allow binding to occur, after which time the amount bound is determined and related back to a solution concentration. The major advantage of solid-phase immunoassays is the ability to concentrate molecules from solutions of low concentration onto a surface for facilitated detection. Easy-to-use test strip kits based on heterogeneous immunoassays exist for pregnancy, ovulation and hepatitis, providing reliable results in under 15 minutes. However, not all heterogeneous immunoassays are transferable to the test strip format, so that many are still carried out manually or with automated benchtop instruments, with more than 15 minutes required for a result[33]. In these cases, the capture molecules are immobilized on the walls of a small plastic vial or well of a microtiter plate. Detection of bound analyte is accomplished using radioactive or fluorescent labels. Automation of heterogeneous immunoassays has generally followed a robotic route for fluid handling, where aliquots of solution are taken from reservoirs and delivered by pipette-like tools to open reaction wells. These instruments tend to be relatively complex and bulky, restricting their use to centralized clinical laboratories. Though precision may be improved, overall analysis times can still be very long. Transport of samples from the patient to the lab may contribute to long delays between sampling and delivery of a result to the medical professional. Long incubation times are also required in many instances to ensure binding of sufficient amounts of analyte for analysis. In most cases, diffusion must be relied on to transport molecules to the reactive surface, a slow process which can take a lot of time, as described in Chapter 1. An IgG

molecule, which has a diffusion coefficient, D, of 4×10^{-7} cm^2/s, would require about 3 hours and 30 minutes to diffuse 1mm. While most analytes of interest are smaller than IgG, and hence diffuse somewhat faster, incubation in conventional assays can still take several hours. For reasons of both long analysis time and the limited portability of most immunoanalyzers, immunoassay test results do not generally play a big role in point-of-care diagnostics. To widen the scope of immunoassay application, analysis times must be shortened, and new, less complex fluid handling instrumentation developed.

Researchers have addressed the issues associated with heterogeneous assays in a number of different ways. The incorporation of the reaction chamber into a flow system has been popular, as it allows controlled transport of the required solutions over the modified surface rapidly and in an efficient manner. Flow systems are also by nature closed, which means they are less susceptible to contamination from external agents or evaporation of solvent. Increasing the reactive surface area in the flow chamber is usually accomplished by using modified beads as the solid phase. These are held in the chamber by means of some kind of barrier, which still allows flushing with the sample and the various reagents[34-36].

Microfluidic chips offer the additional advantage of potentially faster solution delivery in a more compact format. The combination of beads and microfluidics is a powerful analytical tool[16, 37, 38], but using beads effectively in a chip is not an easy task. Micromachined chambers surrounded by filter structures or barriers were recently integrated into microfluidic devices for bead-based DNA analysis[37], chromatography[38], and immunoassay[16]. However, most of these structures require more than one

photolithographic step for their fabrication, making them more complex than etched channel networks.

The approach taken in this study sees the immobilization of immunoreagents directly onto microchannel walls, taking advantage of the inherently high surface-to-volume ratio of micrometer-dimensioned channels[39-41]. Three different microfluidic chips were designed and realized for this work. In all three cases, the reaction chamber consisted of a microchannel segment nested within a microfluidic network for delivery of samples and reagents. Electrokinetic pumping was explored as a means of fluid propulsion through the channels, due to its suitability for miniaturization with flowrates on a pL/s to nL/s scale. The binding of rabbit immunoglobulin G (rIgG) to protein A (PA) was chosen as the test system for the first and second prototypes (DEVICE 1 and DEVICE 2), since PA is not only relatively easy to immobilize on glass, but could also provide a foundation for immobilization of antibodies for immunoaffinity chromatography[35] or other immunoassay applications[33]. The third prototype (DEVICE 3) was designed for a three-layer system for analysis of goat anti-rIgG (g-anti-rIgG), using PA to tether rIgG to microchannel walls. The mode of chip operation in fact resembled affinity chromatography, with analytes being bound to the PA phase during continuous flow incubation steps, followed by elution using a low pH buffer and fluorescence detection of the eluted labeled species. The design, preparation, and operation of the microfluidic chips for heterogeneous assay are described in detail below. The advantages and disadvantages of competitive assays done in different flow-through formats on chip will be discussed.

2.2 Experimental

2.2.1 Chip fabrication and design

The three prototypes were fabricated following the general technological procedure described in the introduction, which is presented here in more detail. The microfluidic networks are fabricated in a 10-cm-diameter, 500-μm-thick Pyrex 7740 wafer (Guinchard, Yverdon, Switzerland for DEVICE 1, and Sensor Prep Services, USA for DEVICE 2 and DEVICE 3) using standard photolithographic techniques. First, a 200-nm-thick layer of polysilicon is deposited on the wafer by low-pressure chemical vapour deposition in a furnace at 570 °C for 1 hour. After the surface is passivated using a silanization treatment with hexamethyldisilazane (Laporte Electronics, Riddings, UK), AZ-1518 photoresist (Clariant GmbH, Wiesbaden, Switzerland) is spin-coated onto the wafer and prebaked for 1 minute at 100°C on a hotplate. The resist is exposed through a chromium mask with 55 mJ of UV light (λ = 365 nm) with an Electronic Vision AL 645 mask aligner (Electronic Vision, Schärding, Austria). It is then developed in 4:1 DI water/AZ351B developer solution for 1 minute, and postbaked for 1.5 minutes at 110 °C on a hotplate. Reactive-ion etching is used to open the polysilicon layer which was exposed during resist development, thus transferring the channel pattern. The photoresist is stripped in MOS (microelectronic) grade acetone (Laporte Electronics, Riddings, UK), followed by a rinse first in MOS-grade isopropanol (Laporte Electronics, Riddings, UK), and then doubly distilled, deionized (DI) water. The wafer is then immersed in 50% HF for approximately 2 minutes to etch into the glass surface at the polysilicon mask openings. The exact etch time depends on the etch rate of the HF bath, which is subject to

variation as the bath ages. Generally, though, etch rates are about 10 μm/min for the Pyrex 7740 substrate used. The polysilicon is then removed by placing the wafer in a KOH bath at 60 °C for five minutes. A Pyrex coverplate containing diamond-drilled holes (Stecher AG, Thun, Switzerland for DEVICE 1, and Sensor Prep Services for DEVICE 2 and DEVICE 3) which align to the ends of the channels is bonded to the etched wafer with a fusion bonding procedure[42].

The design of DEVICE 1 took the following requirements into consideration:

1) The channels should be short enough to minimize transport distances to the reaction chamber, but long enough to decrease the effects of hydrostatic pressure-induced flow[43-45]. This may arise when solution levels are unequal, causing flow from overfilled to underfilled reservoirs. Since pressure-driven flows depend on channel length and cross-section, as given by Equation 1.4, increasing channel flow resistances by increasing length and/or decreasing diameter can minimize these effects[46].

2) Channels should be deep enough (several μm) to have a certain detectable volume, but shallow enough to avoid hydrostatic pressure effects.

3) The channel layout should include a supply channel for each sample and reagent, to avoid cross contamination and facilitate automation of the system.

DEVICE 2 had much shorter channel lengths, thus reducing hydraulic flow resistances and making the device more susceptible to hydrostatic pressure effects, which can perturb flow paths and limit flow control as a result. Nevertheless, this design allows more flexibility since it incorporates more reservoirs, and shorter transport distances should

reduce transport times and hence contribute to reduced analysis times. The other advantage of DEVICE 2 lies in the geometry of its reaction chamber, which no longer incorporates side channels for solution delivery. The absence of these channels means that loss of sample at channel junctions as sample passes through the chamber is eliminated. This will be discussed in more detail below. The multi-inlet chip design provides a certain freedom for sample number and type of analysis. Also, each channel used for sample delivery can be rinsed between tests to remove biomolecules sticking to channel walls and thus avoid clogging of the channels.

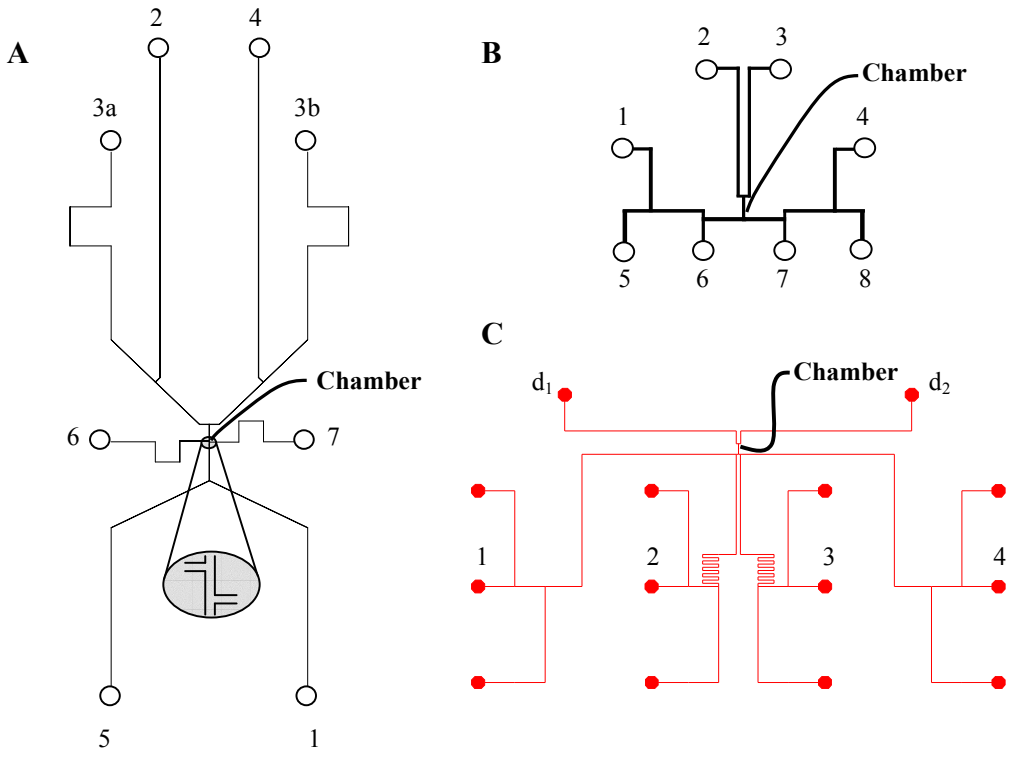

Figure 2.1: The three different prototypes a) DEVICE 1: overall chip dimensions (OCD) = 6.7 x 2.8 cm, b) DEVICE 2: OCD = 2 x 3 cm and c) DEVICE 3: OCD = 2.7 x 4.8 cm. Channel dimensions: are all 50 µm across the top, 20 µm deep.

The layout of DEVICE 1 is presented in Figure 2.1A. The reaction chamber consists of a 200-µm-long channel section at the center of a so-called double-T junction, formed by

channels 6 and 7 intersecting with the main channel. All channels have 50 µm x 20 µm cross-sections, so that the volume at the double-T intersection is 165 pL, making the chamber a true "picowell". The layout of DEVICE 2 is presented in Figure 2.1B. Overall chip dimensions (OCD) are 2 by 3 centimeters, a much smaller footprint than first-generation devices, which occupied an area of 6.7 x 2.8 cm^2. Channels are also 50 µm wide, 20 µm deep, and range from 5 mm to 16 mm in length. This is about 5 times shorter than in the first-generation layout. Chamber length varies between 400 µm and 800 µm to give chamber volumes of 330 pL and 660 pL, respectively. The idea of increasing chamber size was to preconcentrate and elute more bound molecules to increase sensitivity. The biochemical model chosen to characterize both chips was a system based on the affinity of surface-immobilized PA for the antibody, rIgG. The PA was attached to the chamber walls by first silanizing the chamber and then physisorbing the PA.

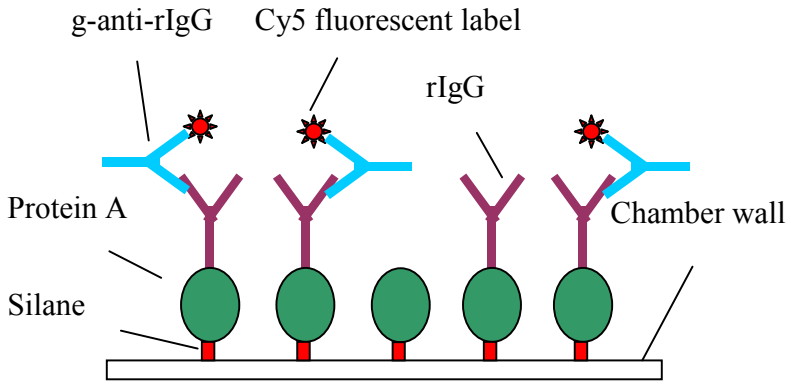

Figure 2.2: Sandwich assay schematic.

After having tested the first two devices, DEVICE 3, which respected the same design points as DEVICE 1, but incorporated more channels to obtain the operational versatility of DEVICE 2, was designed for a sandwich-type assay. Experience gained with the two

previous designs strongly influenced this design. The assay consisted of surface-immobilizing PA, incubating it with rIgG, and finally reacting with g-anti-rIgG as schematically shown in Figure 2.2. Hence, bound IgG could be determined by binding to labeled g-anti-rIgG. Alternatively, rIgG could be used as a probe molecule to assay for g-anti-rIgG. This assay configuration benefits from the fact that g-anti-rIgG has a low affinity for PA, reducing non-specific interaction of this analyte with the PA layer. The layout of this device is shown in Figure 2.1C.

2.2.2 Reagents and solutions

rIgG (polyclonal), g-anti-rIgG and PA were purchased from Sigma Chemicals (Buchs, Switzerland). The silanization agent was a solution of chlorodimethyloctadecylsilane (CDMODS) (40mg) dissolved in anhydrous toluene (1 mL) (Aldrich Chemicals, Buchs, Switzerland). 25 mM glycine/HCl (pH 2.0) and 25 mM tris/HCl (pH 7.5) buffers were made from glycine and tris(hydroxymethyl)aminomethane (tris) powder (Fluka Chemicals, Buchs, Switzerland), 1 M HCl solution and DI water. 1 M HPCE-grade NaOH, filtered over a 0.2 μm membrane prior to packaging, was also obtained from Fluka. 32 mM carbonate buffer (pH 9.6) was made from anhydrous sodium carbonate and sodium hydrogen carbonate powders (Merck AG, Dietikon, Switzerland), and DI water. The Cy5 monoreactive fluorescent dye labeling kit was from Amersham Pharmacia Biotech (Dübendorf, Switzerland). This dye has an excitation wavelength, λ_{ex}, of 649 nm, and an emission maximum, λ_{em}, around 670 nm. All previously unfiltered solutions were filtered with 0.2 μm aqueous filters (Semadeni, Ostermundingen, Switzerland) before being introduced into the chip. Labeled rIgG and labeled g-anti-rIgG samples were prepared by diluting 1 mg rIgG or g-anti-rIgG in 32 mM carbonate buffer

(pH 9.6) and adding 200 μg of Cy5. This mixture was left to react for 1 hour with periodic agitation. Sample was separated from excess dye with a separation column containing Sephadex G-50 (Amersham Pharmacia Biotech, Dübendorf, Switzerland) using 25 mM tris/HCl buffer (pH 7.5). Sample concentration was determined with UV absorbance using an HP 8453A UV spectrophotometer (Hewlett Packard, USA). Samples used for competitive assays were prepared by using a fixed volume of 300 μL of 1.5-μM labeled rIgG in tris/HCl buffer, adding a certain volume of a 2.5-μM stock solution of non-labeled rIgG in tris/HCl buffer, and completing to a volume of 600 μL with tris/HCl buffer.

2.2.3 Instrumentation

The power supply system was built in-house with high-voltage power supplies (Elstar Electronic, Wettingen, Switzerland) incorporating a computer interface. Computer control was achieved using the National Instruments software, LabVIEW™, along with a data acquisition card AT-MIO-16XE-50 with NI-DAQ software (Ennetbaden, Switzerland). The optical setup for fluorescence detection consisted of an L 25x/0.35 NPL FL objective (focal length: 2 cm, numerical aperture: 0.35, magnification: 25x) (Leica, Renens, Switzerland) attached to a microscope body (Melles Griot, Etoy, Switzerland) with an H5701-50 photosensor module (Hamamatsu Photonics, Schüpfen, Switzerland). The fluorescence signal was filtered with a 670-nm optical interference filter (Vomag Optoelectronic, Bubendorf, Switzerland) and imaged through a 100-μm pinhole (Melles Griot, Etoy, Switzerland) onto the photomultiplier. The excitation laser diode was a 3-mW, 650-nm Imatronic LDM115G/650/3 (Global Laser Technology LTD,

Abertillery, South Wales, U.K.). Fluorescence images were taken with a thermoelectrically cooled, high sensitivity CF 8/4 DXC black-and-white CCD camera (Kappa, Gleichen, Germany) mounted on an inverted epifluorescence microscope Axiovert 100S (Zeiss, Zürich, Switzerland) equipped with a mercury lamp and a dichroic mirror set for Cy5 (excitation wavelength bandpass at 640 nm, dichroic mirror reflecting below 660 nm, transmission wavelength (high pass) above 680 nm).

2.2.4 Immobilization of PA

For immunoassays, there is a major advantage when using the PA layer and not directly attaching the rIgG to the surface. PA contains four high-affinity binding sites for certain IgG's, but only two can be used simultaneously[19]. If the antibody is non-covalently bound directly to the surface, it will bind in a random fashion and will not necessarily be oriented in the correct position to accept the antigen. However, when the antibody binds to the PA, it will already be correctly oriented to facilitate binding with the antigen[2, 3] as described in the Introduction (Chapter 1). Also, it has been observed that when proteins are attached to polystyrene, denaturation can result, limiting antibody recognition[3, 47]. Using the PA intermediate layer could also prevent this potential problem in the case of glass surface contact. Other advantages of PA include its strong affinity for particular IgG subclasses in many species, with little or no binding to others[48]. An immobilized PA layer may therefore be used to distinguish between IgG subclasses[33] or simply to analyze for strongly binding IgGs using a competitive format. Alternatively, PA can bind a primary antibody layer, which then serves as the bound reagent for other immunoassays. One relevant example for this work is the use of PA affinity

chromatography for kinetic chromatographic sequential addition immunoassays for transferrin and albumin in human serum, described by Cassidy et al[35].

For DEVICE 1, all chip channel surfaces were first conditioned with 1 M HPCE-grade NaOH. This was done by filling all reservoirs with 1 M NaOH, and applying vacuum at single reservoirs for a total of 20 minutes, and then rinsing with DI water for 10 minutes. Methanol was then drawn for 5 minutes in the same way through the channels to remove the remaining water. This was followed by a 5-minute rinse with anhydrous toluene to flush away the methanol. At this point, the chip was ready for localized PA deposition in the double-T geometry, using the side channels from reservoirs 6 and 7 (Figure 2.1A) to introduce the silanization and PA solutions. The silanization procedure was carried out by pumping the silanization reagent (2% CDMODS in dry toluene) from reservoir 6 to reservoir 7[49, 50]. This reagent was introduced to reservoir 6, while all other reservoirs with the exception of reservoir 7 were filled with toluene. Application of vacuum from an in-house line to reservoir 7 caused CDMODS reagent to be pulled from reservoir 6 through the double-T intersection. At the same time, toluene was drawn from the other reservoirs to reservoir 7 as well. As these solvent flows were all towards the picowell, they confined the silanization reagent to the double-T intersection, preventing it from spreading to other sections of the system. Surface treatment was thus restricted to the picowell area. (Experiments were tried with all reservoirs except for 6 empty, but it was found that the resulting passage of air through the reaction chamber caused precipitation of the CDMODS.) After 5 minutes, reservoirs were switched, with CDMODS solution being filled into reservoir 7. Vacuum was applied to reservoir 6 for a further 5 minutes, after which time excess CDMODS was washed away with toluene for 5 minutes. The

toluene was then removed with methanol for 5 minutes, which in turn was finally rinsed away with DI water for 10 minutes. The chamber was then ready for protein physisorption by pumping PA solution, containing 0.1 mg PA dissolved in 1 mL 25 mM tris/HCl buffer (pH 7.5), from reservoir 6 to reservoir 7 and vice versa, for 5 minutes in each direction. Again, all other reservoirs contained buffer during this procedure. The timing for the NaOH conditioning is one commonly used in many laboratories engaged in conventional capillary electrophoresis[51]. Other solution treatment times are relatively arbitrary and have not been optimized for this application, although they seem appropriate.

For DEVICE 2, PA adsorption was performed with the same chemistry as for DEVICE 1 but chamber size definition was a bit different. The chamber consisted of a 400- to 800-μm-long channel which formed a bridge between reservoirs 2 and 3, and reservoirs 1, 4, 5, 6, 7 and 8 of the chip. The chamber was first silanized by aspirating the silanizing agent from reservoirs 2 to 7 for 10 minutes. PA (0.1 mg/mL in tris/HCl buffer, pH 7.5) was then aspirated along the same path for 10 minutes for physisorption to the silanized surface. After this, the other channels were reconditioned to remove protein and silane, by first drawing 1 M NaOH from reservoirs 2 to 3 and then from reservoirs 6 to 7, each for 10 minutes. In this way, the PA coating was confined to the vertical channel at the center of the chip.

For DEVICE 3, a similar procedure was used. Silanizing agent was drawn from reservoirs 2 and 3 to d_2 by application of vacuum. PA was then physisorbed to the modified surface along the same path. Finally, the reactive surface area was defined by

drawing 1M NaOH from reservoirs 2 to 3 and from d_1 to d_2, limiting it to the 1-mm-long vertical segment.

2.2.5 Chip characterization

With the computer-controlled setup, it was also possible to characterize the flowrates at which the solutions flow throughout the fluidic system, with subsequent determination of electro-osmotic mobilities. As described in the Introduction (Chapter 1), EOF strongly depends on surface properties through the zeta potential. Therefore, measuring the electro-osmotic mobility before and after a surface modification such as silanization and PA adsorption gives an indirect way of verifying that changes have taken place. Electro-osmotic mobility was measured in DEVICE 1 along the flow path from 6 to 7 after each modification step using a current monitoring method, depicted schematically in Figure 2.3. If a channel is filled with a buffer solution and a voltage is applied to its ends, the current measured across the channel will be constant.

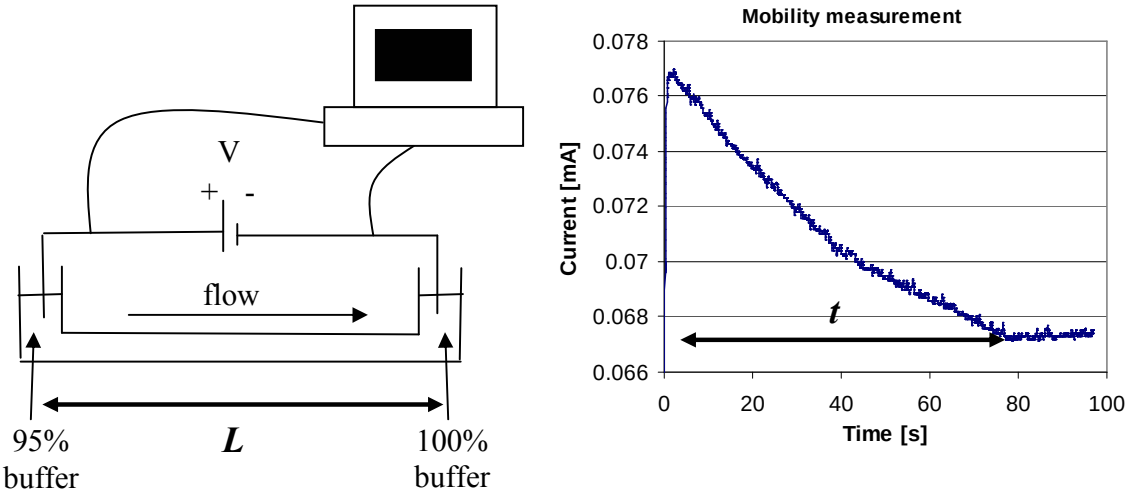

Figure 2.3: Current monitoring method used for EOF mobility measurement.

If, however, the reservoir at the positive electrode is filled with the same buffer but at 95% of the original concentration, and voltage is applied, this lower conductivity buffer

will start migrating through the channel to replace the original buffer. As a result, the current will continue to drop until the buffer reaches the end of the channel, at which time the current will stabilize. The channel length, L, divided by the time, t, taken for the buffer to go from one end of the channel to the other yields the velocity of the buffer, which is directly related to the electro-osmotic mobility by Equation (1.6)[52]. The applied voltage, V, is related to the induced electric field, E, by:

$$V = E \cdot L \tag{2.1}$$

where L = Channel length

Buffer velocity, v, is given by:

$$v = L/t \tag{2.2}$$

With equations (1.6), (2.1) and (2.2) we obtain the electro-osmotic mobility:

$$\mu_{eof} = v/E = L^2/V \cdot t \tag{2.3}$$

The buffers used for these mobility measurements were 25 mM tris/HCl (pH 7.5) as 100% buffer, and 23.75 mM tris/HCl (pH 7.5) as the 95% variant.

After chamber conditioning, μ_{eof}'s were also checked in the supply channels of DEVICE 1 to ensure that these had been sufficiently cleaned of toluene and surfaces restored to initial conditions. Channels above and below the chamber were reconditioned with NaOH to ensure good electro-osmotic mobility after protein immobilization. For reconditioning the top half of the chip, reservoirs 3a, 2 and 4 were filled with 1 M NaOH and vacuum was applied at reservoir 3b for 20 minutes, after which the channels were rinsed with DI water for 10 minutes. Similarly, for the bottom half, reservoir 5 was filled with solution

and vacuum applied at reservoir 1. μ_{eof}'s in all the channels were remeasured after this reconditioning to see if flowrates returned to values observed before chamber conditioning.

The current was monitored throughout the whole experiment along each active flow path, as it is a sensitive indicator of chip operation. Bubble creation in a channel system results first in current oscillation and finally in breakdown of electrical contact and interruption of the current, once the bubble has grown to span the channel. Such an event can immediately be diagnosed by current monitoring. It was also possible to follow the different steps of analysis and ascertain their degree of completion with continuous current measurement, as will be described below.

2.2.6 Surface imaging/flow visualization

For all three devices, surface imaging with a fluorescence microscope was used to monitor the chamber after each step of a full analysis cycle, to determine whether a good PA surface coating was achieved and localized binding of labeled rIgG or g-anti-rIgG in the chamber could be observed. Observation of Cy5-rIgG attachment to the PA-coated chamber walls, or Cy5-g-anti-rIgG attachment to PA-bound rIgG, allows verification of binding specificity and proper functioning of the chip throughout the analysis.

For DEVICE 2, binding specificity of rIgG in the PA-modified chamber was tested. To check this, a sample containing Cy5 only was introduced into the chamber, after which excess sample was removed with tris/HCl buffer. The chamber was then observed under a fluorescence microscope to see if any dye molecules had non-specifically attached themselves to the chamber walls. A Cy5-rIgG sample was then introduced, followed by a

washing sequence, and the chamber was re-examined under the microscope to see if rIgG had bounded to the PA chamber.

For DEVICE 3, electrokinetic flow patterns were visualized using a fluorescent solution of 104 μM tetramethylrhodamine-labeled dextran in 25 mM tris/HCl buffer (pH 7.5) to reveal flow patterns.

2.2.7 Chip operation

Once the PA was immobilized in the chamber, the chips were ready to be tested. Solution reservoirs were formed by punching holes of ca. 0.5 cm i.d. in a slab of poly(dimethylsiloxane) (PDMS) (Dow Corning, USA supplied by Distrelec AG, Dietikon, Switzerland), which was then reversibly sealed onto the glass wafer with reservoirs aligned to holes in the coverplate for DEVICE 1 and DEVICE 3, both relatively large chips.

A different approach was used for DEVICE 2, which was much smaller. In this case, the chip was mounted in a poly(methylmethacrylate) (PMMA) chip holder with integrated reservoirs and an optical window for fluorescence-based detection, as seen in Figure 2.4. Each reservoir is 4 mm high and 4 mm in diameter, which gives a total volume of 50 μL. Viton O-rings are used to seal the chip/chip holder interface. Electrodes immersed in all reservoirs served as electrical contacts for application of electric fields to generate electro-osmotic flow.

The different operation procedures are illustrated in Figure 2.5, Figure 2.6 and Figure 2.7. Arrows indicate the movement of solution during each step, with voltages being applied at the reservoirs at the end of each flow path. Table 2.1, Table 2.2 and Table 2.3 present

the different steps for the operation of the 3 different chips in detail, including the solution(s) being pumped, time elapsed, and voltage applied.

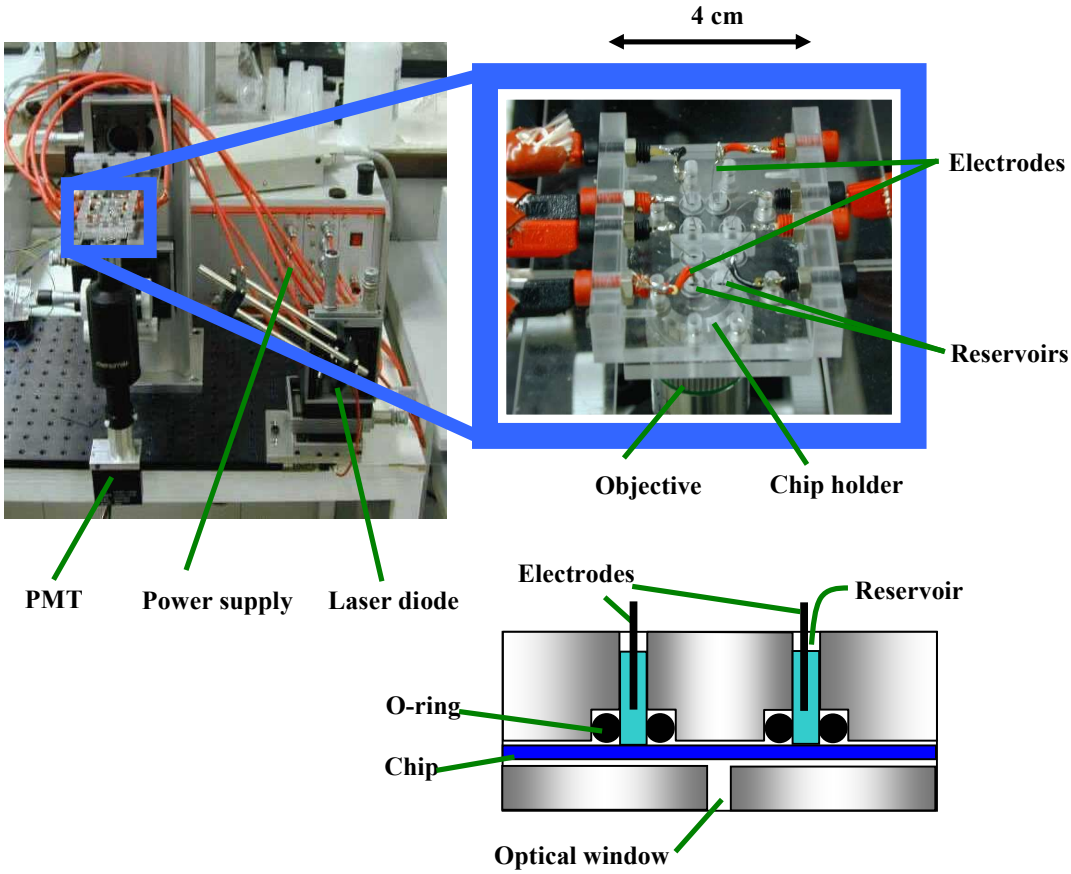

Figure 2.4: Chip holder for 2nd prototype.

All microfluidic channels are filled with buffer before analyses are begun. Computer-controlled, high-voltage power supplies connected to singly addressable electrodes were used to create electric fields through the channels, thus inducing electro-osmotic flow (EOF). This enabled precise control of fluid flow throughout the microchannel network. Each analysis is initiated with an rIgG incubation step, whereby sample is pumped from its reservoir to a waste reservoir for a period of 30 – 300 seconds. For DEVICE 1, voltages applied simultaneously at reservoirs 6 and 7 ensure a small auxiliary flow of buffer from these side channels, to prevent leakage of sample into these channels. This is

a procedure known as "pinching", as described in the introduction, to keep sample confined to the main channel[53].

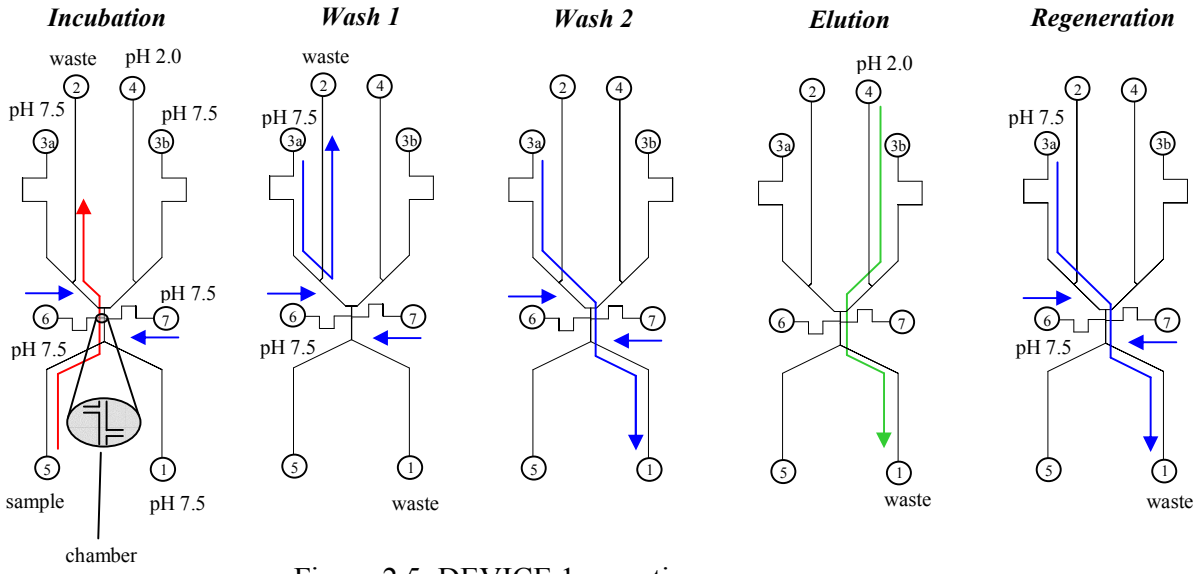

Figure 2.5: DEVICE 1 operation sequence.

Step	Solution being introduced into chamber	Duration of introduction	Reservoirs and flow path
Incubation	Cy5-rIgG sample in 25 mM Tris/HCl (pH 7.5)	30-300 sec	5 to 2 with pinch at 6 & 7 (-5kV at 2, GND at 5, 6, 7)
Wash 1	25 mM Tris/HCl (pH 7.5)	15-30 sec	3a to 2 with pinch (-5kV at 2, GND at 3a, 6, 7)
Wash 2	25 mM Tris/HCl (pH 7.5)	20-50 sec	3a to 1 with pinch (-5kV at 1, GND at 3a, 6, 7)
Elution	25 mM glycine/HCl (pH 2.0)	30-60 sec	4 to 1 no pinch (-5kV at 1, GND at 4)
Regeneration	25 mM Tris/HCl (pH 7.5)	20-40 sec	3a to 1 with pinch (-5kV at 1, GND at 3a, 6, 7)

Table 2.1: Chip operation steps for a full analysis cycle in DEVICE 1. Total cycle analysis time between 1 min 55 sec and 8 min.

After sample incubation, excess sample is rinsed away with a tris/HCl (pH 7.5) buffer. For DEVICE 3, this is followed by a g-anti-rIgG incubation step and another rinsing step. Finally, bound sample is eluted from the picowell using a glycine/HCl buffer (pH 2.0) and detected directly after the reactor. The chip is then regenerated for the next cycle. Experiments used either rIgG or g-anti-rIgG labeled with the fluorescent dye, Cy5 ($\lambda_{excitation}$ = 649 nm, $\lambda_{emission}$ = 670 nm), and signal was detected and recorded using a laser diode-based fluorescence detection system.

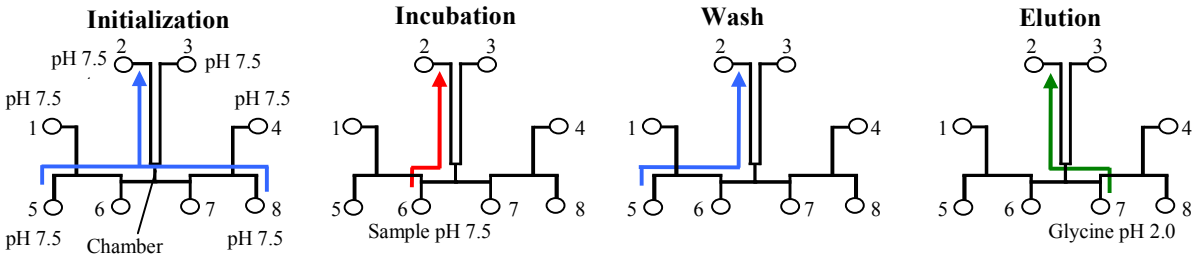

Figure 2.6: DEVICE 2 operation sequence.

Step	Solution being introduced into chamber	Duration of introduction	Reservoirs and flow path
Initialization	25 mM Tris/HCl (pH 7.5)	10 sec	5 and 8 to 2 (-2 kV at 2, GND at 5 and 8)
Incubation	Cy5-rIgG sample in 25 mM Tris/HCl (pH 7.5)	10-300 sec	6 to 2 (-2 kV at 2, GND at 6)
Wash	25 mM Tris/HCl (pH 7.5)	20-60 sec	5 to 2 (-2 kV at 2, GND at 5)
Elution	25 mM glycine/HCl (pH 2.0)	80-100 sec	7 to 2 (-2 kV at 2, GND at 7)

Table 2.2: Chip operation steps for a full analysis cycle in DEVICE 2. Total time required for one analysis: 2 min to 7 min 50 sec.

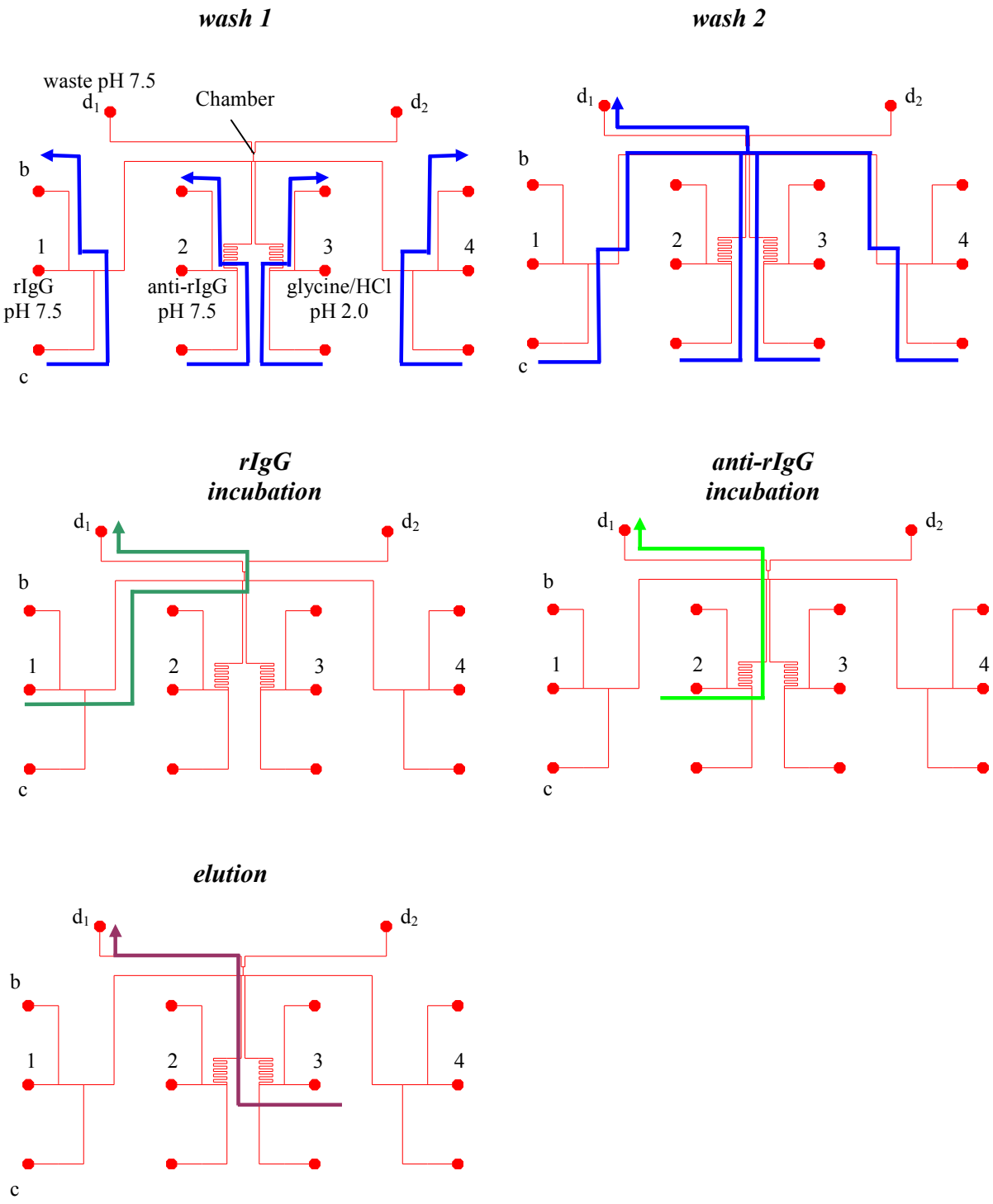

Figure 2.7: DEVICE 3 operation sequence steps. All unlabeled reservoirs are filled with 25 mM tris/HCl buffer (pH 7.5), as are d_1 and d_2. Note that the wash 1 and wash 2 steps are repeated between the rIgG incubation steps and between the anti-rIgG incubation and elution steps.

Step	Solution being introduced into chamber	Duration of introduction	Reservoirs and flow path
Wash 1	25 mM Tris/HCl (pH 7.5)	60 sec	all c's to all b's (-1kV at all b's, GND at all c's)
Wash 2	25 mM Tris/HCl (pH 7.5)	150 sec	all c's to d_1 (-4kV at d_1, GND at all c's)
rIgG Incubation	rIgG sample in 25 mM Tris/HCl (pH 7.5)	200 sec	1 to d_1 (-4kV at d_1, GND at 1)
Wash 1	25 mM Tris/HCl (pH 7.5)	60 sec	all c's to all b's (-1kV at all b's, GND at all c's)
Wash 2	25 mM Tris/HCl (pH 7.5)	150 sec	all c's to d_1 (-4kV at d_1, GND at all c's)
Anti-rIgG Incubation	Anti-rIgG sample in 25 mM Tris/HCl (pH 7.5)	300 sec	2 to d_1 (-4kV at d_1, GND at 2)
Wash 1	25 mM Tris/HCl (pH 7.5)	60 sec	all c's to all b's (-1kV at all b's, GND at all c's)
Wash 2	25mM Tris/HCl pH 7.5	150 sec	all c's to d_1 (-4kV at d_1, GND at all c's)
Elution	25mM glycine/HCl pH 2.0	300 sec	3 to d_1 (-4kV at d_1, GND at 3)

Table 2.3: Chip operation steps for a full analysis cycle in DEVICE 3.

2.3 Results and discussion

2.3.1 Characterization of the sealed, Protein A-modified picowell (DEVICE 1, DEVICE 2)

Values of μ_{eof} depend on surface properties and buffer solution composition. If a glass surface is coated with a long-chain alkyl silane covered by a layer of protein, there will be fewer available charge sites for generation of EOF. The consequence is a decrease in

ζ, with a resulting reduction in μ_{eof}. EOF was measured along the flow path from 6 to 7 in DEVICE 1 after silanization and PA adsorption, using the current monitoring method and 25 mM tris/HCl (pH 7.5) buffer. After silanization, μ_{eof} was reduced to about 50 % of the initial value measured in a non-treated channel, see Table 2.5. EOF mobility was reduced even further after protein adsorption, to 36% of the original value. After PA immobilization, the reagent and sample delivery channels leading into the chamber were reconditioned with 1 M NaOH as described in Section 2.2.5. μ_{eof} was then measured along flow paths 3a to 2, 2 to 1, 4 to 5 and 3b to 1, and found to be about 95% of the initial value. As expected, the 200-µM-long picowell (DEVICE 1) did not figure significantly in determining the μ_{eof} of flow paths of which it is a small part. These results, together with those in Table 2.4, indicate a significant change in surface characteristics in the sealed chamber when compared to the rest of the chip.

Surface modification step	μ_{eof}
Without treatment	$4.2 \cdot 10^{-4}$ cm^2/V·s
After silanization	$2.0 \cdot 10^{-4}$ cm^2/V·s
After protein adsorption	$1.5 \cdot 10^{-4}$ cm^2/V·s

Table 2.4: Electro-osmotic mobilities measured between reservoirs 6 and 7 (DEVICE 1) at various times during surface modification, using 25 mM tris/HCl (pH 7.5) buffer and electric fields varying between 340 V/cm and 690 V/cm. Protein solution: Protein A (0.1 mg/mL) in 25 mM tris/HCl (pH 7.5). Silanizing agent: $CH_3(CH_2)_{17}Si(CH_3)_2Cl$ (40 mg/mL) in anhydrous toluene.

The uniformity of the PA layer is important, since bubbles tend to form in the treated, hydrophobic channels from 6 and 7 if this coating is uneven. The presence of bubbles in the side channels is critical, as they disrupt chip operation. Different PA concentrations were tried for formation of this layer in the assay chamber. Examination of the chip using

a microscope confirmed that channel walls were covered with a rough film when bubbles developed; surfaces appeared fouled, due most likely to precipitation of PA from a reagent solution which contained high concentrations of PA (1 mg/mL or more). Bubbles originated from dissolved gases in the sample and reagent solutions, which were not degassed prior to use. Our experience has shown that in microfluidic devices, rough surface/liquid interfaces provide ideal nucleation points for micro bubbles. These then absorb other gas from solution, and grow large enough to obstruct the channel. On the other hand, no bubble formation was observed when channel surfaces bearing a PA layer were visibly smooth. In this case, the PA concentration of the reagent used to deposit the protein was lower (0.1 mg/mL). Therefore, irregular PA coatings appeared to lead to increased surface roughness, which promoted increased bubble formation. A good PA coating lasted for at least 20 days when dried and stored in the refrigerator. To date, the chips usually fail due to clogging rather than deterioration of the protein layer. It has been possible to keep certain chips functioning for more than a year with a simple cleaning technique, using 1 M NaOH between 65 and 100 °C to remove organic particles or dust. The pressure created by heat-induced evaporation of the fluid itself pushes NaOH throughout the chip, thus unclogging obstructed channels. After such a cleaning procedure, a PA immobilization can be successfully carried out again.

Direct tests for the presence of adsorbed PA were carried out using an inverted fluorescence microscope. For DEVICE 1, the surface in the picowell was incubated with 2.5 μM Cy5-labeled rIgG by drawing sample from all reservoirs to reservoir 7 for 3 minutes, using vacuum. After excess sample was removed, the picowell was examined under the microscope. Figure 2.8(a) and (b) provide a comparison of the region before (a)

and after (b) sample incubation. The emitted Cy5 fluorescence is clearly visible in the latter, indicating the presence of rIgG, and hence, the underlying PA layer. This is supported by the observation that the background signal in the channel entering from underneath is less in regions where no PA was deposited than in the chamber itself. The silanization and subsequent PA reagent deposition followed laminar flow streamlines from the upper left side channel to the lower right. This is evidenced by the well-defined border between Cy5-rIgG bound and non-bound areas in the lower region of the well. Dye solution aspirated from 6 together with buffer from other reservoirs was observed to round the corner upon entering the channel to 7 in a similar flow pattern. It appears in Figure 2.8(b) that PA was also adsorbed beyond the intersection at the top of the image, creating a larger modified surface than initially thought.

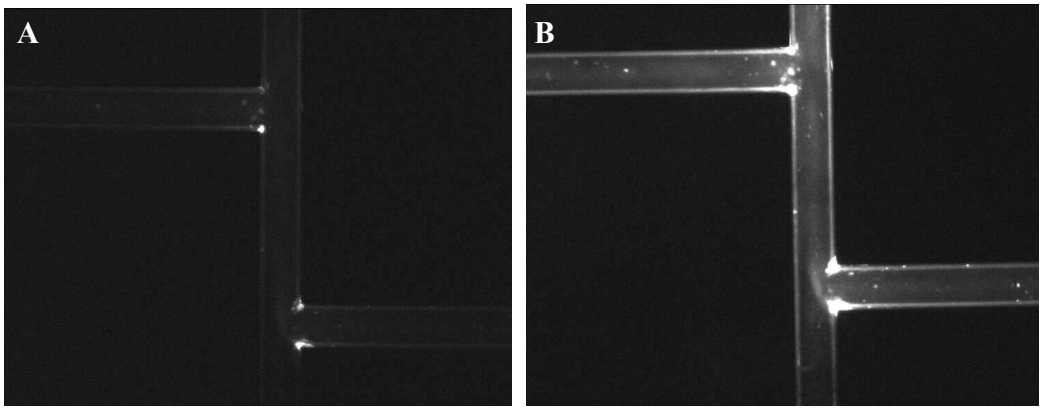

Figure 2.8: Double-T of DEVICE 1 a) before and b) after incubating with [Cy5-rIgG] = 2.5 μM sample. Sample was drawn from all reservoirs to reservoir 7 for 3 minutes by applying vacuum at reservoir 7.

A test for non-specific binding was performed in DEVICE 2, as seen in Figure 2.9. First, a 5-μM Cy5-containing solution was incubated in the channel. No signal was observed after rinsing. This was followed by incubation with a 990-nM Cy5-rIgG sample, which gave a large signal located inside the reaction chamber. The PA-coated chamber is well

defined, due to the NaOH reconditioning of supply channels leading into it, which removes coating in these channels.

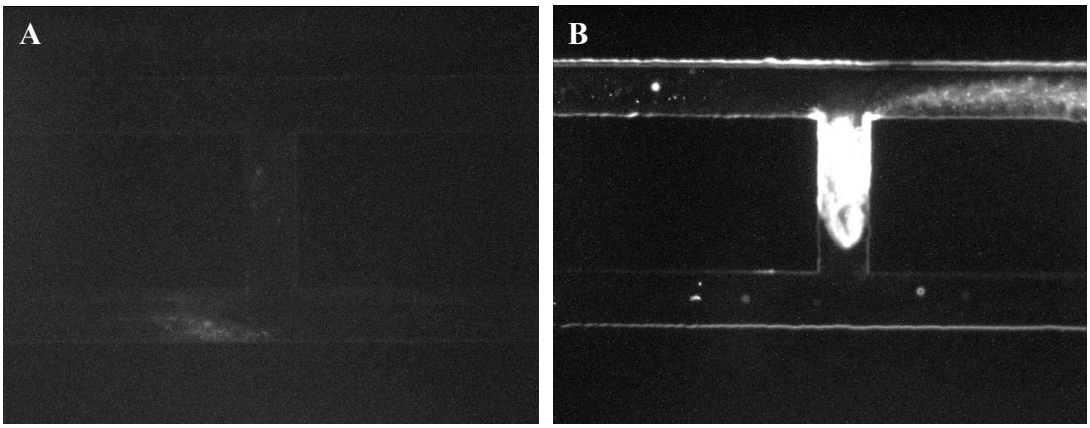

Figure 2.9: Chamber of DEVICE 2. Difference in observed signal between a) 5 μM Cy5 sample b) 990 nM rIgG-Cy5 sample. Chamber length is approximately 400 μm. Incubation time was 120 seconds. All solutions were pumped by aspiration, applying vacuum at a reservoir.

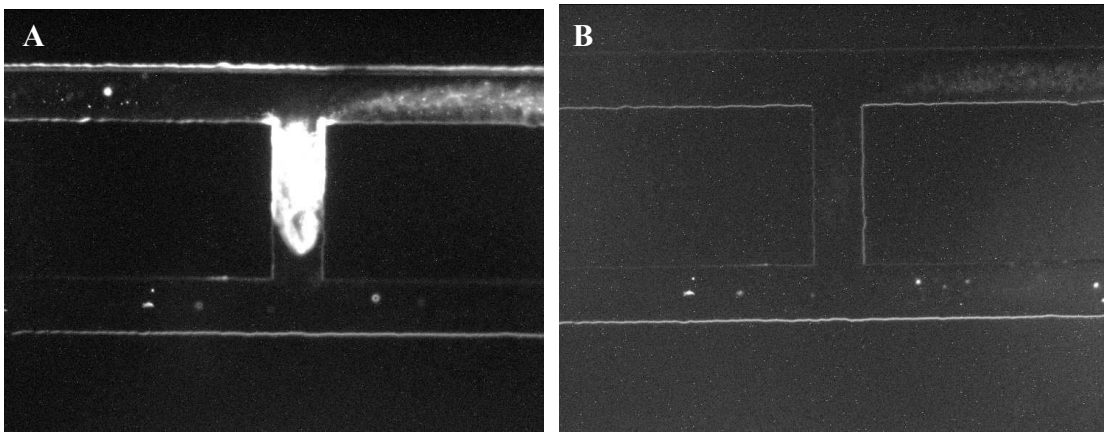

Figure 2.10: Chamber of DEVICE 2. a) After 120 seconds of incubation with 990 nM Cy5-rIgG sample followed by a washing step with tris/HCl buffer b) After elution. Chamber length is approximately 400 μm.

Sample was eluted with glycine/HCl (pH 2.0) buffer, as seen in Figure 2.10(b). Solution was aspirated in (a) and pumped electrokinetically for elution (b). In the latter case,

pumping of glycine buffer by aspiration did not result in elution of bound sample. The reason for this is not known.

2.3.2 DEVICE 1: Test of chip operation

Figure 2.11 shows the fluorescence trace recorded using the laser diode-based detector placed about 50 µm below the picowell, during execution of a Cy5-rIgG binding experiment in DEVICE 1. Incubation, wash, and elution steps are clearly visible in this figure. The elution of bound Cy5-rIgG was carried out using a chaotropic buffer containing glycine at pH 2.0. Dissociation of the bound species was instantaneous and irreversible, so that elution can lead to the stacking or concentration of rIgG into a narrow zone.

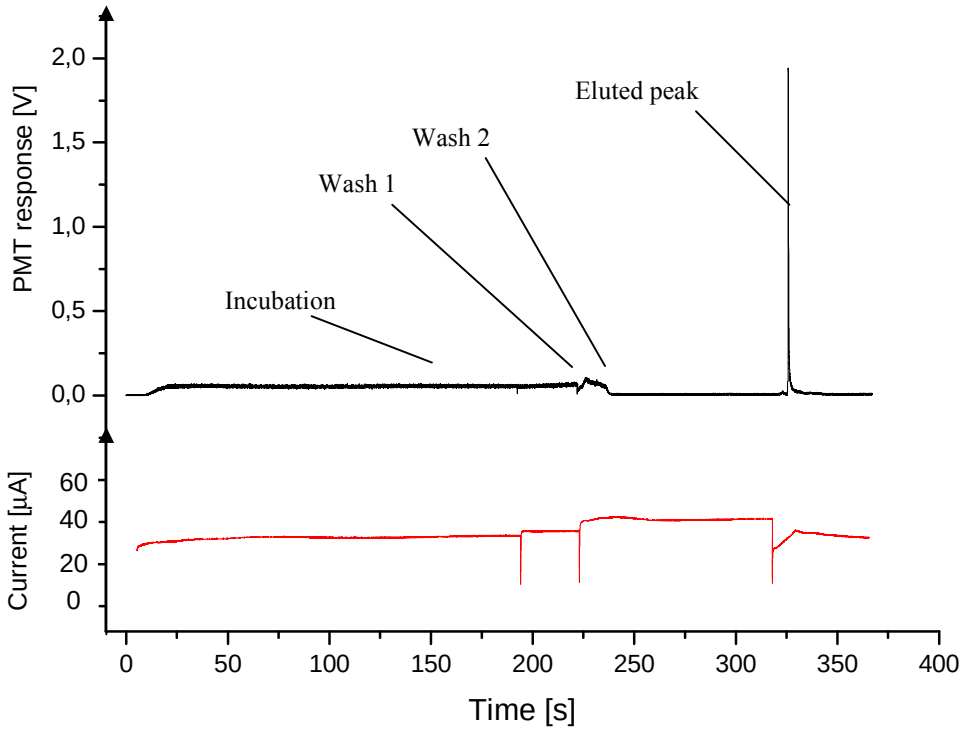

Figure 2.11: Photomultiplier (PMT) response measured simultaneously with current for a complete cycle. [Cy5-rIgG] = 1.5 µM.

One of the inherent advantages of heterogeneous immunoassays is that molecules are effectively concentrated when they bind to a surface-immobilized species, assuming the surface layer is a relatively uniform monolayer and binding sites are abundant. This is particularly true for samples with very low starting concentrations, provided incubation times are sufficient. In this case, the sample contained 1.5 μM of Cy5-rIgG, and signal was detected after an incubation time of 200 s, which was enough to saturate the surface (see below). An estimate of the number of PA molecules attached to the surface of the chamber can be made to illustrate the concentration aspect of this experiment. The available glass surface of the chamber (Figure 2.12) is 24'500 μm^2 ($L \cdot [2\pi \cdot r/2 + 2(w+r)] = 200\mu m \cdot (2\pi \cdot 20\mu m/2 + 2(10\mu m + 20\mu m)]$). A PA molecule occupies approximately 20 nm^2 of surface[3], and a maximum of 2 rIgG can bind to each PA[19]. This means that 2.5×10^9 molecules of rIgG, equivalent to 4.1×10^{-15} moles, could potentially bind to the picowell surface. Recall that the corresponding volume is 165 pL.

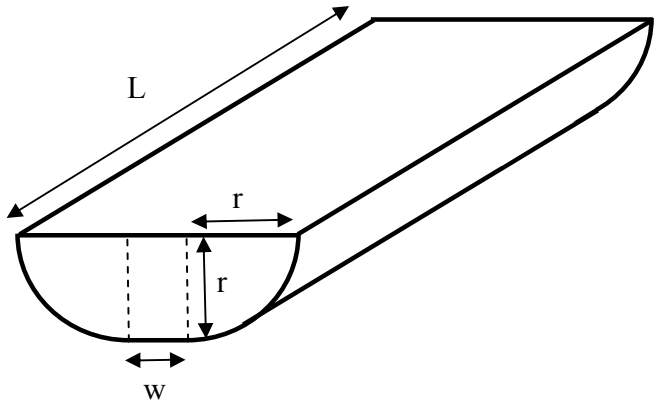

Figure 2.12: Calculation of chamber size.

Assuming the volume of eluted sample to be equivalent to one picowell volume, the concentration of eluted sample would be approximately 25 μM on average, or about 17

times greater than that of the original sample, creating a concentration effect. The eluted peak produced by the 1.5 μM sample is actually about 28 times larger than the incubation signal. This difference may be explained by a larger modified surface area than expected, as suggested in Figure 2.8(b), where rIgG is found beyond the chamber. The required elution volume may also be smaller than the assumed 165 pL. It should be noted that the 200-s incubation time corresponds to approximately 118 nL of sample analyzed, estimated using the incubation time, the applied flowrate (see below) and the channel cross-section (830 μm^2). This represents a significant reduction when compared to microtiter wells ranging between 10 μL and 100 μL.

Current monitoring of channels between reservoirs where potentials have been applied provides information about chip operation. A whole cycle with good functioning of the chip can be seen in Figure 2.11. For example, when the high-conductivity pH 2.0 buffer is supplied for the elution, the current increases until pH 2.0 buffer has filled the entire flow path, at which point the current stabilizes. The peak detected by the photomultiplier due to eluted sample should appear during this increase. Reproducibility of current traces for consecutive measurements is a good indication of system stability.

The high voltage power supplies deliver 5 kV at each step, resulting in electric fields varying between 330 and 660 V/cm, depending on the chip operation step. A μ_{eof} of 4.2×10^{-4} $cm^2/V \cdot s$ for the pH 7.5 buffer in an uncoated channel means that buffer velocities range between 0.139 and 0.277 cm/s, resulting in flows between 1.15 and 2.30 nL/s. This range of flowrates is commensurate with the microfluidic network being used, and provides efficient reagent delivery.

The μ_{eof} of the glycine buffer (pH 2.0) was measured to be of 2.0×10^{-4} $cm^2/V \cdot s$. When elution occurred, the current trace in Figure 2.11 indicates that it took only 13 seconds for this buffer to travel 3.4 cm when the 660 V/cm electric field was applied, corresponding to an apparent μ_{eof} of 3.9×10^{-4} $cm^2/V \cdot s$. This was because the glycine buffer was displacing the higher mobility, lower conductivity pH 7.5 buffer, leading to both discontinuous zeta potential and electric field gradients[54]. The pH 7.5 buffer region experienced a higher electric field, and thus traveled at a higher EOF than the region containing pH 2.0. The larger μ_{eof} of the pH 7.5 buffer further exacerbated the effect. To conserve continuity of flow, the pH 7.5 buffer remaining in the system essentially dragged the chaotropic reagent with it. The EO flow profile at the buffer interface would be distorted as a consequence and the flowrate of the pH 2.0 buffer was greater than expected. The velocity of the combined train of buffers was 0.262 cm/s, which yielded a flowrate of 2.2 nL/s, 84% faster than that of the glycine buffer on its own. The sensitivity of EOF to changes in solution composition must be taken into account if this pumping mechanism is to be used to manipulate widely different liquids one after the other. However, an appropriate combination of low- and high-mobility buffers in one channel may in fact prove useful to pump slow-moving solutions more quickly, as in this case.

A series of 10 sequential measurements was performed to check reproducibility of signal in DEVICE 1, using 300 nM Cy5-rIgG and a 100-s incubation period; the results are presented in Figure 2.13. Each complete analysis from incubation to elution took 4 minutes, and analyses were carried out sequentially with no pause between measurements. The signal reproducibility for eluted rIgG from the chamber was ± 13% for peak area, a result which is close to the ± 10% which is accepted for interassay

coefficients of variation[55]. The cause of these variations most probably resides in the incubation step. The channel used to drive the sample to the chamber was not cleaned between cycles, so that rIgG collected on the channel walls. This modified EOF, preventing new sample to flow into the chamber at the same rate as the previous cycle. Continued sample injection eventually led to clogging of the channel. However, the implementation of current monitoring as shown in Figure 2.11 could allow some feedback control of incubation times to compensate for varying sample flowrates. In disposable systems, of course, the issues associated with repeated chip use cease to be important.

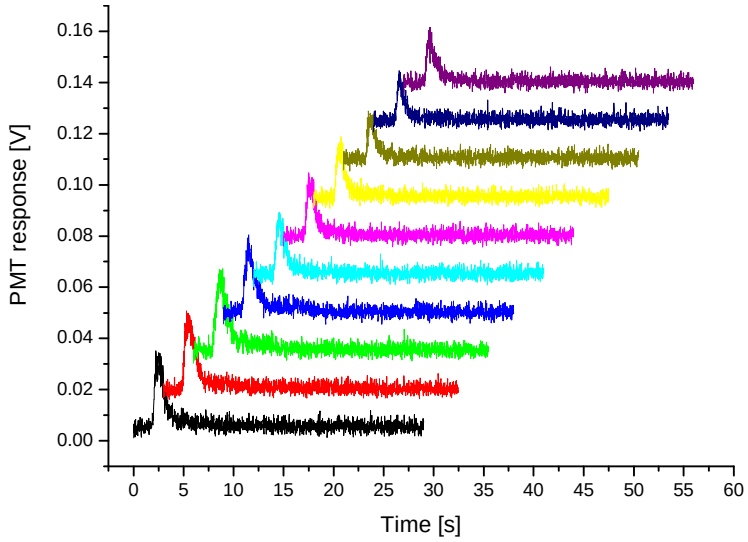

Figure 2.13: 10 sequential measurements of a 300 nM Cy5-rIgG sample in DEVICE 1.

2.3.3 DEVICE 2: Test of chip operation

The fluorescence trace for a full cycle performed in DEVICE 2 can be seen in Figure 2.14. The peak is much broader than in DEVICE 1, which makes this device less interesting in terms of sample preconcentration for detection limits. In this case, the total

amount of sample analyzed was 435 nL for an incubation time of 100 s. The incubation-step flowrate is 7.4 times faster than in DEVICE 1 (see below). The amount of analyzed sample has been increased because chamber size is larger. This requires more IgG to bind to the increased number of available PA binding sites at the chamber surface. The increased chamber size might explain the increase of peak width from 2 to 25 seconds.

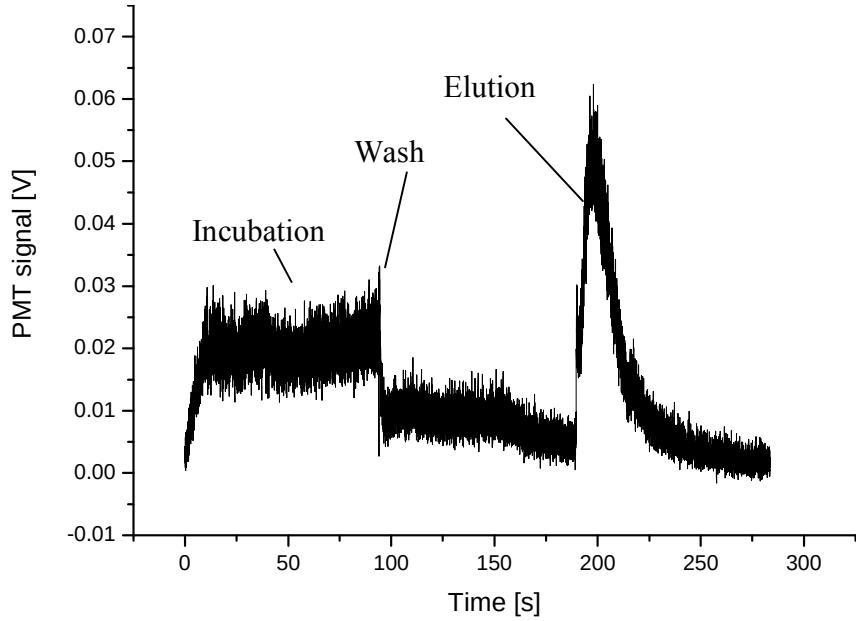

Figure 2.14: Full cycle performed in DEVICE 2. [Cy5-rIgG] = 1.5 μM. Incubation time is 100 seconds.

Unfortunately, reproducibility was difficult to achieve in DEVICE 2. Having demonstrated the chemistry and principle of chip function with the fluorescence microscope images, it was concluded that irreproducibility probably originated from a fluidic aspect of the system. Because the channels are very short, and therefore have little resistance to flow, they are very susceptible to adverse hydrostatic pressure effects. Therefore, fluid levels in all the reservoirs must be exactly equal to avoid hydrostatic pressure-induced flows which can inhibit proper chip functioning. It was observed with the fluorescence microscope that when the reservoirs were not perfectly equilibrated,

sample did not follow the desired path and flowed throughout the whole chip. Very often, no peak was obtained during elution because fluid control was not optimal. Also, leakage into side channels would create large plugs of fluorescence located in various regions of the device which would be pushed back in front of the detector and be detected. This type of plug could, in some cases, be confused with eluted bound sample since in this device, elution peaks are relatively broad. In order to check for spurious peaks, before beginning a series of experiments, full cycles were recorded with the PMT for a Cy5 sample first, followed by a Cy5-rIgG sample, to check for any potential difference in response during the elution step. In Figure 2.15, it is obvious that there is no signal when only Cy5 is analyzed. Therefore, the signal resulting from a Cy5-rIgG sample is truly due to bound sample.

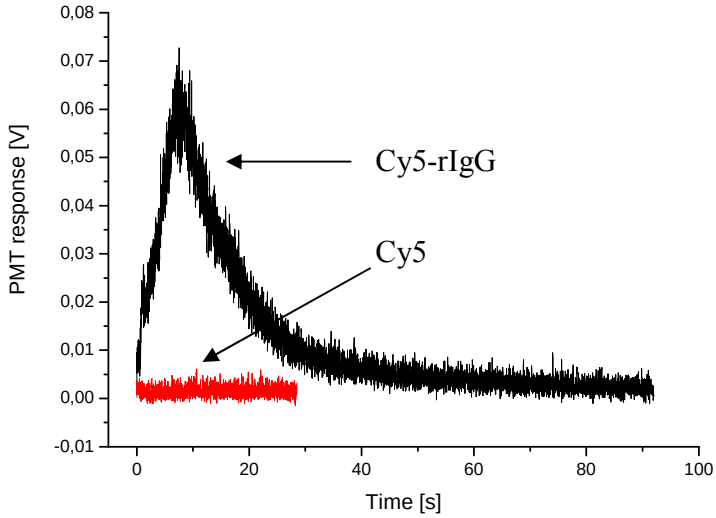

Figure 2.15: Comparing elution steps of an experiment performed in DEVICE 2 with a 1.5 µM sample of Cy5-labeled rIgG and one done with a 5 µM Cy5 only sample. Chamber length is approximately 800 µm. Incubation time is 200 seconds.

The absence of spurious peaks or high background signal indicates that leakage of sample from side channels was not a problem in this particular experiment. Both samples and

reagents followed flow paths through the chip as expected, with no undesired escape of sample into side branches of the network. However the type of result shown in Figure 2.16 was not always possible, making this device much less reliable than DEVICE 1. This lack of fluidic control must be prevented for improved liquid handling in view of implementing more complex assays. The advantage of the design is that it is possible to perform assays without channel clogging. This is because the channels utilized for sample and reagent delivery can be rinsed in between each step during the analysis.

2.3.4 Signal as a function of incubation time

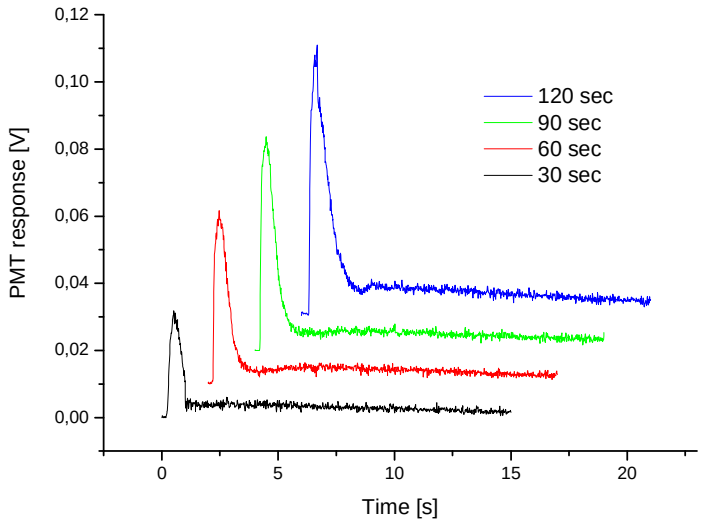

Figure 2.16: Elution peaks as a function of incubation time in DEVICE 1. [Cy5-rIgG] = 2.5 μM. All peaks appear at the same elution time. Traces are offset for the sake of clarity.

Since the incubation in these devices is carried out in a flowing stream, non-equilibrium conditions for binding prevail, and amount bound will depend on sample concentration and the amount of solution flushed over the surface of the picowell. In this case, the longer the incubation time for a particular sample, the more sites will be occupied and the higher the signal will be, as shown in Figure 2.16.

At some point, saturation of the PA sites will occur, corresponding to a maximum peak height. Figure 2.17 shows eluted peak area as a function of incubation time for a sample concentration of 2.5 μM in DEVICE 1. Similarly, for DEVICE 2, a 1.5-μM sample was used, and peak height was plotted as a function of incubation time (Figure 2.18). In both cases, peak area and peak height, respectively, begin to level off at about 150 s.

The binding of the Cy5-rIgG to the PA column may be described by

$$S + L \underset{k_2}{\overset{k_1}{\leftrightarrow}} SL \tag{2.4}$$

where S = binding site

L = ligand

SL = immuno-complex

The second-order differential equation describing this reaction is [56]

$$d[SL] / dt = k_1 [S][L] - k_2[SL] \tag{2.5}$$

where k_1 = association constant of rIgG and PA

k_2 = dissociation constant of rIgG and PA

[S] = concentration of available PA binding sites

[L] = concentration of ligand, here being Cy5-rIgG

[SL] = concentration of bound complex

t = total reaction time, here being the incubation time

The relation between [S]and [SL] is

$$[S] = S_0 - [SL] \tag{2.6}$$

where S_0 = initial number of available binding sites

The solution for the differential equation (2.5) is

$$[SL](t) = \frac{k_1[L]S_0}{k_1[L] + k_2}\left(1 - e^{-(k_1[L]+k_2)t}\right) \tag{2.7}$$

Literature sources confirm that the dissociation constant k_2 can be neglected[36, 57] which gives the final equation:

$$[SL](t) = S_0\left(1 - e^{-k_1[L]t}\right) \tag{2.8}$$

By fitting the data in Figure 2.17 using a function of this form, we obtained in DEVICE 1, for [Cy5-rIgG] = 2.5 μM, $k_1[L]$ = 0.00988 s^{-1} and S_0 = 0.0950 V·s, with an R^2 value of 0.945. This yields a forward rate constant k_1 = 3950 ± 700 $(M \cdot s)^{-1}$, which is in the range of biospecific adsorption rate constants for immunoaffinity chromatography, lying between 10^3 and 10^5 $(M \cdot s)^{-1}$ [36]. The deviation of data points from the curve arises as a result of the sample introduction channel not being reconditioned between experiments, since these measurements were performed in a serial manner.

For DEVICE 2, a binding rate constant of k = 7330 ± 1720 $(Ms)^{-1}$ and S_0 = 0.0842 V·s was found, with an R^2 value of 0.981, using the data in Figure 2.18 obtained for a [Cy5-rIgG] of 1.5 μM. The difference in k between the two devices is most likely due to the difference in flowrate applied during the incubation step.

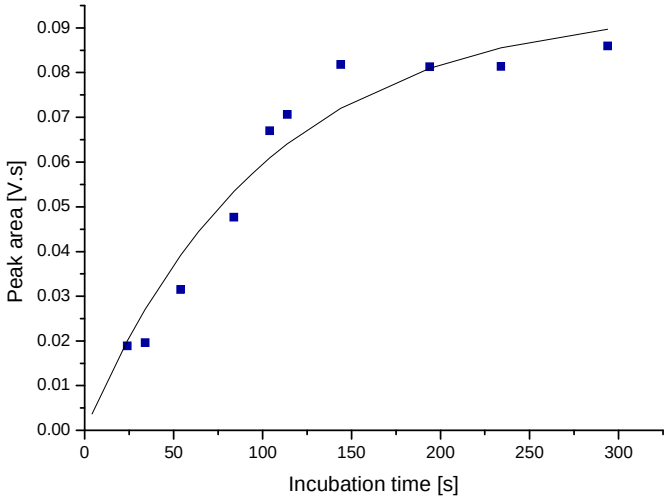

Figure 2.17: Eluted peak area in DEVICE 1 as a function of incubation time, with fitted curve. Chamber length is approximately 200 µm. [Cy5-rIgG] = 2.5 µM. Minimum total assay time = 2 minutes (for an incubation of 25 s)

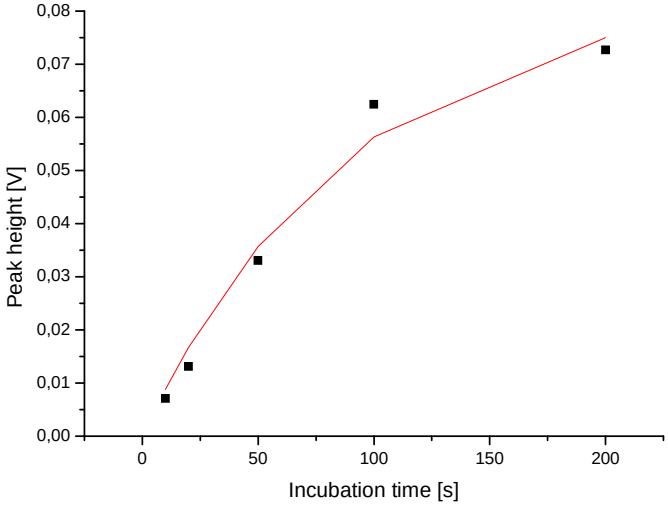

Figure 2.18: Peak height as a function of incubation time in DEVICE 2, with fitted curve. [Cy5-rIgG] = 1.5 µM. Chamber length is approximately 800 µm. Minimum total assay time = 2 minutes (for an incubation time of 10 s).

The variable S_0 yields an estimate of the number of binding sites initially available. The signal S_0 in Figure 2.17 (DEVICE 1) is given in Volts·second, which should be converted into a number of molecules. To calculate this, the conversion factor for fluorescence

signal in V to number of fluorescent molecules was first determined. The signal area due to a certain number of molecules passing the detector can be determined using the fluorescence recorded during incubation, since sample concentration, [L], and flowrate, f, are known. N, the number of molecules passing by the detector per second is given by:

$$N = N_A \cdot [L] \cdot f \qquad (2.9)$$

where N_A is Avogadro's number. In DEVICE 1, f = 0.593 nL/s and [L]= 2.5 μM, giving N = 8.9×10^8 molecules/s. Integrating the incubation signal over 1 second, an area of 0.015 V·s is obtained. Unit signal area is then 5.9×10^{10} molecules/V·s. Converting, then, S_0 obtained from a kinetic fit of the data is equivalent to 5.6×10^9 molecules of Cy5-rIgG. For comparison, the area under the peak obtained under saturation conditions, where full occupation of binding sites is assumed, was 0.0859 V·s, corresponding to 5.1×10^9 molecules. These values agree relatively well, though coverage is twice that predicted by assuming a monolayer of PA in the volume defining the picowell (see above). This could be due to PA immobilization extending slightly beyond the boundaries of the double-T intersection, as has already been described in Figure 2.8 (b), or to a denser layer of PA than assumed above. More experimentation is required to establish the direct correlation of S_0 with total number of available binding sites.

For DEVICE 2, the electric field applied during the incubation step was 1250 V/cm, giving a flowrate f = 4.36 nL/s. [L]= 1.5 μM, which gives N = 39.3×10^8 molecules/s. Integrating the incubation signal over 1 second, an area of 0.025 V·s is obtained. Unit signal area is then 15.7×10^{10} molecules/V·s. Converting, then, S_0 obtained from a kinetic fit of the data is equivalent to 13.2×10^9 molecules of Cy5-rIgG. The peak obtained

under saturation conditions, where full occupation of binding sites is assumed, was 0.117 V·s corresponding to 18.4×10^9 molecules. This is more molecules than in the chamber of DEVICE 1, which is to be expected since the chamber of DEVICE 2 is larger.

2.3.5 DEVICE 1: Dose-response curve

Figure 2.19 shows a dose-response curve for Cy5-rIgG binding to PA obtained in a DEVICE 1 chip. Incubation time in this case was 200 seconds, giving a total cycle time of 4 minutes and 45 seconds per point. The lowest concentration considered was 50 nM, which approaches desired clinical detection limits for IgG[33, 58] As implied in Figure 2.16, Figure 2.17 and Figure 2.18, longer incubation times could lower detection limits. This is because more sample would be delivered to the surface, concentrating analyte until enough molecules were bound to produce an adequate detector response.

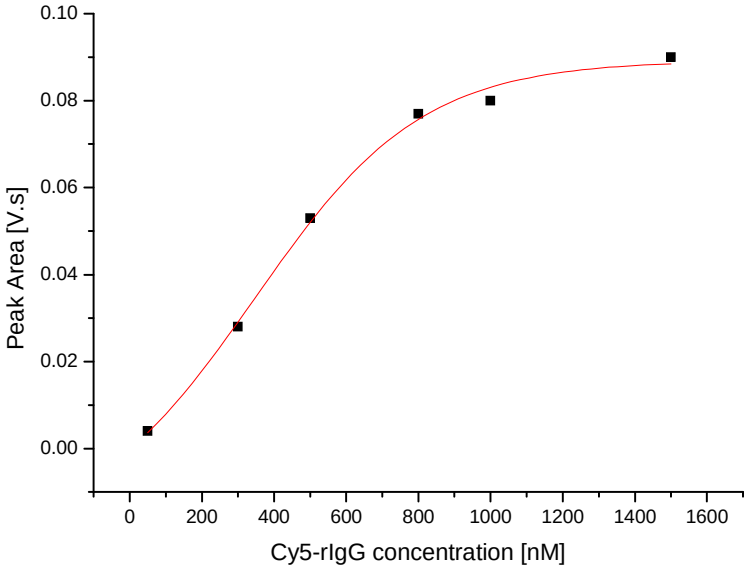

Figure 2.19: Signal as a function of [Cy5-rIgG]. Incubation time: 200 s, total cycle time: 4 min 45 s. Curve for sake of clarity.

In other words, the microfluidic device provides an approach which is not dependent on analyte concentration. This should provide for greatly increased flexibility in assay development, with greater scope of application as a result. In this mode of chip operation, a signal-to-noise ratio of 3 was obtained for a 50 nM concentration, giving the limit of detection characteristic for this device and incubation time.

2.3.6 DEVICE 1: Competitive assays

In conventional systems, competitive assays have to fulfill a sine qua non condition for obtaining results, namely, competition only takes place if the number of binding sites is smaller than the number of labeled and unlabeled molecules combined in the sample[33]. Here, the number of binding sites is fixed, but sample quantity can be chosen simply by varying incubation time.

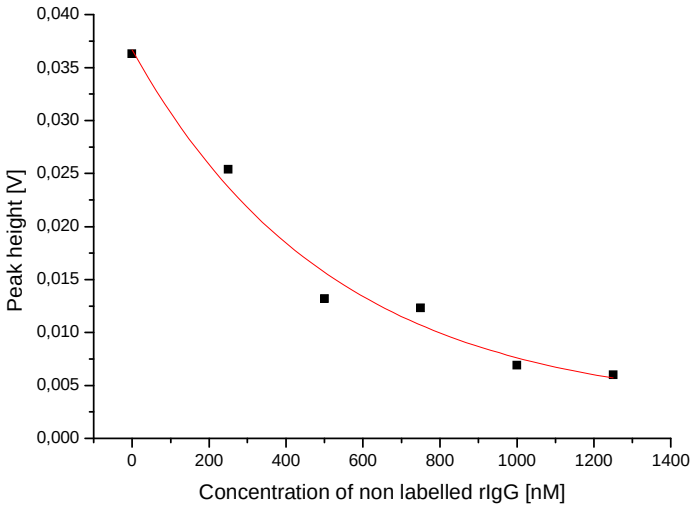

Figure 2.20: One-step competitive assay with [labeled rIgG] = 750 nM, 300-second incubation time, and a total cycle time of 7 min 35 s for each point. Curve for sake of clarity.

Two ways of performing a competitive assay based on binding between PA and rIgG are presented here, and could for example be used to distinguish between IgG subclasses.

The first and more conventional approach involves mixing a known amount of Cy5-rIgG with the unlabelled rIgG in the sample. When the concentration of non-labeled antibody changes, the signal due to the bound labeled species, or tracer, changes, and a dose-response curve can be obtained. This situation is illustrated in Figure 2.20, where eluted peak heights due to bound tracer are inversely related to the concentration of the unlabelled species.

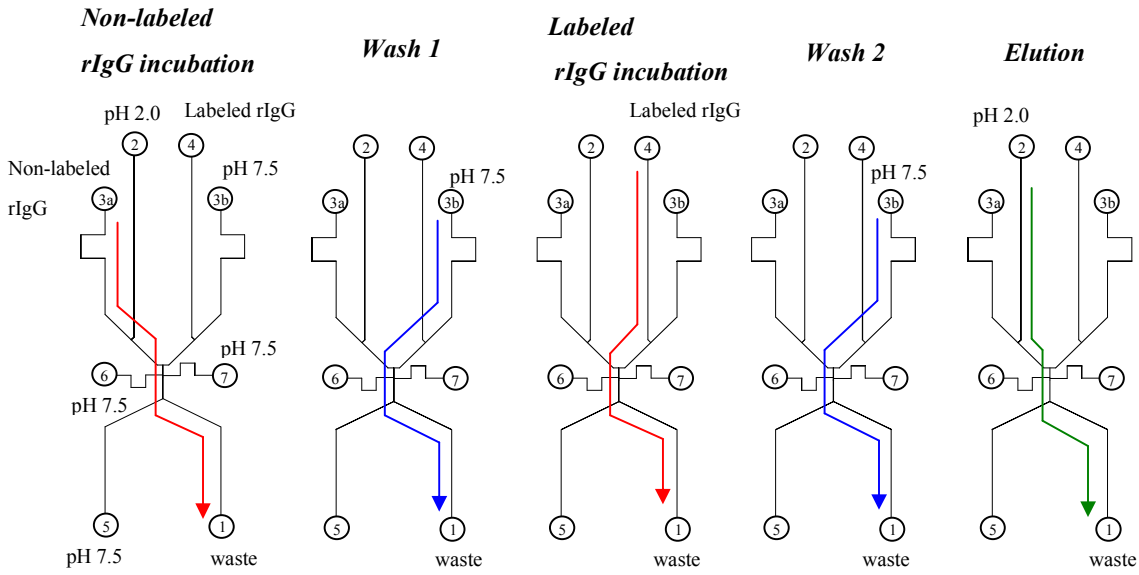

Figure 2.21: Operation sequence for two-step competitive immunoassay.

The second approach that this device affords involves the sequential incubation of unlabelled rIgG alone, followed by a mixture of labeled and unlabelled species. Theory shows that delayed addition of tracer to a competitive assay mixture, to allow the analyte to equilibrate with the binding molecules, increases the sensitivity of the measurement for a batch-type immunoassay[59]. Intuitively, this is to be expected, since the rate of formation of bound analyte-complex will slow down as the number of available binding sites decreases. If the surface sees only analyte initially while there are still abundant

binding sites remaining, more analyte will be bound per unit concentration than for the tracer later on. Sequential-addition, competitive immunoassays based on immunoaffinity chromatography have also been reported and the same considerations apply[36].

It was therefore of interest to see whether DEVICE 1 could be operated in a sequential addition format. The experiment was carried out using the operational procedure depicted in Figure 2.21. Note that there was no pinching of sample flow from the side channels in this case.

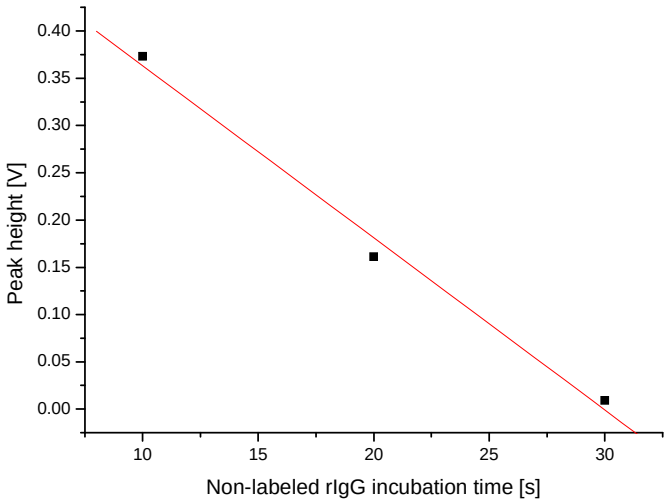

Figure 2.22: Sequential addition competitive assay. [Non-labeled rIgG] = 1.0 µM, [labeled rIgG] = 1.5 µM, with 2-min incubation time. Curve for sake of clarity.

The concentration of non-labeled antibody was set at 1.0 µM, and its incubation time was varied. This solution was incubated in a continuous-flow fashion first, followed by a wash step to remove excess unlabelled antibody and a subsequent 120 s incubation with 1.5 µM Cy5-rIgG. A dramatic decrease in eluted tracer concentration was observed for an initial rIgG incubation time of only 30 s, as shown in Figure 2.22. This is in sharp

contrast to the one-step competitive assay shown in Figure 2.20, where a greatly reduced tracer peak was obtained for 1.0 μM rIgG after 300 s. The difference is due to chip operation, since application of pinching voltages at 6 and 7 affect the electric field gradient between the sample reservoir and the picowell, decreasing it significantly. (The reduction may be estimated by modeling the microfluidic device as an electrical resistor network, and calculating the potential at the T junctions of the chamber[60]. Hence, the sample delivery rate is also much reduced in the pinching case, and sample is bound more slowly. Pinching also dilutes the sample stream somewhat, lowering effective sample concentration. This large difference in required incubation times resulting from pinched versus non-pinched modes of operation underlines the importance of chip design for optimized sample incubation. This experiment also demonstrated the flexibility of operation offered by this chip layout, by virtue of its multichannel network.

2.3.7 DEVICE 3: Sandwich assay

A three-layer, PA-rIgG-g-anti-rIgG sandwich assay was performed in DEVICE 3. In this assay, rIgG molecules tethered to the PA layer served as the probes for analysis of g-anti-rIgG in solution. Elution with pH 2.0 buffer resulted in the entire rIgG-g-anti-rIgG complex being released from the PA layer. To check the fluidic aspects of the assay, flow visualization was first performed in order to see the different fluids moving throughout the relatively complex fluidic network. Figure 2.23 shows fluorescence microscope images of electrokinetic solution flows into the chamber of DEVICE 3 during reagent addition or wash steps. An important aspect that can be seen in these images is that the flow paths for the rIgG and g-anti-rIgG incubation steps and the glycine/HCl elution step are not well superimposed. This means that the molecules bound to the substrate will not

all be eluted, resulting in fewer detected molecules. This problem can of course seriously affect the sensitivity of the assay.

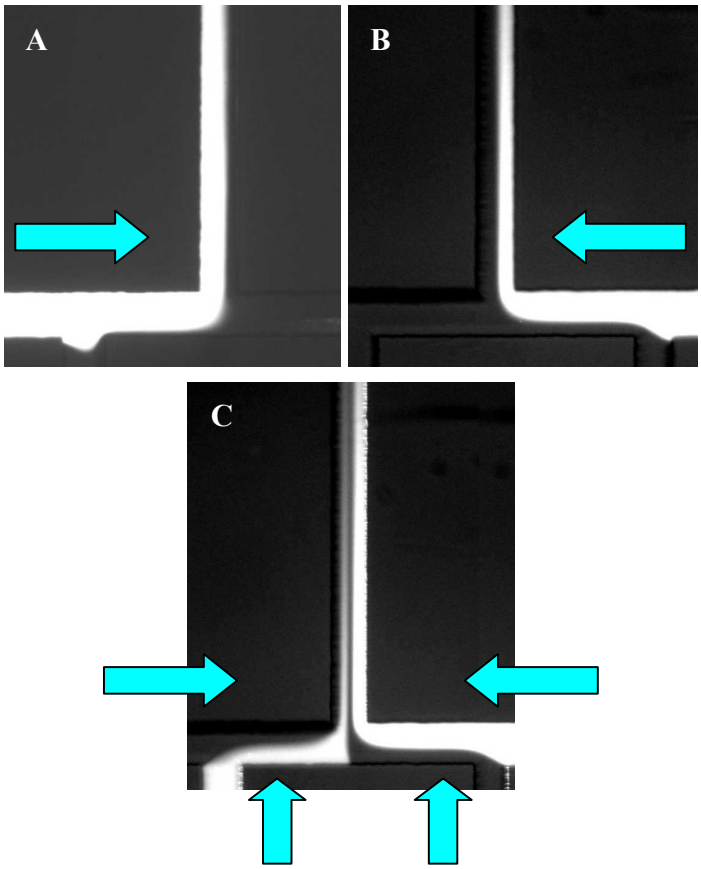

Figure 2.23: Flow control in the chamber. Arrows indicate flow. a) rIgG flow b) glycine elution c) four flows corresponding to washing sequence.

To be sure that binding occurs, images of the chamber of DEVICE 3 were taken during the last two sequences of a full cycle (Figure 2.24). After the incubation of g-anti-rIgG, followed by the cleaning sequence, there is a strong signal at the chamber surface, indicating bound sample (Figure 2.24A). The white lines show chamber boundaries. As mentioned earlier, because the flow paths are not superimposed properly over the whole width of the chamber, sample is bound only along half of the chamber width.

Introduction of glycine buffer results in zero signal (Figure 2.24B), because PA/rIgG bonds were broken and the bound IgG-anti-IgG complex was eluted from the chamber.

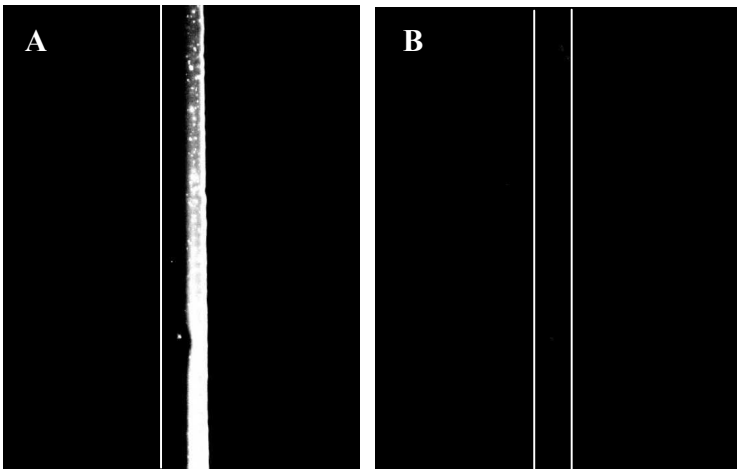

Figure 2.24: Chamber images in DEVICE 3 a) after incubation of 1 µM Cy5-labeled anti-rIgG sample and cleaning sequence b) after elution.

Figure 2.25 shows the elution peak recorded at the top of the chamber. The peak height obtained is very low. This is again due to design considerations and can be explained by the flow paths observed in Figure 2.23. In the case illustrated in Figure 2.23, the rIgG flow covers the whole chamber width but the elution flow does not. This means that the eluted sample will not contain all the bound sample, but only the sample in the path of the glycine/HCl buffer. In Figure 2.24, bound g-anti-rIgG is only present along half of the chamber width, meaning that the rIgG and g-anti-rIgG flow paths in this experiment only superimposed over half of the chamber. So, if the three rIgG, g-anti-rIgG and glycine/HCl flows are not well superimposed, a strong decrease in peak height can be expected. To avoid this, the design would have to be modified in order to optimize flow paths. Nevertheless, the presence of bound g-anti-rIgG in Figure 2.24 and the peak obtained in Figure 2.25 prove that it is possible to observe and quantify a three-layer

sandwich assay. To the best of our knowledge, this is the first-ever sandwich assay performed on chip.

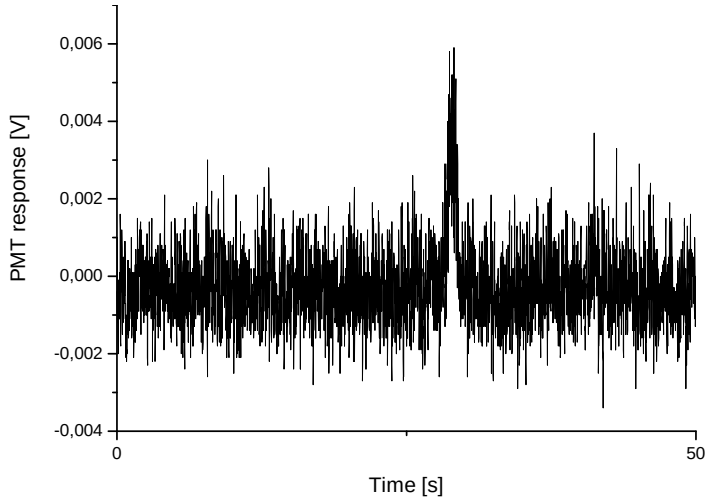

Figure 2.25: Peak obtained for the elution of 1 μM Cy5-labeled anti-rIgG flowing for 300 seconds over a layer of rIgG bound to PA.

2.4 Conclusions

Microfluidic platforms for automated heterogeneous immunoassay have been designed and characterized using an immobilized PA/rIgG affinity model. Since the assays were carried out in a flowing system, and therefore under non-equilibrium conditions, it was possible to benefit from shortened analysis times, generally less than 5 minutes. Optimization of incubation conditions through improved chip design has the potential to shorten this even further. It was also possible to run immunoaffinity chromatography-type competitive assays in both single and sequential addition modes. These assays are intrinsically flexible when done in fused silica capillaries, achieved by injecting well-defined volumes of the sample and reagents using an injection valve. In contrast, injected

volumes on chip are defined by the duration of voltage application, making the chips even more versatile, since no injection valve is required.

There are a multitude of applications where immobilized antibodies or other molecules exhibiting biospecificity are of interest. In particular, the combination of a modified picowell with CE should lead to highly selective and sensitive assays[9, 61]. Sample could be preconcentrated on the biomolecular layer before further analysis, improving attainable detection limits. There are many situations where not just one compound but several may be captured. Subsequent elution and separation would yield information not just about sample content, but would give a good indication as to affinity of a mixture of compounds for a particular antibody. Alternatively, mixed layers of immobilized antibodies could be applied, since the separation step would ensure resolution of captured species. Clearly, this has implications for the development of fast screening and/or multi-analyte assays. The use of antibodies immobilized directly onto fused silica capillaries for so-called immunoaffinity CE has been reported[61, 62]. This is, however, the first time, to the best of our knowledge, that microfluidic chips using locally immobilized biospecific layers and operated electrokinetically have been reported.

3 TEMPERATURE CONTROL IN MICROFLUIDIC SYSTEMS

This chapter is adapted from:

Chemical Reactions for Integrated Temperature Control in Microfluidic devices

A. Dodge, R.M Guijt, G.W.K. van Dedem, N.F. de Rooij, E. Verpoorte, Lab on a Chip, 3, pp. 1-4, 2003.

Thermal Dehybridization of Surface-Bound DNA in a Microfluidic Device for Nucleic Acid Analysis

A. Dodge, G. Turcatti, I. Lawrence, N.F. de Rooij, E. Verpoorte, Submitted to Analytical Chemistry.

Integrated temperature control system for microfluidic devices

A. Dodge, R.M Guijt, G.W.K. van Dedem, N.F. de Rooij, E. Verpoorte, Presented at the μTAS '2002 Conference, Nara, Japan, Proceedings pp. 617-619, Nov. 1-5, 2002.

Development of a microfluidic device for genetic analysis based on hybridization of surface-bound DNA

A. Dodge, G. Turcatti, P. Mayer, N.F. de Rooij, E. Verpoorte, Presented at the SmallTalk2002 Conference, San Diego, CA, USA, Jul. 28-31, 2002.

Microfluidic devices are a promising new tool for studying and optimizing (bio)chemical reactions and analyses. Many (bio-)chemical reactions require accurate temperature control, such as PCR, described in Chapter 1. PCR thermal cycling times are strongly reduced in a microsystem. It is also possible to thermostat a microchamber to enhance a chemical reaction[29] or to decrease non-specific binding of analytes at modified surfaces[22]. An example of the latter is the hybridization of oligonucleotides to surface-bound probes at slightly elevated temperatures, which improves the stringency of the reaction (fewer basepair mismatches). Surface chemistry combined with heat can be a powerful tool for certain types of biochemical analyses. A good example was recently reported, where single nucleotide polymorphism (SNP) analysis was performed by thermal dehybridization of surface-bound oligomers[63, 64]. The temperatures at which oligomers dehybridized were lower for sequences containing a SNP than for fully hybridized strands. Another technique which is growing in importance is the amplification of DNA when it is bound to a surface and no longer in solution[20, 21]. This allows the formation of random arrays of DNA colonies, which can then be sequenced in situ using a "sequencing by synthesis" technique[20, 21]. This also requires surface chemistry combined with precise temperature control.

Here, two different methods for controlling temperature are presented. The first is a classic resistive layer approach using the Joule effect to heat a microdevice. This resistive heating device is used in Chapter 4 to perform a temperature-dependent solid-phase DNA analysis. The second approach is a new, integrated temperature-control system for microfluidic devices, using endothermic and exothermic chemical and physical processes to locally control temperature. Also, a novel non-invasive technique is used to calibrate

temperature inside the microchannels embedded in both types of device, using molecular beacons as temperature sensors.

3.1 Introduction

3.1.1 Heating and cooling in microdevices

Since the introduction of the miniaturized total chemical analysis system (μTAS) concept in 1990[65], the development of so-called 'lab-on-chip' devices has been an area of exponential growth. Miniaturization of chemical systems allows faster chemical reactions, due to reduced diffusion-driven transport times, and faster and more efficient separations. Working on a small scale reduces the risks involved in manipulation of explosive and unstable mixtures required for chemical reactions. Additionally, working with a microchip format dramatically reduces the consumption of sample and reagents, and allows the performance of multiple analyses in parallel, thereby lowering the price per analysis. Large surface-to-volume ratios also make better thermal control possible. Heating and cooling of small liquid volumes can be accomplished in much shorter periods of time. The small thermal mass of the chips themselves also contributes to increased heating and cooling rates.

Enhanced heat transfer introduces the potential for improved control of chemical process conditions in microreactors. Certainly, the excessive heat build-up which often leads to runaway reactions in conventional reactors can be avoided[66]. Precise temperature control is also required in certain (bio)chemical reactions, such as DNA amplification using the polymerase chain reaction (PCR)[67], and the investigation of reaction kinetics. PCR is a biochemical reaction requiring rapid and precise thermocycling of reagents at

three different temperatures between 50°C and 100°C. The potential of faster temperature ramping and more precise temperature control has been the impetus for the integration of PCR into microfabricated devices. The earliest examples of this development were presented by Northrup *et al.* in 1993[68]and Wilding *et al.* in 1994[69]. More recently, efforts in a number of groups have resulted in several examples of PCR on chip. The techniques used for thermocycling on a chip can be divided into different subgroups as described in Table 3.1.

External non integrated components		**Integrated systems**
Contact	**Contactless**	
Peltier element (heat/cool) Clamped[69] Glued[70]	Infrared light (heat) [25]	Resistive layer (heat) [68, 71, 72]
Contact with copper block (thermostatting) [73]	Convection by blowing air (cool) [25, 71, 74]	Micropeltier (heat/cool) [75]
Induction activated heater (heat) [76]		Flowing a cold fluid inside a microchannel (cool) [77, 78]
Thermoresistive tape (heat) [74]		

Table 3.1: Classification of temperature control methods

In the devices described in references (25, 69, 70, 73, 74, 76), thermal control was implemented using bulky external components, whereas in references (68, 71, 72), heating elements were incorporated in the device through integration of resistive layers heated by the Joule effect. In reference (71), temperature control of exothermic reactions in micromachined chemical reactors using integrated heaters in microreaction chambers

was presented. Another example describes a battery-powered device which heats by using induction. An oscillating current, created in a primary piloting copper coil surrounding a ferrite core, induces a current in a cylindrical resistive heater[76]. Until now, cooling of microfluidic devices has only been done with external components or by convection. It has been achieved by clamping[69] or gluing[70] the microfuidic device to an external Peltier element, or by contacting the microdevice with a copper block, passively cooled by contact with cooling fins[73]. The convection technique primarily consists of using the heat exchange between the device and ambient air, an effect which may be enhanced by blowing compressed air or nitrogen gas over the microdevice[25, 71, 74]. Only two integrated cooling techniques have been presented, neither of them for microfluidic devices but for microelectronics. In one case, an integrated cooling system utilizing a microchannel in a printed circuit board (PCB) was described. Either water or methoxy-nonafluorobutane were used as coolants and pumped through the microchannel, removing heat from the electronics[77]. The heat was dissipated in a heat exchanger, positioned elsewhere on the PCB. A comparable system using microfluidics in combination with a heat exchanger for cooling electronics has been described elsewhere[78]. In the second case, integrated cooling of microelectronic devices took the form of the "fridge-on-a-chip"[75]. Here, microPeltier elements were integrated during the microfabrication process on the back of microelectronic devices.

Most of the cooling systems described above require external and often bulky components, hereby limiting the possibilities of integration in a microfluidic device. Even the microfluidic cooling system integrated on the PCB[77] required a heat exchanger elsewhere on the device, complicating the microfabrication process and increasing the

footprint of the device and fabrication costs. Similarly, heating small volumes on-chip involves the use of external elements, or additional fabrication steps for integration of heating elements.

Here, two different methods for controlling temperature are presented. The first is a resistive-layer approach using the Joule effect to heat a microdevice, similar to references (68, 71, 72). By regulating the voltage applied to the resistive layer, one can control the current flowing through it, and therefore the heat it creates. By measuring the temperature at the surface of the resistive heater (RH) and using it as a feedback signal, it is possible to precisely regulate the temperature of the device. The resistive layer used in this work is an indium-tin-oxide (ITO) layer. This material was chosen because it is transparent, making optical detection inside a treated microchannel possible through this layer. The use of ITO is novel, as most integrated resistive heaters to date have been based on platinum or other metals. The use of ITO was described by Daridon *et al.*[29] for performing chip-based flow injection analysis, using absorption as a detection method to detect an on-chip chemical reaction. In that case, temperature was kept constant to enhance a chemical reaction, whereas in our case, temperature can be varied and regulated using a home-made electronic circuit and appropriate control software.

The second approach for chip-based temperature modification presented here is quite different, as it is based on the exploitation of endothermic or exothermic chemical or physical processes in microchannels to respectively cool or heat solutions in an adjacent microchannel. The temperature control channels (TCCs) are directly integrated in the chip at the same time that the microfluidics are fabricated by simple single-level microfabrication. Localization of the cooling or heating effect is controlled by positioning

the endothermic or exothermic, physical or chemical process (EEPCP) at the reactant flow interface.

3.1.2 Molecular beacons: a novel way of performing temperature calibration

During a temperature-dependent event happening within a microdevice, the temperature of interest which should be monitored is the one located inside the microfabricated reactor. Different direct measurement techniques, involving insertion of a thermocouple directly inside a microchamber[70, 74], have been reported. However, the presence of a foreign body in the small cavity could affect temperature uniformity or inhibit certain types of biochemical reactions. A different approach was to measure temperature on the outside of a device, either by using a commercially available sensor taped to the device[29], or by integrating platinum resistors onto the device to act as temperature sensors[71, 72]. A non-invasive method was also developed using backscatter interferometry[79]. Alternatively, the use of thermochromic liquid crystals has been reported[80]. In general, precise temperature calibration in a microdevice is not a trivial problem. Moreover, it has not been a popular research topic, with most of the few published references considering this issue cited here. Most of the solutions reported to date use sensors put directly into contact with the fluid to be heated. This contribution proposes a novel, non-invasive way of calibrating temperature inside a microchannel using molecular beacons as temperature probes. Molecular beacons are molecules that have recently been developed in order to recognize and report the presence of specific nucleic acid sequences[81-86]. They possess a hairpin-loop structure, with the hairpin consisting of a DNA double strand, with a fluorophore attached to the end of one strand and a molecule acting as a so-called “quencher” to the other. When the hairpin is closed

(i.e. the DNA is hybridized in this portion of the molecule), the fluorophore and the quencher are close together, quenching possible fluorescence.

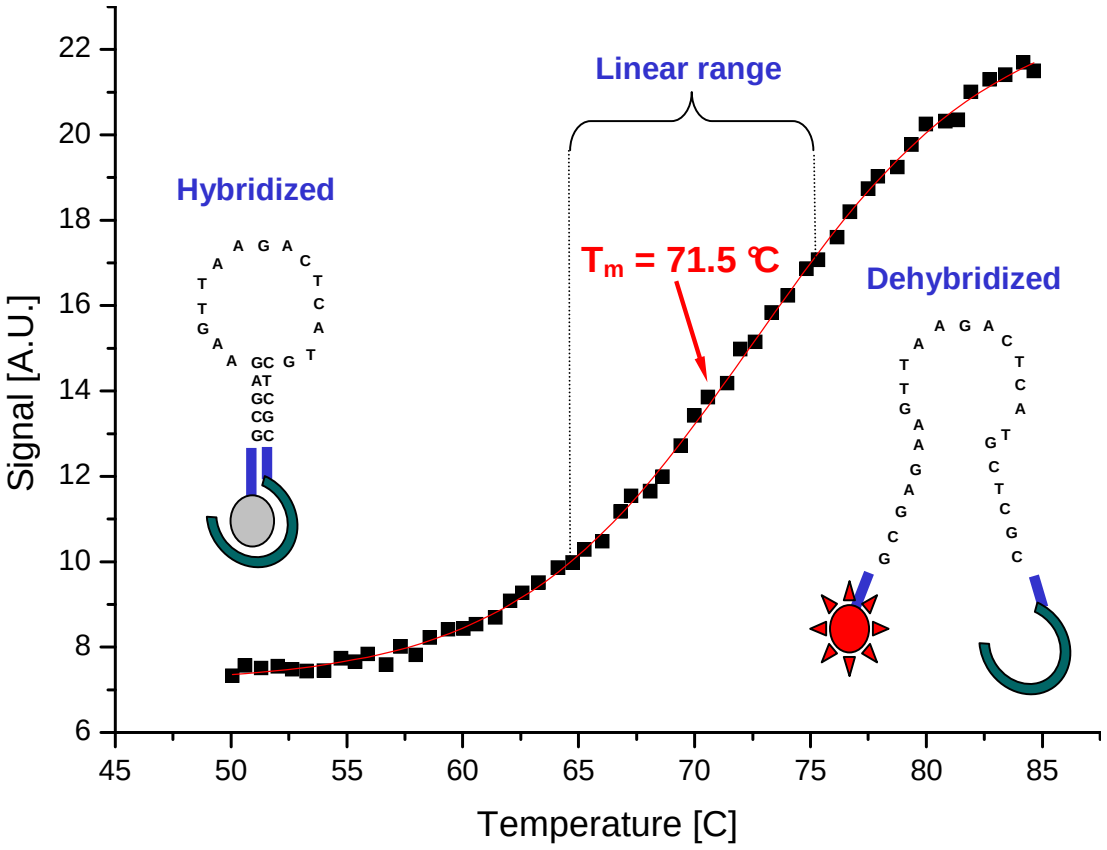

Figure 3.1: Melting curve for a molecular beacon. Signal increases as the beacon's double strand denatures to release the fluorophore from the quencher at higher temperatures. Beacon used here is a Cy5-Black Hole Quencher (Cy5-BHQ3) beacon (vide infra).

The loop consists of a single strand that can hybridize to a complementary target. If hybridization occurs, its force is strong enough to straighten the loop, which leads to breaking of the hairpin's double-stranded structure. The fluorophore spatially separates from the quencher as a result, making it possible to detect fluorescence upon excitation[81-86].

Another way of separating the double strand is to bring it to its melting temperature (T_m)[81-84]. The T_m of the beacon's double strand depends on its length and composition, and is very specific. When temperature is slowly increased, the double-strand denatures progressively, and fluorescence increases as the fluorescent moiety is released from the quencher (Figure 3.1). By ramping up the temperature and measuring fluorescence, one obtains a melting curve from which it is possible to extract the T_m of a beacon, as seen in Figure 3.1. T_m is defined as the inflexion point of the fitted curve.

The method for controlling temperature inside the RH device was performed using an ITO resistive heater on the bottom surface of the prototype and measuring temperature via a sensor glued to the ITO surface. As this was an indirect means of monitoring temperature inside the microchannels, it was possible that the actual temperature inside a chamber of the device differed from the externally measured temperature, as observed by Yamamoto *et al.* [87]. Thermal calibration of the system thus becomes necessary. This was performed by measuring the melting curve of a molecular beacon in a chip, and comparing the linear range of this curve with one measured in a conventional system. Simulations were carried out to confirm the hypotheses necessary to extrapolate real temperatures inside chambers from temperature data obtained using the external temperature sensor and the molecular beacon melting curves.

3.2 Experimental

3.2.1 RH chip fabrication

A schematic of the RH device with its cross-section can be seen in Figure 3.2. Each reactor chamber consisted of a 2-cm-long straight channel, having widths of 500 or 1000

µm, and etched to depths of 10 or 20 µm, respectively, in a 500-µm-thick, 10-cm-diameter Pyrex 7740 wafer. The reason for having such large channels was to have a large detection surface for heterogeneous assays. It was found that optical detection was best performed through an unstructured, 200-µm-thick glass substrate when working with an inverted fluorescence microscope. Therefore, the bottom plate of the device, through which detection was performed, had to be transparent and could not have fluidic channels etched into it. Hence, the chambers were etched into the top coverplate. The coverplate, which had predrilled access holes, required a non-standard photolithography as a result. It was not possible, for instance, to create a uniform layer of photoresist on this wafer using a standard spin-coating process, due to the access holes. First, a 400-nm-thick layer of polysilicon was deposited by low-pressure chemical vapour deposition in a furnace at 570°C for 1 hour.

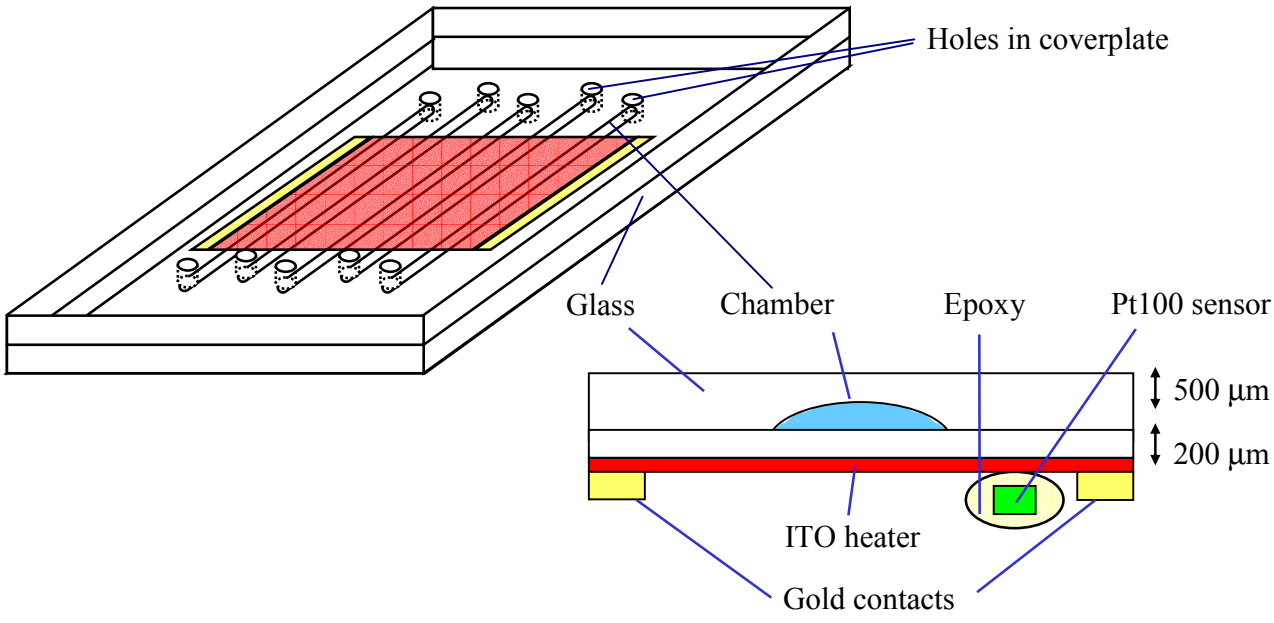

Figure 3.2: Resistive layer device with cross-sectional view

The surface was then coated with hexamethyldisilazane (HMDS) (Laporte Electronics, Riddings, U.K.) by exposure to HMDS vapour, in order to increase adhesion of the photoresist. A 3:2 mixture of AZ4562 photoresist (Clariant GmbH, Switzerland)/propylene glycol methyl ether acetate (PGMEA) solvent (Aldrich, Switzerland) was sprayed, rather than spin-coated, onto the substrate to obtain a 6-µm-thick photoresist layer.

The resist layer was prebaked at 85°C for 35 min in an oven, exposed, developed and finally postbaked at 125°C for 30 min, again in an oven. Pattern transfer and microchannel fabrication was performed as described previously [88]. The coverplate containing the access holes and the channels was sealed by fusion bonding to a 200-µm-thick Pyrex 7740 wafer. The integrated heater consisted of a transparent, 50-nm-thick ITO layer sputtered onto the bottom wafer, as previously reported (Kroll Thin Film Technologies, Neuchâtel, Switzerland) [29, 89]. Strips of 50-nm-thick chromium topped off by 150-nm-thick gold were evaporated along the sides of the ITO layer as electrical contacts, in order to obtain a uniform electric field throughout the resistive heater. Scotch™ tape was used as a mask to spatially define the heater during deposition of the different resistive layers onto the device. A Pt100 platinum sensor (Minco, Aston, France) was glued with thermally conductive, electrically insulating H70E EPO-TEK epoxy (Epoxy Technology, Polyscience AG, Cham, Switzerland) cured at 100°C in an oven, to measure the temperature at the ITO surface

3.2.2 Concept for EEPCP temperature control

Under the usual operating conditions for microfluidic devices, fluid flows are laminar. That is, the velocity at any one point in a channel is predictable and unchanging, and streamlines are well-defined. When two fluids coming from two different reactant channels (RC) are merged together into a single microfluidic channel (Figure 3.3), they generally follow laminar streamlines and flow side-by-side. The stream from RC_2 flows along the side of the TCC closest to the central channel (Figure 3.4). The relative widths of the fluid flows are determined by the flowrate ratio. At the interface, chemical reactions or physical processes can occur. In the examples presented here, two-reagent reactions were used.

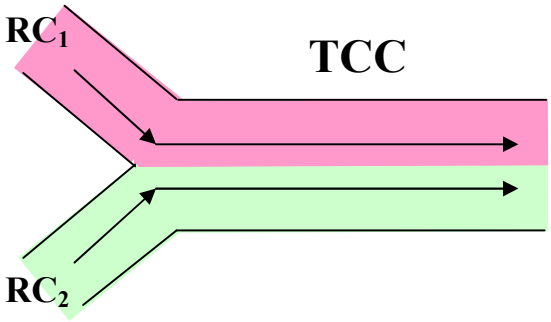

Figure 3.3: Two RC channels merging into a TCC channel.

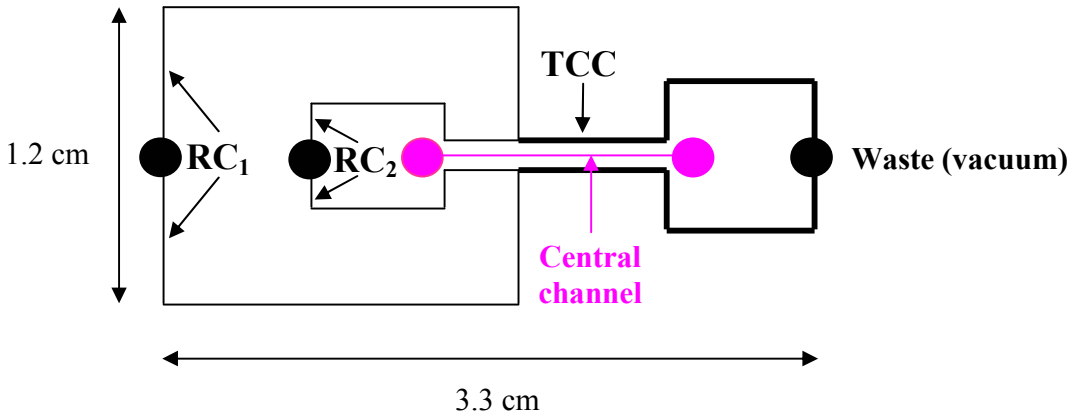

Figure 3.4: Layout of the device. Distance between the central channel and TCC: 30 µm. Channel depths are 19 µm, TCC width is 108 µm and RC widths are 54 µm.

For cooling, the evaporation of acetone was used as an endothermic reaction. In the TCC, air flows from RC_1 alongside acetone from RC_2, cooling down the central channel. For heating, the violently exothermic dissolution of concentrated H_2SO_4 in water was used, with water in RC_1 and H_2SO_4 in RC_2.

A microfluidic structure (layout in Figure 3.4) was etched into a glass substrate using the techniques described in the Introduction and Chapter 2. For cooling experiments, a closed microchannel system was formed by reversible bonding of the glass substrate with poly(dimethylsiloxane) (PDMS). For all heating experiments and some cooling experiments, thermally bonded glass-glass devices were used. Vacuum applied at the end of the TCC was used to draw in the reagents from RC_1 and RC_2 into the TCC, initializing the chemical reaction and thus inducing the thermal effect. TCCs were integrated along both sides of the central channel to obtain a symmetric temperature effect.

3.2.3 Instrumentation

A homemade electronic circuit hooked up to a Hewlett Packard power supply regulates the current flowing through the resistive ITO layer via a National Instruments (Austin, Texas, USA) DAQPad-6020 data acquisition board controlled by Labview^{TM} PID software. A temperature control precision of ± 0.5 °C was obtained with increasing temperature ramps of 10°C/sec. Fluorescence images were taken with a CF 8/4 DXC black-and-white CCD camera (Kappa, Gleichen, Germany) mounted on an Axiovert S 100 fluorescence microscope equipped with a DC halogen lamp and a dichroic mirror set for Cy5 (excitation wavelength bandpass at 546 nm, dichroic mirror reflecting below 580 nm and transmitting above 590 nm) (Zeiss, Feldbach, Switzerland). Images were pixel-processed with Lispix freeware to obtain quantitative intensity data.

Experimental denaturation curves (melting curves) in solution assays for fluorescent beacons were generated in a Jasco FP 750 spectrofluorometer equipped with a temperature controller and stirring unit (Jasco ETC-272T). Excitation and emission wavelengths were fixed at 620 nm and 660 nm for Cy5. Oligonucleotides, diluted to a final concentration of 200 nM in 100 mM Tris-HCl buffer containing 1 mM $MgCl_2$ (pH 7.8), were introduced into a 0.5 × 1.0 cm quartz cuvette (Hellma). Samples were stirred continuously with a magnetic bar during the measurements.

3.2.4 Reagents

100 mM Tris/HCl buffer containing 1 mM $MgCl_2$ (pH 8.0). was made from tris(hydroxymethyl)aminomethane (Tris) (Fluka Chemicals, Buchs, Switzerland) and $MgCl_2$ powder (Merck, Buchs, Switzerland) diluted in doubly-distilled deionized (DI) water. 97% H_2SO_4 was purchased from Merck, Buchs, Switzerland. Electronic-grade ethanol, acetone and 1M HCl was purchased from Laporte Electronics, Riddings, U.K. Cy5-Black Hole Quencher 3 (Cy5-BHQ3) beacon was purchased from Biosearch Tech (USA). Tetramethylrhodamine-Dabcyl (TAMRA-Dabcyl) beacon was purchased from Eurogentec, Belgium. 5 μM beacon solutions were prepared in the Tris buffer described above.

3.2.5 Temperature calibration in the RH device

As described in the introduction of this section, a non-invasive method was used to calibrate the internal temperature as a function of the externally applied temperature, using molecular beacons as temperature sensing compounds. The melting temperature T_m of the beacon double strand depends on its length and composition, and is very specific.

Molecular beacons with different T_m's are available. The one chosen here to calibrate temperature was a Cy5-BHQ3 beacon. Temperature calibration was performed by measuring the melting curve of the molecular beacon. This measurement was first performed in a conventional spectrofluorometer equipped with a temperature controller and stirring unit, using a 200-nM beacon solution prepared in 100 mM Tris-HCl (pH 7.8) containing 1 mM $MgCl_2$. Fluorescence was measured as the fluorescent moiety was released from the quencher. A beacon sample at a concentration of 5 μM in a 100-mM Tris/HCl buffer containing 1 mM $MgCl_2$ (pH 8.0) was then introduced in the device, and temperature was increased by heating with the ITO layer. Temperature was regulated by measuring temperature with the Pt100 sensor glued to the surface of the ITO layer. Images were taken using an inverted fluorescence microscope and a digital camera. Pixel processing of the images enabled generation of quantitative data, allowing calculation of the effect of temperature on fluorescence intensity. The resulting curve is sigmoidal in shape, with the T_m being defined by the inflexion point of the fitted curve using Origin™ software. The melting curve possesses a linear range, as seen in Figure 3.1. The data in the linear range of beacon response obtained with external temperature measurement was compared to that obtained in the conventional system to correct for differences in internal versus applied temperature.

Simulations were performed with CFD-ACE™ software (CFD Research Corp., Huntsville, AL) in order to confirm the relationship between externally measured and actual temperatures inside the microchambers.

3.2.6 Temperature calibration in the EEPCP device

To estimate the temperature changes achieved in the central channel, a different fluorescence-based calibration method was used. In this case a temperature-sensitive compound acting as an optical thermometer over a large range of temperatures was needed. The fluorescent compound chosen was rhodamine B. The fluorescence of rhodamine B strongly depends on temperature, with fluorescence decreasing as a function of increasing temperature[90-93]. A calibration plot was made in the glass device by filling the central channel with this thermo-sensitive fluorescent dye and ramping temperature up while acquiring fluorescence data. These measurements were done in a manner similar to the molecular-beacon melting curve measurements. Temperature was ramped by applying voltage to an ITO layer deposited onto the bottom of the EEPCP device using the RH setup (Section 3.2.3). Images were taken using an inverted fluorescence microscope and a digital camera. Pixel processing of the images enabled generation of quantitative data, allowing calculation of the effect of temperature on fluorescence intensity. This calibration curve was obtained by measuring fluorescence as a function of the temperature of the ITO layer, which was not the same as inside the microchannel containing the dye. The temperature axis of this curve was corrected using the molecular beacon technique.

3.3 Results

3.3.1 Temperature calibration

The internal temperature inside the RH device needed to be calibrated as a function of the externally applied temperature at the ITO layer, to ensure optimum DNA hybridization-

dehybridization conditions (Chapter 4). This was done by recording the fluorescence-versus-temperature melting curves for the Cy5-BHQ3 beacon in both conventional (reference) and RH device systems. The T_m of the beacon was always determined using melting curves normalized to the maximum value of fluorescence recorded. The beacon yielded a T_m of 72.6°C ± 0.4°C (n=3) in the conventional system versus 55.3°C ± 0.3°C (n=3) for the RH chip, which gives an apparent temperature shift, ΔT, of 17.3 °C. The melting curves are presented in Figure 3.5.

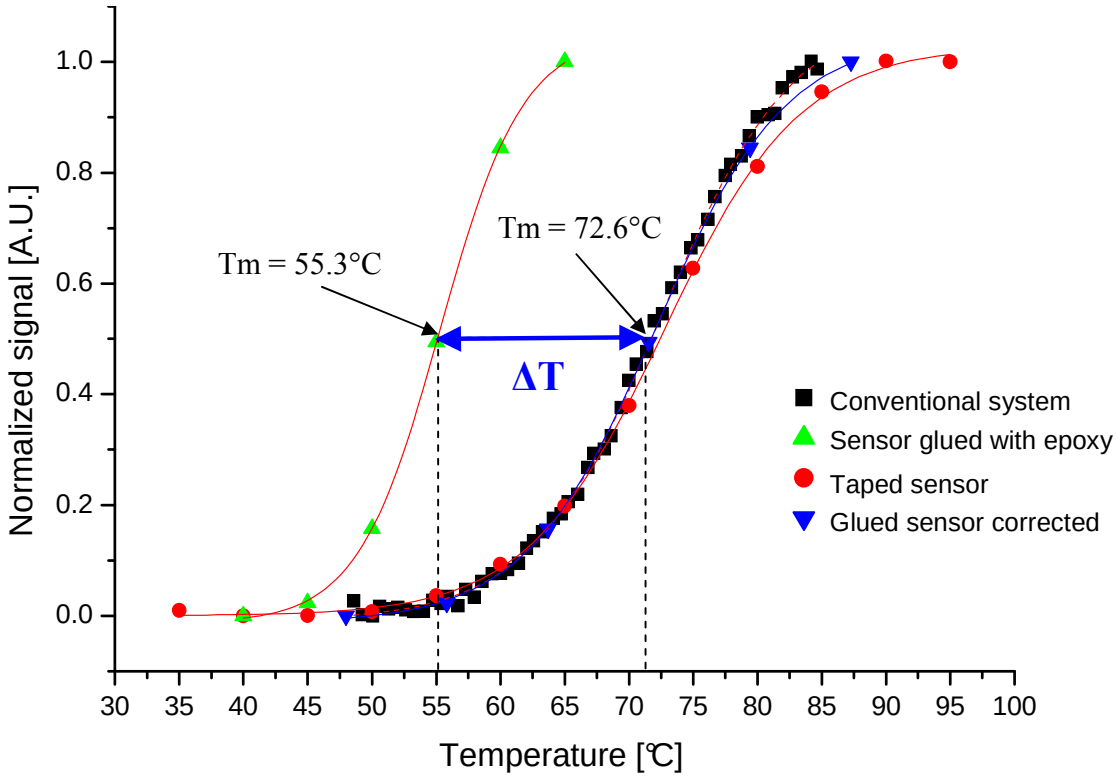

Figure 3.5: Different normalized melting curves for the Cy5-BHQ3 beacon. Curves corresponding to the conventional T_m determination method, taped-sensor method and extrapolated glued-sensor method match well. Beacon concentration: 5 µM in 100 mM Tris/HCl buffer containing 1 mM $MgCl_2$ (pH 8.0) for all measurements.

The measurements indicated by the squares (■) correspond to signal measured in a conventional system, while the triangles (▲) represent the measurements performed with

the microdevice. The two curves are very similar in shape, regardless of the strong shift along the temperature axis. One can assume that the curve measured in a conventional system is a reliable reference, since the instrument was well thermostatted, and temperature was measured directly in the beacon solution by immersing a thermocouple into the cuvette.

Hence, the measured external temperature applied at the ITO layer is clearly lower than the actual temperature inside the microchannel. This is somewhat surprising, as generally more heat must be applied than needed in a reaction volume alone, due to losses by dissipation and the additional thermal mass of system components. Pt100 sensor functionality was verified by dipping it in boiling water to see if it gave the expected readout. As this was the case, it was concluded that this sensor was properly calibrated. After some consideration, the problem was pinpointed to the epoxy used to glue the Pt100 sensor to the ITO heating layer. This epoxy, though touted to be heat-conductive (thermal conductivity of 1.4 W/mK), did not provide an adequate contact to the ITO layer. This was demonstrated by means of a control experiment, in which the Pt100 sensor was simply attached to the ITO heating layer using common Scotch^{TM} tape. The resulting melting curve obtained in the microchannel is given in Figure 3.5 (circles). Clearly, this curve is in better agreement with the melting curve determined conventionally than the curve measured initially with the glued sensor. The temperatures recorded by the Pt100 sensor when taped to the ITO layer are shifted to somewhat higher values with respect to the reference curve. However, this is to be expected, since heat transfer from the ITO layer to the microchannel will not be 100% efficient, and some extra heat is required to achieve the desired internal temperature (as discussed above).

As much of the data collected in this study was obtained using the Pt100 sensor embedded in epoxy (Chapter 4), it was desirable to calibrate the internal temperature of the system for these conditions. This required the establishment of a reliable relationship between the temperature measured with the Pt100 sensor in epoxy, T_{ext}, and actual temperature inside the channel, T_{act}. To do this, the linear regions of the Cy5-BHQ3 melting curves obtained in conventional and microchip systems were compared. The differences in actual versus external temperature, ΔT ($=T_{act}-T_{ext}$), were calculated for each normalized fluorescence value that fell within the linear regions of both curves. (The difference in T_m was measured in the same way (Figure 3.5).)

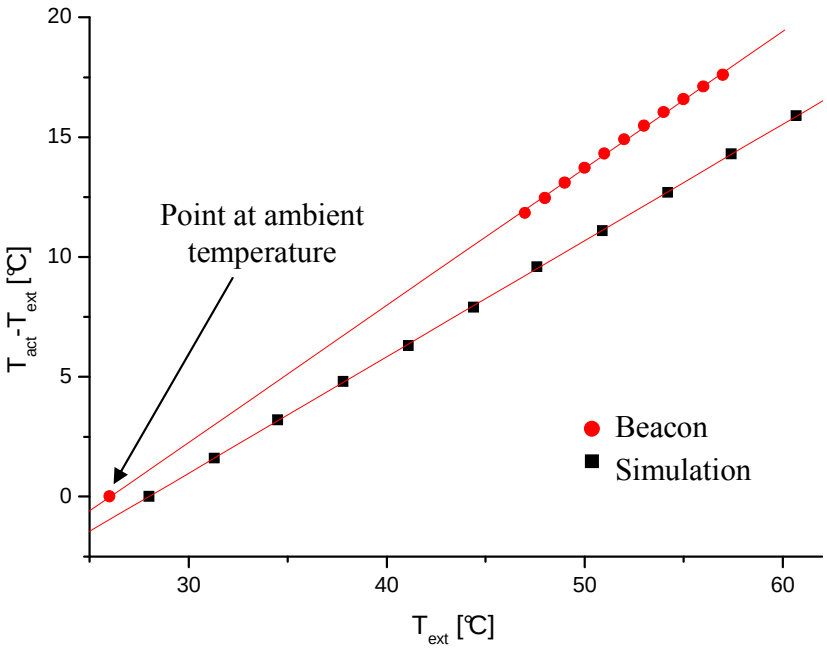

Figure 3.6: Difference in temperature, ΔT, between actual temperature inside the microchannel (T_{act}) and external temperature measured using the epoxy-embedded Pt100 sensor (T_{ext}), plotted as a function of T_{ext}. Plots calculated from experimental (●) and simulated (■) data are given. For the "beacon" curve, ΔT was calculated from the linear regions of the Cy5-BHQ3 melting curves obtained in conventional and microchip systems, as explained in the text. The experimental and simulated ΔT curves were both linear. Thus, a reliable model exists for extracting T_{act} inside a microchannel from T_{ext}, measured with the Pt100 sensor.

For the microchip curve, the linear region extended between 47 and 57 °C. In the conventional case, the linear region fell in the range 60 °C to 75 °C. The ΔT values were then plotted as a function of T_{ext}, as shown in Figure 3.6 (circles). This plot is linear, and indicates that ΔT in fact increases with increasing applied external temperature. Moreover, ΔT is 0 at around 26 °C, which will have been close to room temperature (actual room temperature on the day of the experiment is not available).

To confirm the validity of the calibration plot of ΔT ($=T_{act}-T_{ext}$) as a function of T_{ext}, simulations were performed with CFD-ACE™ software, using a model system with the geometry shown in Figure 3.7. This represents a block of the RH device composed of:

1) A microchannel segment machined in Pyrex
2) An ITO layer deposited onto the lower Pyrex surface
3) Epoxy over the ITO layer
4) A Pt100 block embedded in epoxy.

The characteristics of the different materials involved in the simulation are given in Table 3.2.

	Pyrex	Epoxy	ITO	Pt100	Buffer
Density [kg/m^3]	2320	2000	2698.9	2698.9	997
Specific heat [J/kg·K]	830	900	900	900	4179
Thermal conductivity [W/mK]	1.144	0.1	210	0.1	0.613
Viscosity [kg/m·s]					$8.55 \cdot 10^{-4}$

Table 3.2: Material characteristics for the simulation.

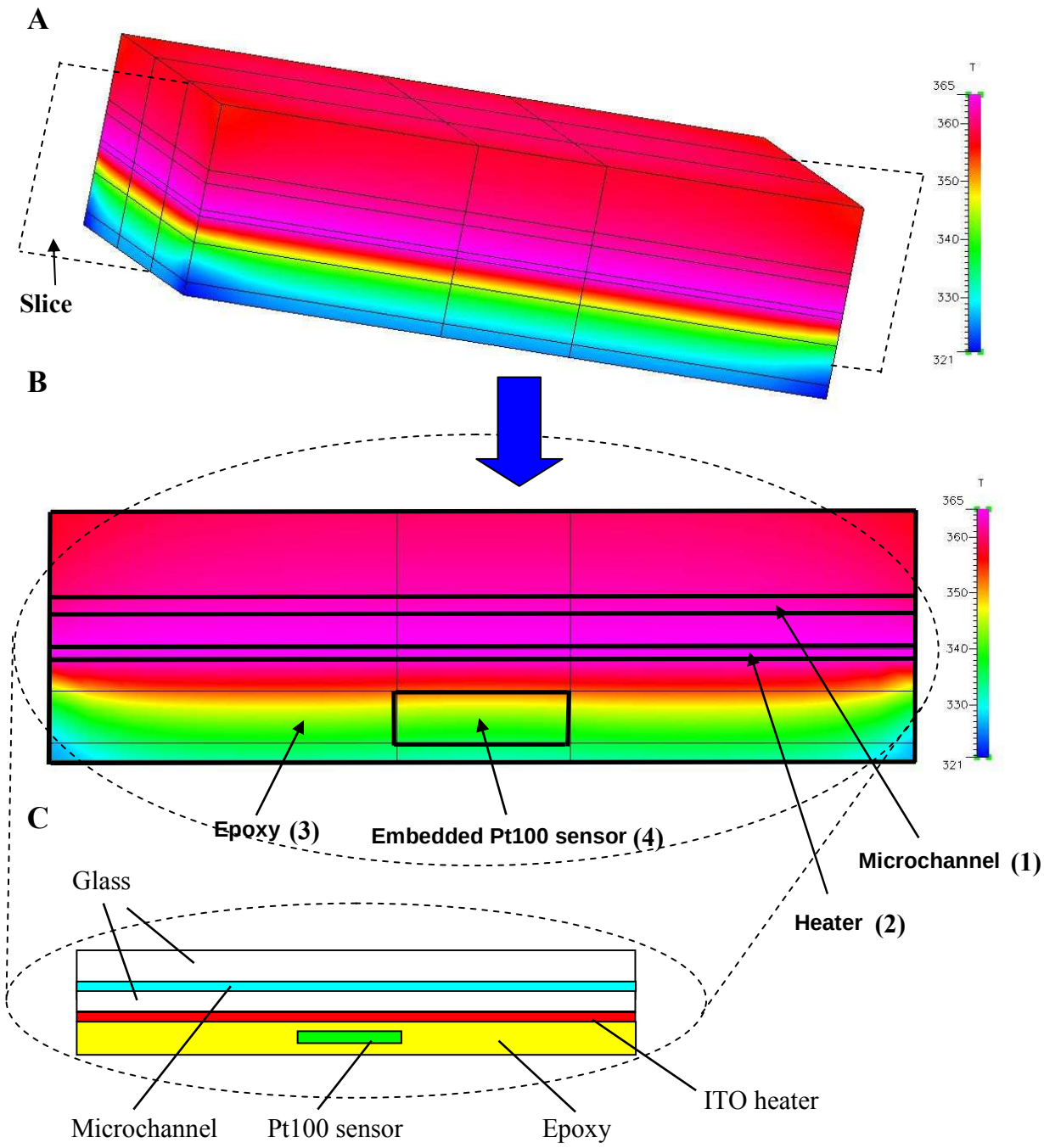

Figure 3.7: a) 3D heat simulation with resistive heater sandwiched between glass substrate and epoxy. The Pt100 sensor is embedded in the epoxy to determine the thermal gradients induced by low thermal conductivity of the epoxy. b) 2D slice inside the device where the Pt100 is located. c) Schematic of the 2D cut. In this simulation, a temperature of 365 °K was applied to the ITO layer resulting in T_{act} = 363.2 °K and T_{ext} = 342.5 °K.

The different simulation parameters were chosen as follows

1) Pyrex parameters were the same as Pyrex.
2) ITO parameters were similar to platinum, except for the thermal conductivity.
3) Buffer parameters were assumed to be the same as for water.
4) Epoxy parameters were taken from the epoxy data sheet for the most part. However, since it did not conduct so well, the thermal conductivity parameter was decreased from the listed value of 1.4 W/mK.
5) Pt100 parameters were the same as for the epoxy, except that a density approaching that of platinum was used.

Simulated temperature values were collected at the Pt100 sensor block and compared to the values obtained in the center of the microchannel for a range of temperatures applied at the ITO layer. The difference between the two yield ΔT values, which were plotted as a function of the temperature values obtained at the Pt100 block. The resulting plot, also depicted in Figure 3.6 ("simulation"), exhibits a linear relationship, in agreement with the experimental values. This supports the assumption that the relationship between ΔT and T_{ext} is linear, providing a model for correcting T_{ext} values. Yamamoto *et al.* also observed a linear relationship between T_{ext} and T_{int} for a PDMS microreactor array in contact with a thin-layer heater device [87].

Hence, the experimentally obtained $\Delta T(T_{ext})$ plot can be used to correct the temperature axis of the Cy5-BHQ3 melting curve obtained using the Pt100 sensor embedded in epoxy, so that this axis represents actual temperature inside the microchambers. A line

was fitted by linear regression to the measured data points in Figure 3.6 to yield the following equation:

$$T_{act} = 1.57 \cdot T_{ext} - 14.9 \qquad (3.1)$$

The corrected melting curve for the glued-sensor measurement is also given in Figure 3.5 (▼), and agrees well with that obtained in the conventional fluorimeter under controlled thermostatted conditions. In this way, the determinate error introduced by the poor thermal contact between the Pt100 sensor and the ITO layer could be corrected.

For the EEPCP device, the rhodamine B fluorescence-versus-temperature calibration curve was first measured by measuring fluorescence while ramping up the temperature in a device incorporating an ITO layer as heater. A Pt100 sensor was used to provide a feedback signal to regulate the ITO heater. Fluorescence signal was collected with a CCD camera mounted on a fluorescence microscope, and pixel-processed to obtain quantitative data. The resulting curve is the "measured" curve presented in Figure 3.8. As mentioned above, temperature was monitored at the ITO layer and not inside the microchannel. To account for any differences between external and internal temperatures, the molecular beacon technique described above was used to correct the temperature axis of the rhodamine calibration curve. The circular data points make up the corrected fluorescence-temperature data set. Basically, the temperature axis has been corrected for the difference in applied temperature versus actual temperature in the microchannel. Thus, temperature values for this curve are internal microchannel temperatures. The corrected curve is shifted to higher temperatures, as a result of the poor thermal contact between the Pt100 sensor and the heating layer (discussed above).

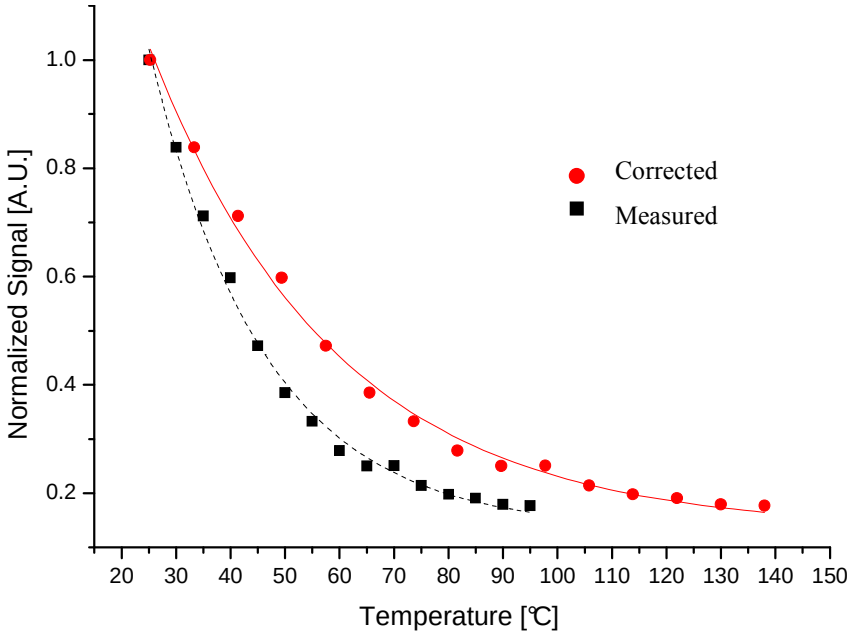

Figure 3.8: Fluorescence intensity of 1 µM rhodamine B in water as a function of temperature.

3.3.2 Cooling and heating in EEPCP device

During cooling experiments, RC_2 was filled with acetone, RC_1 with air, and vacuum was applied to the waste reservoir at the end of the TCC. The central channel was filled with a solution of 1 µM rhodamine B in water. In Figure 3.9, images of the central channel show the fluorescence increase as a function of the temperature decrease obtained by the evaporation of acetone in the TCCs. This is as expected (Figure 3.8).

The extent to which liquid is cooled in the microchannel depends on the evaporation rate of acetone, and can be influenced by varying relative flowrates from RC_1 and RC_2. These latter parameters can be controlled by varying the flow resistance of the channels involved. Flow resistance depends on channel cross-section and length, as well as fluid viscosity.

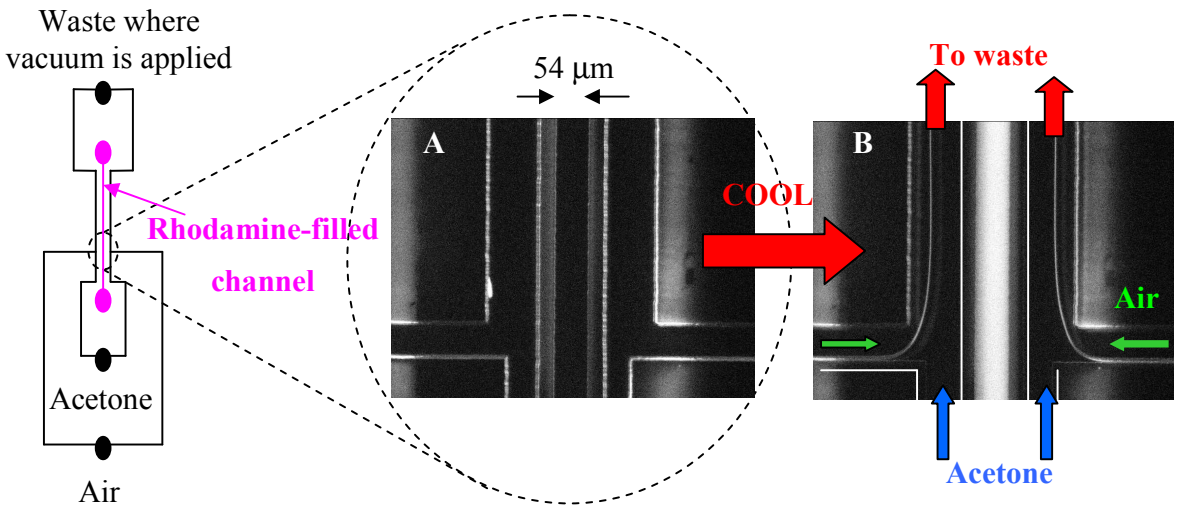

Figure 3.9: Chip design with fluorescence microscope images taken (A) before and (B) during cooling of a 1 µM rhodamine B solution. Note the difference in fluorescence in the central channel. Signal increases as temperature decreases.

If a certain pressure P is applied to a channel i, the flow Q_i induced through the channel is given by:

$$Q_i = 2A_i \cdot D_i^2 P_i / C_i \cdot \eta_i \cdot L_i \qquad (3.2)$$

where: A = area of channel cross-section

D = hydraulic diameter (dependent on channel cross-section)

C = geometric constant (dependent on cross-section shape)

η = viscosity of the fluid in the channel

L = length of the channel

In our device, the vacuum applied to the waste reservoir simultaneously creates the same negative pressure at the ends of RC_1 and RC_2. They also both have the same cross-sectional area, and therefore, using equation 3.2, the flowrate ratio between RC_1 and RC_2 becomes:

$$Q_1/Q_2 = \eta_2 \cdot L_2 / \eta_1 \cdot L_1 \qquad (3.3)$$

Q_1/Q_2 depends only on channel lengths and viscosities of the fluids used, providing some flexibility in setting the flowrate ratio in the TCC.

Two different structures were tested to verify the difference in the cooling effect induced by varying the flow ratio in the air and acetone channels, as presented in Table 3.3. Using equation 3.3, we obtain 0.3:1 and 7:1 air-to-acetone flow ratios for L_{RC1} of 766 mm and 30 mm respectively (L_{RC2} remained constant). The temperatures in the central channel are approximated at 5°C and -3°C respectively using the corrected rhodamine calibration curve in Figure 3.8, demonstrating the influence of the flow ratio on the cooling effect.

Cooling in glass-glass devices was less efficient than in the glass-PDMS hybrids. We think this is because acetone vapor also escapes through the gas-permeable PDMS, thereby driving the acetone evaporation process more strongly and augmenting the cooling effect. This implies that a larger air-acetone contact surface would be required for efficient cooling in a fully glass device.

reagent$_1$-reagent$_2$	L_{RC1}: L_{RC2} (mm)	Flowrate ratio	Estimated T (°C)
air-acetone (COOL)	**766 : 12**	0.3 : 1	5
	30 : 12	**7 : 1**	**-3**
water –H_2SO_4 (HEAT)	**766 : 12**	0.4 : 1	76
	30 : 12	**11 : 1**	**36**

[#]viscosities of reagents at 20°C: air, 18.10^{-6} ; acetone, $0.32.10^{-3}$; water, 1.10^{-3} and H_2SO_4, 25.10^{-3} Pa·s (Handbook of Chemistry and Physics, 1960)

Table 3.3: Achieved temperatures in the central channel using different flowrate ratios.

Heating experiments were performed with rhodamine B in glass-glass devices, with a layout and operating procedure identical to the devices used for the cooling experiments.

Concentrated H_2SO_4 from RC_2 and water from RC_1 were merged in the TCC, where the exothermic dissolution process took place. In Figure 3.10, images of the central channel show the fluorescence decrease as a function of the temperature increase obtained by the dissolution of H_2SO_4 in the TCCs. This is as expected (Figure 3.8). Devices identical to the ones used for the cooling experiments were used to investigate the effect of flow ratio on heating. Since the viscosities of the fluids used in this case were different, the flow ratios changed, as indicated in Table 3.3. For the 0.4:1 water-to-H_2SO_4 ratios, a temperature of 76 °C could be estimated in the rhodamine-containing channel, whereas for the 11:1 ratio, heating to 36 °C was estimated. These results are summarized in Table 3.3.

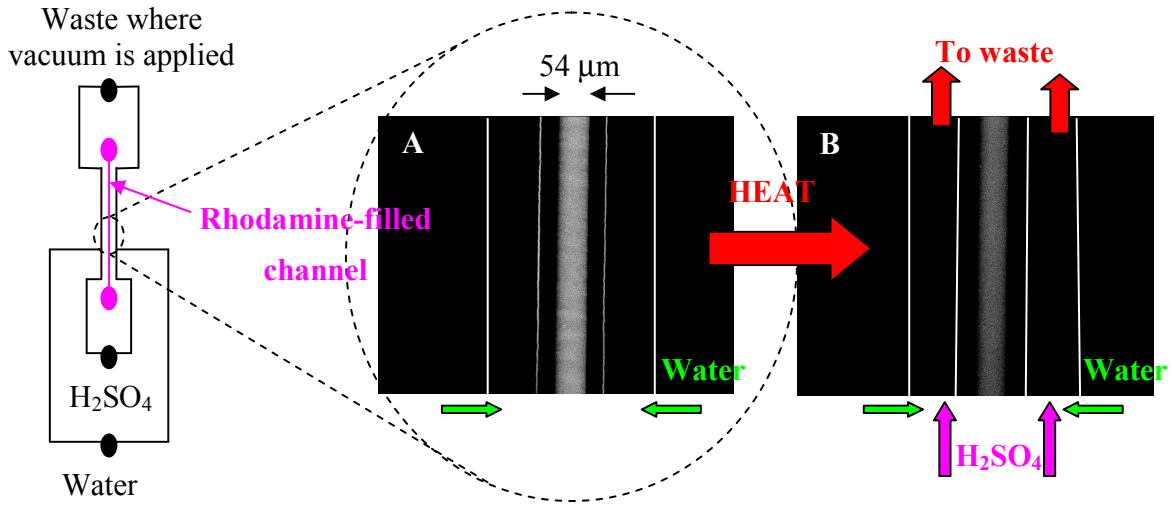

Figure 3.10: Chip design with fluorescence microscope images taken (A) before and (B) during heating of a 1-µM rhodamine B solution. Note the difference in fluorescence in the central channel. Signal decreases as temperature increases.

For additional heating experiments, the central channel was filled with a TAMRA-Dabcyl beacon solution, having a melting point at 54.6°C. In analogy with the experiments described above, water was present in RC_1, and the exothermic reaction was initiated by pipetting 97% H_2SO_4 into RC_2 while vacuum was applied to the waste reservoir. Images

taken before (Figure 3.11A) and after (Figure 3.11B) initiating the heating effect are given in Figure 3.11. The fluorescence increase observed in Figure 3.11B relative to Figure 3.11A is caused by opening of the molecular beacon, demonstrating heating above 54.6°C. The observation of this single biochemical event demonstrates that it is possible to control and influence chemistries inside a microchannel with this device.

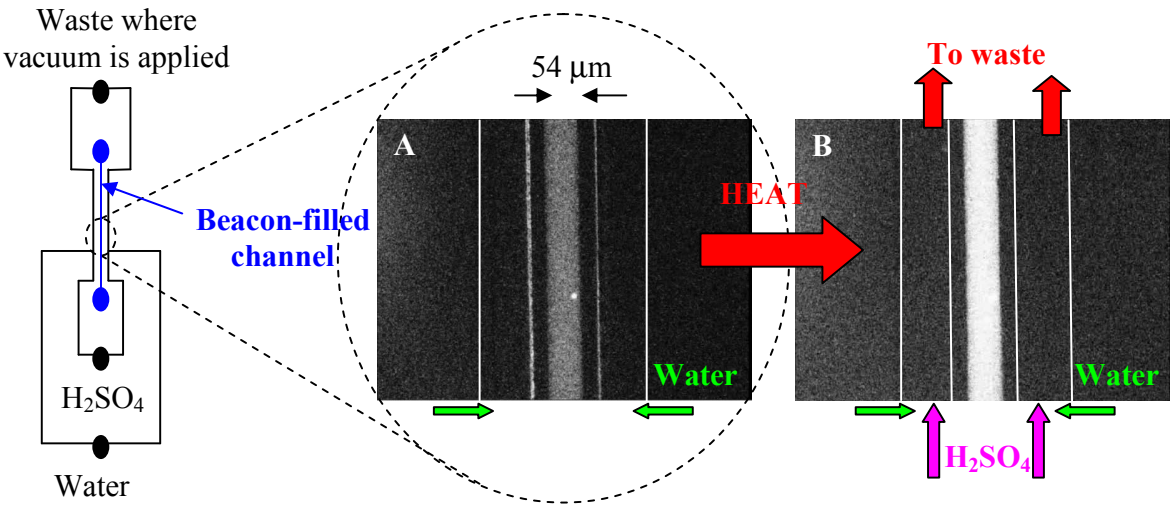

Figure 3.11: Chip design with fluorescence microscope images taken (A) before and (B) during heating of a TAMRA-beacon solution. Note the difference in fluorescence in the central channel. Signal increases above the melting temperature of the beacon (54.6°C).

3.4 Conclusions

A resistive heating device with a transparent resistive layer, for performing fluorescence detection inside a heated glass microchannel, has been fabricated, tested and characterized. Temperature inside the device was calibrated with a novel non-invasive technique using molecular beacons. Beacon melting temperatures, specific to each different beacon, can be used as temperature sensors inside a microchannel. Melting curves (fluorescence as a function of temperature) obtained with molecular beacons thus can provide an unequivocal measure of internal temperature, independent of device

characteristics, and can correct for experimental errors. This is, to our knowledge, the first time that the use of molecular beacons in a microdevice for temperature calibration has been published.

A new, integrated method for spatially localized cooling and heating in microfluidic devices was also presented, using endothermic and exothermic reactions, respectively (EEPCP). The thermal effect was initiated by merging two reagents in a channel by application of a vacuum. The extent of the thermal effect can be controlled by either the flow ratio of the two reactants or by their chemical properties. It is also dependent on the external ambient temperature, though this was not investigated. Integration of the EEPCP temperature control system in microfluidic devices is simple, and does not require additional microfabrication steps. Since the chemical reaction takes place in a microchannel, integration of a temperature control system does not dramatically increase the footprint of a device. Multiple cooling and heating systems could be integrated along a single reaction channel, allowing thermocycling of compounds migrating or being pumped through this channel. The small feature size of the cooling system also allows multiple temperature control units on a microdevice where multiple reactions occur in parallel. Additionally, the driving force of the system is vacuum, resulting in low-power consumption during cooling or heating. The cooling system described might also be attractive for cooling of microelectronic devices.

4 DNA HETEROGENEOUS ASSAY ON CHIP

This chapter is adapted from:

Thermal Dehybridization of Surface-Bound DNA in a Microfluidic Device for Nucleic Acid Analysis

A. Dodge, G. Turcatti, I. Lawrence, N.F. de Rooij, E. Verpoorte, Submitted to Analytical Chemistry.

Development of a microfluidic device for genetic analysis based on hybridization of surface-bound DNA

A. Dodge, G. Turcatti, P. Mayer, N.F. de Rooij, E. Verpoorte, Presented at the SmallTalk2002 Conference, San Diego, CA, USA, Jul. 28-31, 2002.

After having described a heterogeneous assay and different methods for temperature monitoring, this chapter describes a heterogeneous DNA assay combining immobilization and quantification of biomolecules onto modified surfaces, with temperature control performed in a microchamber. It presents a simple microfluidic device used for performing DNA hybridization kinetic studies, and DNA-double-strand melting temperature measurements. It is the first microfluidic device in which thermal dehybridization of oligonucleotides, hybridizes to complementary probes covalently bound to a surface, is performed for measurement of double-stranded DNA melting temperatures

4.1 Introduction

With the huge increase in DNA sequence information resulting from the Human Genome Project, genetics researchers are now focusing on establishing the link between sequence and function. In pharmacogenomics, for instance, the relationship between DNA sequence composition and drug response is of particular interest, as pharmaceutical companies seek to better design medicines to avoid adverse side effects and improve drug therapies generally. Medical diagnostics has also benefited enormously, as more and more tests for inherited diseases rely on testing patient DNA for characteristic mutations by hybridization with DNA probes of known sequence. An integral part of genetics research today involves the discovery of single-nucleotide polymorphisms (SNPs), single-base variations which could potentially play a large role in determining phenotype. Traditionally, DNA analysis has been performed with instruments based on gel electrophoresis, which separate DNA fragments according to size. This method is difficult to perform with high throughput, since analysis times are in the order of hours.

Microfluidic chips have provided a way to downsize this technology, strongly reducing analysis times while maintaining or exceeding the separation efficiencies achieved in macroscopic instruments [10-14, 94]. Multiplexing DNA analysis also becomes possible, simply by reproducing the channel layout many times to form an array of closely spaced separation channels for highly parallel, high-throughput analysis [95-102].

An alternative approach to high-throughput DNA analysis is offered by DNA microarray-based chips, involving the synthesis or immobilization of many thousands of probe oligomers onto a surface as arrays of spots. Analysis is then performed by introducing the target DNA to the liquid volume above the array, and allowing hybridization to occur. Detection is generally accomplished by fluorescently labeling the target DNA beforehand, so that hybridization leads to an increase in optical signal. There is no doubt that this technology has revolutionized genetics research. However, besides the non-negligible cost of the probes and spotting instrumentation, analysis time is still a concern. This is because chip-based hybridization assays still generally depend solely on diffusion of target (sample) DNA to the surface-bound probes, leading to hybridization times of several hours or more [103-105]. To address this problem, DNA array chips have been combined with microfluidic devices designed to mix and circulate hybridization sample over the array surface, to enhance sensitivity and thus provide a route to reduced hybridization times [104, 106]. Lenigk *et al.* spotted probe DNA for four pathogenic bacteria surrogate strains directly into a polycarbonate microchannel, and moved sample DNA through the channel using an integrated pump to accelerate hybridization [103]. Detection could be carried out in only 30 min. Other solid-phase hybridization-based analysis methods have used either novel solid phases and/or DNA transport to achieve improved

performance. In a reversal of the usual assay configuration, Fan *et al.* attached different DNA sample (target) fragments to paramagnetic beads, and perfused these with probe-containing solution to reduce hybridization times from 3 to 18 hours down to just a few seconds [107]. Heller *et al.* immobilized DNA probes onto arrays of individually addressable microelectrodes, and used applied electric fields to electrophoretically transport labeled target DNA to and from specific electrodes to enhance hybridization [108]. Improved interaction with surface-immobilized DNA by reducing diffusional transport distances was also achieved by depositing spots of probe-containing solution on microchannel glass, a porous substrate consisting of vertical microchannels 10 μm in diameter [105, 109]. Recirculation of target-containing sample through the substrate guaranteed efficient delivery of target to the surface. DNA has also been immobilized in porous hydrogel plugs in microfluidic channels. Electrophoretic perfusion of the plugs with complementary DNA allowed hybridization to take place in minutes [110]. All these examples demonstrate that active delivery of hybridization solutions or DNA molecules directly to DNA-probe-coated surfaces strongly enhances the rate of hybridization and the sensitivity of the resulting signal when compared to systems in which transport is solely passive.

One of the applications of interest in this work involving solid-phase hybridization is a recently described method for performing high-throughput DNA sequencing. In this approach, massively parallel amplification of surface-bound sample DNA is followed by *in situ* sequencing by synthesis [21, 111, 112]. Conventionally performed in plastic tubes or on glass substrates, the DNA template to be sequenced is first hybridized to surface-bound primers and subsequently amplified in a commercial thermocycler to create a

random array of DNA colonies, each 1 to 2 μm in diameter. These DNA colonies can then be analyzed in parallel using base-by-base sequencing, a method in which primer extension is carried out using fluorescently labeled, deoxy nucleoside triphosphates (dNTPs). The incorporation of each base into the DNA strand being synthesized can be immediately detected *in situ*, directly at the surface. The distance between any two colonies is important for the accuracy of this technique, and can be modulated by changing the concentration of the target DNA to be hybridized to the attached primers. Clearly, the steps involved in this technique require a lot of fluid handling, from surface conditioning to amplification and especially sequencing [21, 111-113]. The demands on the fluid handling capability of a sequencing instrument increase even further if analysis is to be done reproducibly and with high throughput. Microfluidics can address the different fluid handling and sample delivery problems of this surface-based DNA analysis effectively. The large surface-to-volume ratios characteristic of microfluidic devices also provide for efficient heat transport, and thus greater temperature uniformity and control. This aspect was also important in this study, as it was of interest to decrease thermocycling times through integration of a thin-film heater, as proposed by a number of authors [72, 114-117].

Surface chemistry combined with heat can be a powerful tool for other types of biochemical analyses as well. A good example was recently reported, where SNP analysis was performed by thermal dehybridization of surface-bound DNA in a technique known as *dynamic allele-specific hybridization (DASH)* [64, 118]. Target DNA is immobilized after amplification to a microtiter plate well using biotin-streptavidin chemistry, and hybridized with a probe specific for one allele. Hybridization is visualized

using a double-stranded DNA-specific dye. Monitoring fluorescence as temperature is ramped should then yield a rapid decrease in fluorescence at the denaturing or "melting" temperature, T_m, of the target-probe duplex. T_m's were lower for sequences containing a SNP than for fully hybridized strands, with temperature differences on the order of 6 to 12°C for 15 to 21-mer probes [63, 64, 118]. Thiel *et al.* observed similar values for *in situ* surface plasmon resonance imaging of DNA hybridization at gold surfaces [119].

In order to perform the types of DNA analysis described above on a microfluidic platform, one has to address the issues of sample delivery and small-volume liquid handling generally, as well as temperature control and surface modification in microchannels. In this work, devices have been realized for use in solid-phase DNA hybridization-based analysis. An established oligonucleotide-immobilization technology that has proven to be relatively resistant to high temperatures [21] was transferred to microfluidic channels. The device used was the RH device described in Chapter 3, which was characterized thermally using the molecular beacon technique. A flowing system was foreseen for both surface modification and analysis in order to continuously remove bubbles. The use of this microfluidic device with integrated heaters for measurement of DNA melting curves is demonstrated.

4.2 Experimental

4.2.1 Reagents

100 mM Tris/HCl buffer containing 1 mM $MgCl_2$ (pH 8) was made from tris(hydroxymethyl)aminomethane (Tris) (Fluka Chemicals, Buchs, Switzerland) and $MgCl_2$ powder (Merck, Buchs, Switzerland) diluted in doubly-distilled deionized (DI)

water. 1 M NaOH solution (CE-grade, filtered over a 0.2-μm membrane prior to packaging) was purchased from Fluka Chemicals, Buchs, Switzerland. 97% H_2SO_4 (Merck, Buchs, Switzerland) was diluted to 50%. Electronic-grade ethanol, acetone and 1 M HCl was purchased from Laporte Electronics (Riddings, U.K). The acetone was dried over molecular sieves (400 Å mesh). Silanizing agent (3-aminopropyl)-aminotriethoxysilane (ATS) was purchased from Aldrich (Buchs, Switzerland). Tris(2-carboxyethyl)phosphine hydrochloride (TCEP) and a heterobifunctional cross-linking reagent, m-maleimidobenzoyl-N-hydroxysulfo-succinimide ester (sulfo-MBS), were purchased from Pierce (Socochim SA, Switzerland). Phosphate-buffered saline (PBS) buffer (0.1 M NaH_2PO_4, 0.15 M NaCl, pH 7.2) and NaPi buffer (0.1 M NaH_2PO_4, 0.15 M NaCl, pH 6.5) were prepared from NaH_2PO_4 (Merck, Buchs, Switzerland) and NaCl (Fluka, Buchs, Switzerland) powders, dissolved in DI water and pH adjusted with HCl. 5XSSC buffer (0.75 M NaCl, 0.075 M sodium citrate, pH 7.0) was prepared using chemicals from Fluka, Buchs, Switzerland. Beta-mercaptoethanol (BME) was purchased from Sigma, Buchs, Switzerland. TMN stringent buffer is a solution of 10 mM Tris / HCl (pH 7.5) with 50 mM NaCl and 20 mM $MgCl_2$.

4.2.2 Oligonucleotides

Cy5-Black Hole Quencher 3 (Cy5-BHQ3) beacon was purchased from Biosearch Tech, USA. All the oligonucleotides were purchased from Eurogentec, Belgium. The sequences of the oligonucleotides used in the different experiments are given below.

1) Thiol oligonucleotide fluorescently labeled with Texas Red (TR) (used to assess thiol oligonucleotide binding to the silane-bound cross-linker)

(T) 10-P2-TR: 5'-SH-TTTTTTTTTTGAGGAAAGGGAAGGGAAAGGAAGG-TEXAS RED-3'

2) Oligonucleotides (used in the different hybridization experiments):

(T) 10-P1 (surface-attached probe DNA with thiol group):

5'-SH-TTTTTTTTTTCACCAACCCAAACCAACCCAAACC-3'

TR-REV-P1 (target DNA in solution):

3'-GTGGTTGGGTTTGGTTGGGTTTGG-TEXAS RED-5'

(T) 10-P2 (surface-attached probe DNA with thiol group):

5'-SH-TTTTTTTTTTGAGGAAAGGGAAGGGAAAGGAAGG-3'

TR-REV-P2 (target DNA in solution):

3'-CTCCTTTCCCTTCCCTTTCCTTCC-TEXAS RED-5'

(T) 10-P1 and ***TR-REV-P1*** are complementary, as are ***(T) 10-P2*** and ***TR-REV-P2***.

4.2.3 Instrumentation

The temperature control system was described in Chapter 3 (Section 3.2.3).

Fluorescence images were taken with a CF 8/4 DXC black-and-white CCD camera (Kappa, Gleichen, Germany) mounted on an Axiovert S 100 fluorescence microscope equipped with a DC halogen lamp and a dichroic mirror set for Cy5 (excitation wavelength bandpass at 546 nm, dichroic mirror reflecting below 580 nm and transmitting above 590 nm) (Zeiss, Feldbach, Switzerland). Images were pixel-processed with Lispix freeware to obtain quantitative intensity data.

Experimental denaturation curves (melting curves) for fluorescent beacons in solution were generated in a Jasco FP 750 spectrofluorometer equipped with a temperature controller and stirring unit (Jasco ETC-272T). Excitation and emission wavelengths were fixed at 620 nm and 660 nm for Cy5. Oligonucleotides, diluted to a final concentration of 200 nM in 100 mM Tris-HCl containing 1 mM $MgCl_2$ (pH 7.8) buffer, were introduced into a 0.5 × 1.0 cm quartz cuvette (Hellma). Samples were stirred continuously with a magnetic bar during the measurements.

Denaturation curves of the P2 oligonucleotides were generated in a spectrophotometer (Jasco V550) equipped with a temperature controller (Jasco ETC-505T). Each pair of synthetic complementary oligonucleotides were diluted to a final concentration of 0.7 μM in 1 mL of buffer containing 100 mM Tris-HCl and 1 mM $MgCl_2$ (pH 8.0).

A flow system was used to remove dissociated DNA fragments (to prevent resettling) and bubbles created during experiments at elevated temperatures. This system consisted of a Harvard syringe pump (Harvard, UK) connected to PEEK^{TM} tubing (outer diameter: 1.6 mm, internal diameter: 500 μm) (Upchurch, Switzerland). The tubes were interfaced to the chip with a PEEK™ plug designed in-house and fabricated at MECA (St-Aubin, Switzerland). These fittings were inserted into the coverplate holes, sealing well due to the elasticity of PEEK^{TM}. The tubing was fixed snugly over the flanges of the plugs.

A manometer connected to the house vacuum, with an exhaust valve to regulate the induced negative pressure, was used to control the flowrates of conditioning solutions inside the microchambers.

4.2.4 Surface conditioning prior to oligonucleotide attachment

Surface conditioning was performed by continuously drawing conditioning fluids through the reaction chambers at constant controlled flowrates using vacuum as a pumping mechanism. When there is a difference of pressure, ΔP, between the inlet and outlet of a channel, the flow induced in this channel can be obtained by:

$$Q = \Delta P/R \qquad (4.1)$$

where R is the channel fluidic resistance [120-122]. In this study, channels are much wider than they are deep, and have profiles which can be approximated by a rectangle having a width much larger than the height. R is then given by [120, 121]:

$$R = 12 \cdot \eta \cdot L/w \cdot h^3 \qquad (4.2)$$

where: η = viscosity of the fluid in the channel

L = length of the channel

w = channel width

h = channel height

Flowrate can then be calculated as:

$$Q = w \cdot h^3 \cdot \Delta P/12 \cdot \eta \cdot L \qquad (4.3)$$

From Equation (4.3), it is clear that flowrates, and hence reagent delivery to microchannel surfaces, can be well controlled, assuming a stable source of vacuum is available.

The surface modification procedure adopted here is based on that described in Adessi *et al.* [21]. For all conditioning and reaction steps, solution was drawn through the chamber

under constant flow conditions. Drops of each solution were placed over reservoir holes at one end of a chamber, and vacuum applied to the other end. Chambers were first treated with bases and acids in order to always obtain the same starting surface conditions prior to silanization. The preconditioning sequence consisted of an initial 20-min rinse with 1 M NaOH, followed by a 10-min rinse with DI water. 1 M HCl, DI water, 50% H_2SO_4, and DI water were then sequentially flushed through the chamber for 10 min, 5 min, 20 min, and 5 min, respectively. A 5-min ethanol rinse removed excess water, followed by a 10-min rinse with dried acetone to remove ethanol. Silanization was then carried out by flushing with a solution of 1 % ATS in dried acetone for 10 min. Dried acetone was used to rinse the solution away, followed by an ethanol rinse to prepare the chip for the next step (both rinses were 5 min long). For all conditioning steps, a negative pressure of 7×10^4 Pa was applied to the 500-μm-wide, 10-μm-deep channels. This yields a flowrate of 8.4 μL/min, assuming a η equivalent to that of water. Dividing the flowrate by the area of the channel cross-section gives the average linear velocity, which was 28 mm/s in this case. For the 1000-μm-wide, 20-μm-deep channels, 3×10^4 Pa was applied to generate a linear velocity of 48 mm/s.

Shchepinov *et al.* showed that hybridization yields are enhanced when surface-bound DNA molecules are given more spatial freedom to interact with DNA molecules in solution [(1)]. The use of so-called spacer molecules to increase the distance between the bound DNA and the solid substrate, thereby reducing steric hindrance, is one of the ways to accomplish this. The heterobifunctional reagent, sulfo-MBS, was used both as a spacer and as a cross-linker between the silane and the oligonucleotides. The sulfo-MBS is covalently attached to the amino silane through formation of an amide bond between the

succinimidyl ester moiety of sulfo-MBS and amino groups of the silane. To carry out the reaction, a 5-mM solution of sulfo-MBS in PBS was flowed through the chamber for 10 min, followed by a 10-min PBS rinse, a 5-min DI water rinse, and finally a 5-min ethanol rinse. This procedure was performed at linear velocities of 28 mm/s for the 500-μm-wide chamber and 16 mm/s for the 1000-μm-wide chamber. Concentration of the cross-linker solution had to be kept low in order to avoid non-uniform coatings and eventual clogging of the chamber due to precipitation, as observed previously for physisorption of Protein A to a silanized surface [88]. The formation of microbubbles occurs on hydrophobic surfaces, and was observed here when the cross-linker reaction had more or less gone to completion, saturating the surface.

4.2.5 Probe immobilization

The final step of the procedure for surface modification involved covalent attachment of the probe oligonucleotide via the thiol group on the 5' end to the maleimide portion of the sulfo-MBS cross-linker. The DNA probe molecules include a poly-T (T10) sequence to keep the sequences to be hybridized positioned away from the surface, as previously reported [21]. In experiments to determine the densities of DNA bound to the spacer, a TR-labeled thiol oligonucleotide diluted in NaPi buffer, with 5 mM TCEP added to avoid thiol oxidation, was bound to the cross-linker. The fluorescence emitted by the TR label could then be used as a measure of probe molecule density. The binding step was followed by a 10-min rinse with NaPi buffer and a 10-min capping treatment using a solution containing 10 mM BME in NaPi solution to render all the remaining available cross-linker sites inactive. A 10-min rinse with NaPi buffer was performed to remove the

BME, followed by a 5-min rinse with 5XSSC buffer, a solution in which DNA is stable and can be stored for longer periods of time when refrigerated.

The reproducibility of probe surface density in the 500-μm-wide, 10-μm-deep chambers was assessed by reacting 100 μL of 1 μM TR-labeled thiol oligonucleotide (***(T)10-P2-TR***) solution with the sulfo-MBS-modified surface. This was performed by drawing the solution through the chamber at a linear velocity of 12 mm/s for 30 min. Fluorescence images taken after rinsing away excess sample then allowed the reproducibility of the immobilization reaction to be determined.

Control of probe surface density was demonstrated by varying the reaction times of the oligonucleotide with cross-linker-treated surface. The DNA sequence used for these tests was the fluorescently labeled ***(T)-10-P2-TR***. For the 1000-μm-wide, 20-μm-deep chambers, the flowrates of thiol oligonucleotide (probe molecules) required to achieve linear flowrates equivalent to the smaller chambers were significant, resulting in rapid consumption of reagent. Therefore, an alternative stopped-flow method was used to carry out oligonucleotide immobilization in this case. Probe-containing solution was introduced to a chamber with the controlled vacuum system at 8 mm/s. Once the chamber was filled, the flow was stopped in order to let passive diffusion of DNA to the surface take place for 1 minute. This solution was then removed, and a second volume of probe solution drawn into the chamber for a 1-min stopped-flow reaction, and so on. The total effective reaction time increased with the number of times the solution replenishment process was performed.

4.2.6 Hybridization / dehybridization experiments

For hybridization tests, the non-labeled thiol oligonucleotides, ***(T) 10-P1*** and ***(T) 10-P2***, diluted in the same buffer solution as the labeled thiol oligonucleotide, were bound to cross-linker-treated chambers. Reaction times were kept constant at 30 min. Surface densities of the bound probe DNA were determined by hybridizing with a fluorescent complementary oligonucleotide, either ***TR-REV-P1*** or ***TR-REV-P2***, depending on the experiment. All complementary oligonucleotides were prepared in 5XSSC buffer at a 100-nM concentration, and hybridized in both the small and large chambers using the stopped-flow technique described above. Surface densities of hybridized oligonucleotides could be actively controlled by either varying the concentration of thiol oligonucleotides in the solutions for the immobilization reaction, or by varying incubation times of the fluorescent complementary oligonucleotides.

The degree of hybridization versus non-specific adsorption was determined by measuring the difference in signal-to-noise ratios for binding between surface-immobilized ***(T) 10-P1*** and its complementary strand, ***TR-REV-P1***, versus binding with the non-complementary ***TR-REV-P2***. Probe immobilization reactions were performed for 30 min. Hybridization experiments were carried out using solutions containing 100 nM of the two target DNA species in either 5XSSC buffer or TMN stringency buffer. The duration of the incubation periods for hybridization was 30 min.

Melting curves of surface-bound double strands were obtained using a continuous flow technique. The ***(T) 10-P2*** and ***TR-REV-P2*** complementary pair was used. The probe DNA was first immobilized in a 1000-μm-wide, 20-μm-deep chamber using a 30-min reaction time. Target DNA was then incubated with the probes for another 30 min. A 5

μL/min flow of 5XSSC buffer was continuously pumped through a fully conditioned chamber with the Harvard syringe pump connected to the PEEK™ interface. Temperature was slowly ramped up at a rate of 1°C/sec with the ITO resistive heater, and stabilized every 5 degrees for 5 seconds in order to take a snapshot of the fluorescence image with the CCD camera mounted on the fluorescence microscope. As temperature increased, dehybridization occurred, releasing hybridized, labeled strands which were continuously removed in the applied flow. A decrease in fluorescence signal at the surface was therefore observed. T_m's of the melting curves obtained were determined by first fitting them with a sigmoidal function and then calculating the inflexion points of the fitted curves, as was done with the beacon. Melting curves were also measured in a conventional system in the liquid phase to compare with the results obtained for solid-phase hybridization.

4.3 Results and discussion

4.3.1 Surface conditioning

Using the controlled reagent delivery system in conjunction with the 500-μm-wide, 10-μm-deep structures, a reproducibility of 9% (n=3) was obtained for immobilization of oligonucleotides (Table 4.1). This was better than the 20% obtained on microscope slides[21]. The remaining error can probably be explained by the fact that the precision of the manometer used in the setup was only $\pm 0.5 \times 10^4$ bar, resulting in a flowrate error of ± 0.3 μL/min for the 10-μm-deep channel. Since flowrates range between 3.6 and 8.4 μL/min in the small channel, values for flowrate precision fall between 8 % and 4 %, respectively. Using a high-precision peristaltic pump or a syringe pump with nanoliter-

per-minute flow precision, even better surface conditioning reproducibility could be expected. Nevertheless, this simple system manages to achieve good reproducibility with fast reaction times, with a total procedure time of about 4 hours. This is much faster than the 2 days required in the original publication, in which this DNA immobilization method was applied to glass slides [21]. It should be noted, however, that reaction times have not been optimized in either the slide or microchannel case, and improvements should be achievable in both cases. The advantage that microfluidic devices offer over glass slides is controlled convective transport of reagents over the surface being modified.

	Exp 1	Exp 2	Exp 3	Average with STD [%]
Signal [A.U.]	140	135	160	145
STD [%]	6	5	2	9

Table 4.1: Fluorescence signal of surface-bound thiol oligonucleotide in the 500-µm-wide, 10-µm-deep chamber. Repeated experiments show good reproducibility of surface density. Standard deviations of single measurements obtained by pixel processing of a surface image are dependent on the uniformity of the conditioned surface. The average of the three single experiments yields a standard deviation of 9%. [***10 P2-TR***] was 1 µM in 5XSCC buffer with 5 mM TCEP added.

In the 1000-µm-wide, 20-µm-deep chamber, a stopped-flow reaction technique was used to conserve DNA reagent, as described in the Experimental section. In the standard case, reagent solution was left to incubate for 1 min in the chamber before being refilled by fresh reagent. Total reaction time is then simply the product of the number of refill cycles and the reaction time per cycle. It was possible to vary the density of TR-labeled probe DNA bound to the surface, as evidenced in Figure 4.1. For 1-min incubation times, the surface concentration of TR-DNA approached its maximum after 20 refill cycles, indicating that cross-linker sites available for binding were close to being fully occupied.

A simple test proved that it was not necessary to wait longer than one minute between each chamber refill. Incubation times of 5 min/cycle resulted in a lower fluorescence signal after a total time of 30 min than in the 1 min/cycle case. In fact, the signal was more or less equivalent to that obtained for 1-min times for the same number (6) of refills.

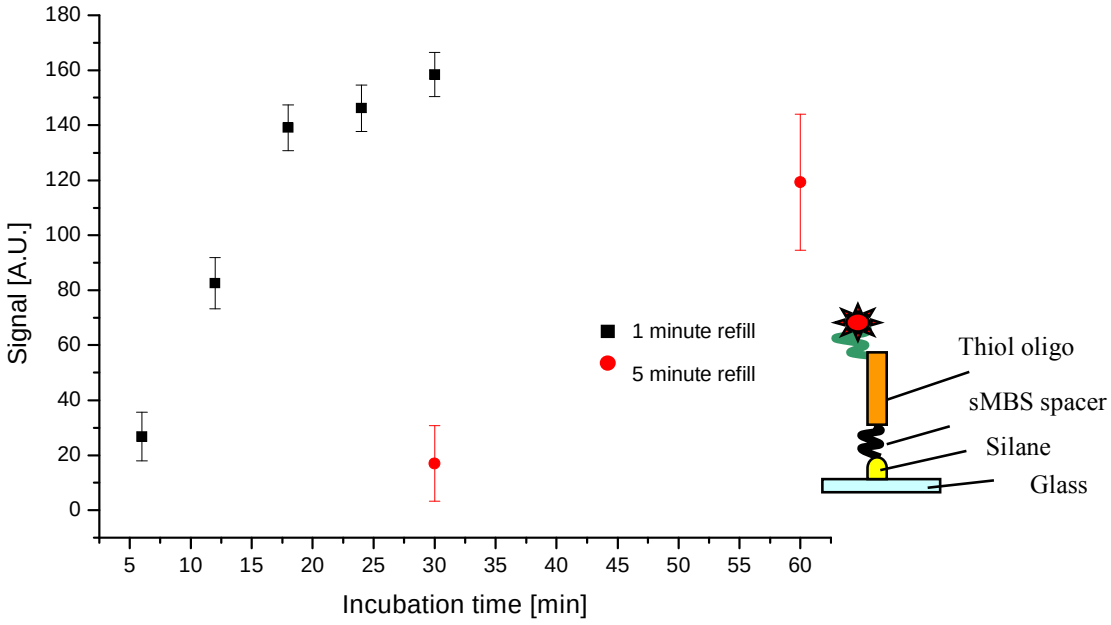

Figure 4.1: Binding of labeled probe thiol oligonucleotide to cross-linker-treated surface in a 1000-µm-wide, 20-µm-deep device. A stopped-flow reaction technique was used in this case. The inset shows the composition of the surface layer being studied. Signal increases with reaction time until all cross-linker sites are saturated for the 1 min reaction / refill case, as expected. DNA solution depletes in less than 1 minute, since signal does not increase when reaction times of 5 min per refill are used. Standard deviations of single measurements obtained by pixel processing of a surface image are dependent on the uniformity of the conditioned surface. [***(T) 10-P2-TR***] was 1 µM in 5XSSC buffer with 5 mM TCEP.

The result at 60 min total incubation time, obtained after twelve 5-min refill cycles, is also lower than after 30 min in the 1 min/cycle case. This indicates that the reagent solution was rapidly depleted, so that reaction rates at the end of the 1-min and 5-min incubation periods were very small and about the same.

For testing specificity of hybridization in the microchannels, the non-fluorescent thiol oligonucleotide ***(T) 10-P1*** was bound to the surface, and a hybridization experiment was performed first with the unrelated labeled target, ***TR-REV-P2***, to measure the mishybridization signal. Stopped-flow conditions were used. The chamber was reinitialized by performing a 20-min 1 M NaOH rinse to remove the immobilized DNA, and fully reconditioned with ***(T) 10-P1***. A solution containing the complementary probe, ***TR-REV-P1,*** was then introduced and allowed to react with the surface. Figure 4.2 shows that hybridization of complementary oligonucleotides produces a strong difference in signal when compared to mishybridization of unrelated probes. Figure 4.2A shows a signal-to-noise ratio of of 9.6 ± 23% for specific hybridization versus 3.5 ± 19% (n=3 in both cases) obtained for mishybridization, when experiments are performed with the 5XSCC buffer. In this case, the specific/non-specific binding signal ratio is 2.7. Figure 4.2B shows that sufficiently stringent surface hybridization conditions (here attained with the TMN buffer) lead to good hybridization specificity for complementary versus unrelated DNA strands. The signal-to-noise ratio decreases to 6.0, but the specific/non-specific binding signal ratio is 6.0, which is 2.2-fold better than that obtained with the 5XSSC buffer.

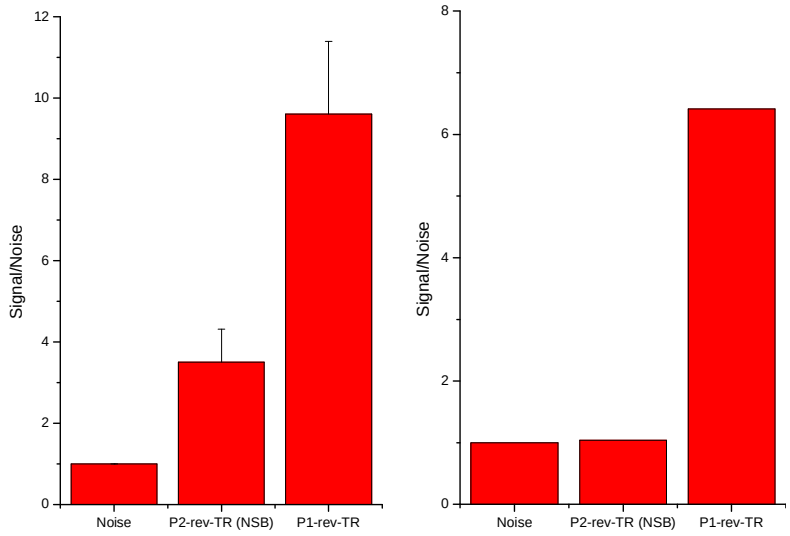

Figure 4.2: Determination of hybridization specificity. ***T (10) P1*** single-stranded oligonucleotide was attached to the surface, and sequentially incubated with the complementary ***TR-rev-P1*** and unrelated ***TR-rev-P2*** labeled oligonucleotides. [thiol oligonucleotide] was 1 μM in 5xSSC buffer with 5 mM TCEP. a) A 500-μm-wide, 10-μm-deep chamber was used. Incubation was performed under stopped-flow conditions. [target DNA] was 100 nM in 5XSSC buffer, 5XSSC buffer rinse. b) [target DNA] was 2.5 μM in stringent buffer (TMN), followed by TMN rinse. Binding and rinsing with stringent buffer decreases the signal-to-noise ratio from 9 to 6, but increases the hybridization/mishybridization signal ratio by 2.2-fold. Mishybridization is thus virtually non-existent. Pumping using a peristaltic pump in the second case led to lower standard deviations than the controlled vacuum pumping setup.

By varying incubation times of complementary target DNA, it was possible to control their surface densities, as seen in Figure 4.3. Signal increases until all available bound probe DNA sites are saturated. Also, by varying the concentration of probe thiol oligonucleotides in the reagent solution but keeping reaction times fixed, it is possible to control surface densities of the covalently bound probe DNA. The maximum signal due to hybridized, fluorescently labeled complementary probes increases as a function of the concentration of thiol oligo in the original solution used for immobilization. These curves are typical for binding experiments from which kinetic data can be extracted. The kinetics of DNA hybridization to surface-tethered probes is a subject of ongoing investigation in a

number of research groups, with second-order (bimolecular) or modified Langmuir adsorption models being proposed [123-125]. In our system, a second-order model neglecting the reverse (dehybridization) reaction was chosen.

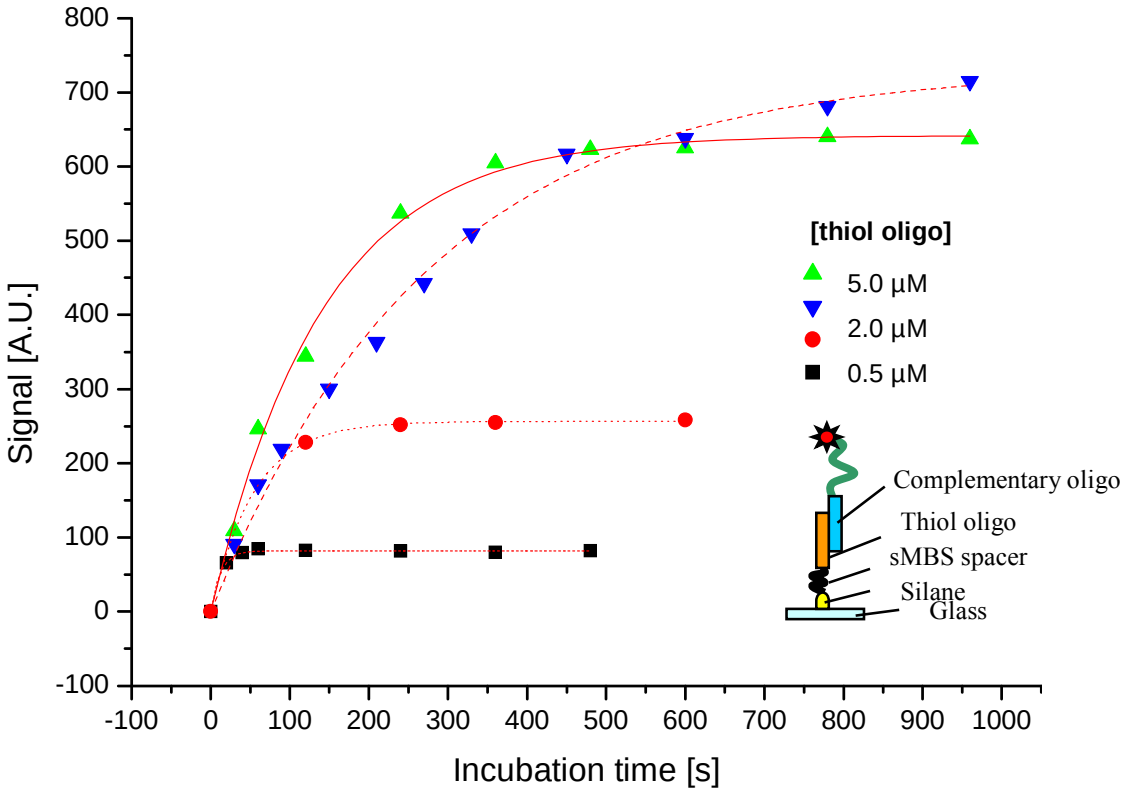

Figure 4.3: Variation of ***T (10) P2*** thiol oligonucleotide concentration in the reagent solution for surface immobilization induces variation of surface density. These experiments were performed in a 500-µm-wide, 10-µm-deep chamber. Bound oligonucleotide density is revealed by hybridization with the fluorescently labeled complementary oligonucleotide. Signal increases until saturation of all available thiol oligonucleotide hybridization sites. Saturation signal increases with surface-bound DNA density. [***TR-REV-P2***] = 100 nM.

The rate equation is given in Equation 4.4.

$$S(t) = S_0 \cdot (1 - e^{-k \cdot [L] \cdot t}) \qquad (4.4)$$

Where S(t) = number of bound molecules

S_0 = total number of available binding sites

k = forward association rate

[L] = concentration of sample in solution

t = incubation time.

By fitting the binding curves using this function, the forward rate constant, *k*, can be deduced. As Figure 4.3 shows, agreement of the fitted curves with experimental data is good, indicating that our kinetic model is appropriate. The four forward rate constants obtained for the curves in Figure 4.3 and plotted in Figure 4.4 reveal an interesting point.

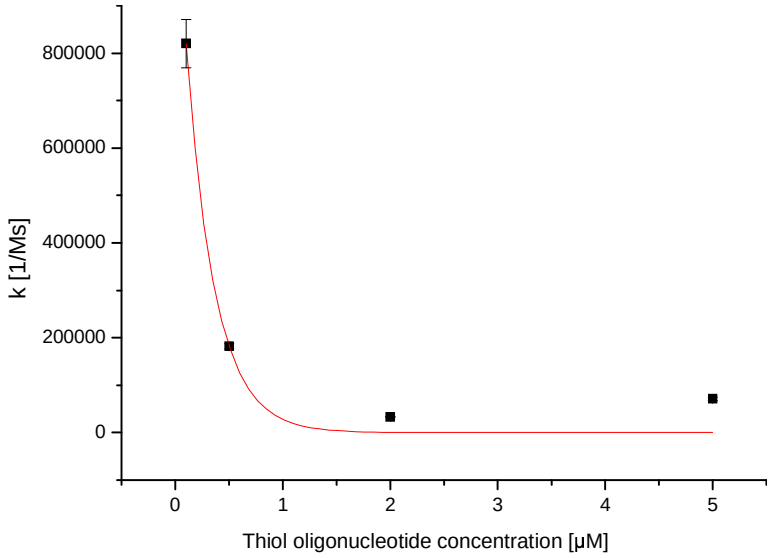

Figure 4.4: Forward rate constant decreases at larger thiol oligonucleotide concentrations because surface-bound oligos are packed closer together, therefore reducing spatial freedom. [***TR-REV-P2***] = 100 nM.

For the lowest surface density of thiol oligo obtained with 0.1 µM primer concentration in solution, $k_{0.1}$ = 820'000 $M^{-1}s^{-1}$. For the highest surface density, k_5 = 71'000 $M^{-1}s^{-1}$, which is a decrease in reaction rate of 91%. This decrease could be due to the fact that the immobilized oligonucleotides are closer to each other when surface densities increase, thereby reducing the spatial freedom which is necessary for hybridization enhancement [1, 126]. Hybridization rate is quite sensitive to surface density of bound DNA, as indicated by the exponential decrease of forward rate constant versus primer concentration depicted in Figure 4.4. From the saturation values of each curve in Figure 4.3, the dose-response curve in Figure 4.5 was obtained, with "dose" being the density of primers bound to the surface.

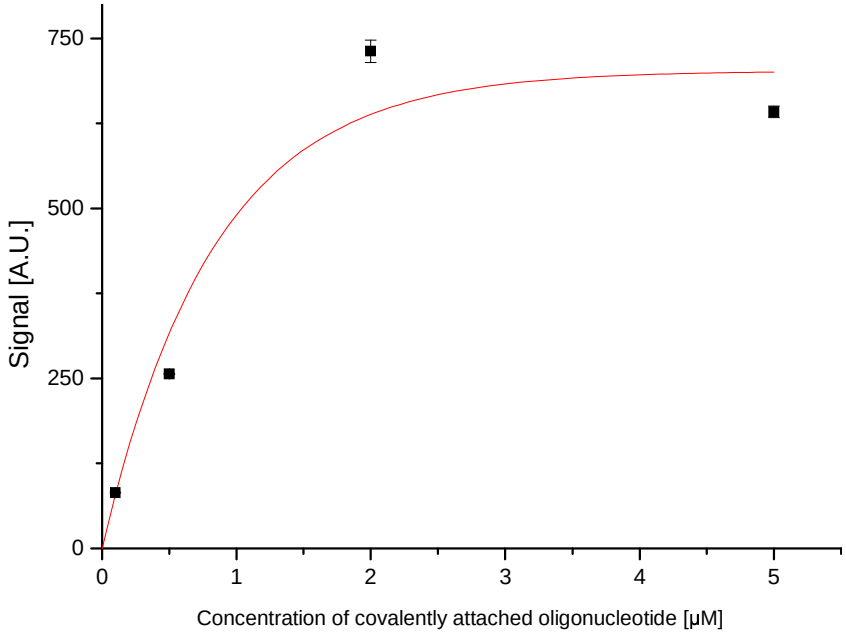

Figure 4.5: Dose-response curve, with the "dose" in this case being surface density. These points are the saturation signals from the curves in Figure 4.3. Signal increases as a function of the concentration of thiol oligonucleotide reagent used for immobilization until saturation. A slight signal decrease was observed at the highest reagent concentration, due to spatial restriction of bound oligonucleotides leading to inhibited hybridization. Curve for the sake of clarity.

The saturation signal increases up to a certain point, and then decreases again with increasing attached oligonucleotide density. This again could be attributed to the fact that hybridization is inhibited when oligonucleotides are too close to each other [1, 126]. Fluorescence quenching may also play a role, as a result of the close proximity of fluorophores in the more compact environment of densely packed hybridized oligonucleotides.

This type of study makes it possible to optimize surface densities in order to obtain a good compromise between hybridization signal and rate of hybridization. The different tests described above show that there is a large degree of flexibility and excellent control of surface definiton possible within a microfluidic system. This is due to the enhanced control of solution transport provided by microfluidic devices, a feature which is difficult to obtain in macroscopic systems.

4.3.2 Heated microflow system

In order to test stability of the modified surface with respect to heat, ***(T) 10-P2-TR*** was bound to the conditioned surface in the larger chamber. Temperature was thermocycled according to a PCR protocol under conditions of continuous buffer flow. The surface was subjected to long heat treatments, with each cycle comprising stages of 95°C for 30 sec, 60°C for 5 min and 72°C for 7 min. As Figure 4.6 shows, a 30% drop in the signal due to labeled, bound DNA was observed during the first cycle, and a total drop of 78% was recorded over 25 cycles. This suggests a strong instability of the chemically modified surface when subjected to these extreme conditions. Chemical bond strength considerations lead to the conclusion that the silane bonds are the ones to break when

energy is introduced to the system. For cycling conditions where the times are reduced to 30 sec, 90 sec and 90 sec for temperatures of 95°C, 60°C and 72°C, respectively, the signal drop is about 40% for 40 cycles.

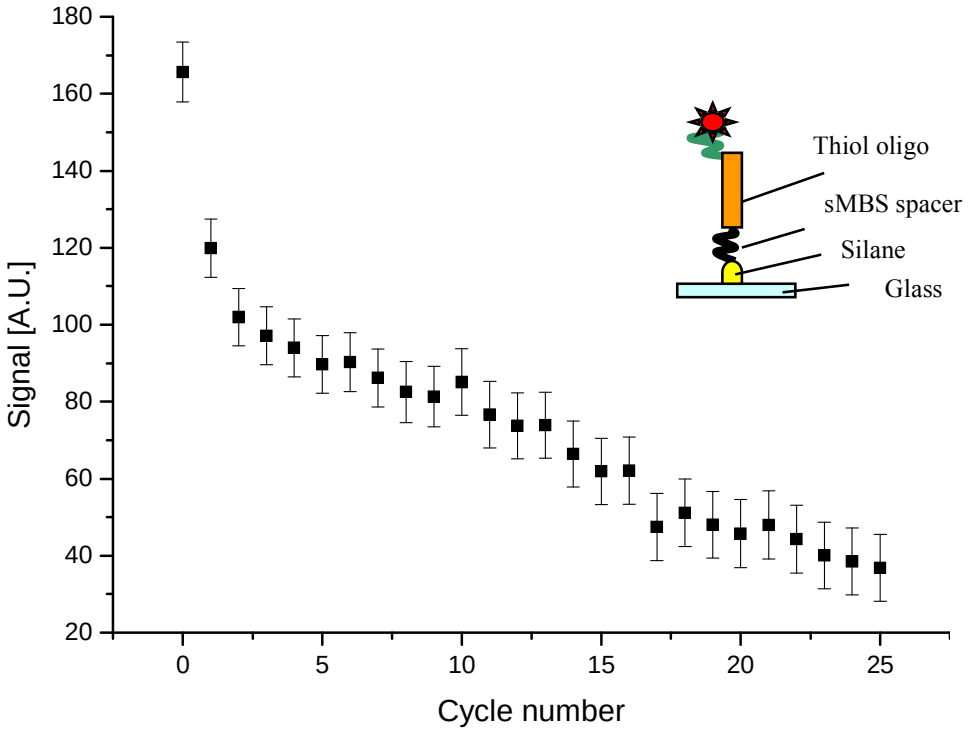

Figure 4.6: Decrease of surface-bound probe density as a function of thermocycle number. The inset illustrates the composition of the surface layer for this experiment. The ***(T) 10-P2-TR*** primer was used in this experiment. A decrease of 30% is observed after the 1st cycle, revealing instability of surface conditioning with respect to elevated temperature. The curve is reproducible, which could allow for signal intensity correction if quantitative analysis is desired.

Photobleaching was measured in a separate experiment, and a drop of 16.3% in signal was observed after 10 minutes of exposure. For the total exposure time of 40 s for this experiment, the decrease in signal corresponding to bleaching was only 3%. Therefore, the contribution of photobleaching in these experiments is negligible. Because the curve

in Figure 4.6 is reproducible, it could in principle be fit with an exponentially decreasing function and used to correct intensity values after each cycle for quantitative analysis[22].

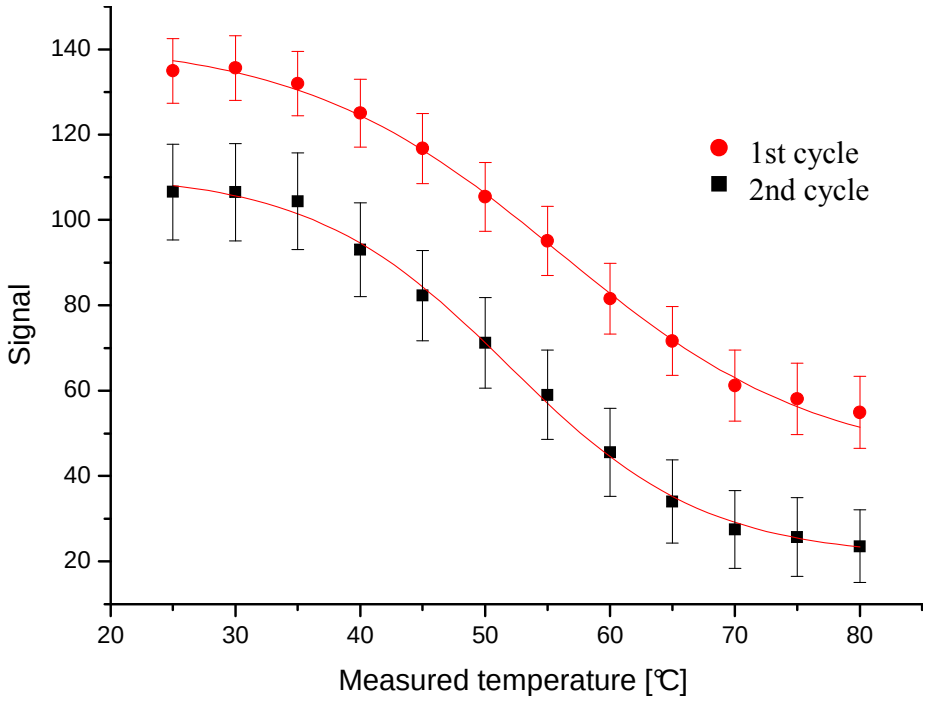

Figure 4.7: Two consecutive melting curve measurements for hybridized ***T(10) P2*** / ***TR-REV-P2***. The initial signal decrease of 20% can be explained by surface instability with respect to heat. The T_m's deduced from the curves nevertheless remain stable. A constant buffer flow of 5 µL/min was applied to remove dehybridizing strands. Temperature was ramped up in steps of 5 °C, and images were acquired with a fluorescence microscope when temperature had stabilized after 5 seconds. [***T(10) P2***] in 5xSSC buffer with 5 mM TCEP added = 1 µM, [***TR-REV-P2***] in 5XSSC buffer = 100 nM.

Dehybridization with the flow setup gave a T_m for the ***(T) 10-P2*** / ***TR-REV-P2*** system of $T_{m,P2device}$ = 56.2°C ± 0.9°C (n=5) for the first cycle (Figure 4.7). Correcting for T_{ext} using Equation 3.1, a $T_{m,P2act}$ of 73.4°C was obtained. This is close to the value obtained in the conventional system, $T_{m,P2liquid}$ = 74.4°C± 0.4°C (n=4). After a first thermal cycle, the system was rehybridized and thermally dehybridized again. The curve for the second

cycle in Figure 4.7 gives the same T_m, but the total intensity has decreased by 20%. The total measurement precision of about ± 1°C for T_m and the reproducibility of curve shapes should enable SNP analysis with this device[63, 64].

4.4 Conclusions

A microfluidic system with surface-bound DNA has been fully characterized in terms of surface modification and thermal control. A novel non-invasive technique for thermal calibration inside a microchannel has been developed and exploited using molecular beacons as temperature probes. Surface treatments are reproducible and highly controllable in a microfluidic channel, and surface-conditioning times are strongly reduced. Kinetic data can be extracted from binding curves in order to optimize surface densities for optimal reaction times. A novel way of performing thermal dehybridization has successfully been used to determine melting temperature measurements of strands of DNA. Taken together, this combined microfluidic / small-volume heating approach represents a powerful tool for surface-based DNA analysis, and could be implemented effectively in applications like SNP analysis.

5 CONCLUSIONS

The main goal of this thesis, namely demonstration of proof of principle of performing heterogeneous assays on chip, has been achieved. The different issues addressed in the various experiments, such as surface conditioning of a microchamber, temperature control inside a microchannel or flow control in a microfluidic network, were resolved with the simplest methods possible. Even these techniques, at first seeming deceptively simple, gave rise to more interesting questions. The Conclusions section at the end of each chapter discuss what the more interesting questions are. These will be left open for future researchers…

The main conclusion that one could come up with after having spent three or more years with microfluidic systems is that it is often not the technology issues which are complex to resolve, but the actual operation of the different microchips. Each device is an animal with its own character, and has to be tamed in its own way. Even if the design modification from one prototype to the next seems almost insignificant, the results are often surprisingly different. Each new design gives rise to new issues and problems, and provides a wealth of information on how devices behave and on what one has to take into account to improve a system for a new design.

Another line of thought which gradually comes to mind when creating new microfluidic devices is more philosophical in nature. Questions arise, such as: “Should my device be as complex as possible with all the features integrated onto it, even if it takes a lot of technological effort to implement and the costs would make it quasi impossible to commercialize, the devices having a very limited lifetime since they eventually clog?” More practical questions come to mind, such as: “I only analyze 100 nL of sample, but in the end I still have to pipette 1 µL of solution into my device to operate it”, or for diagnostic analyses: “by analyzing only 100 nL do I have a significant representation of the sample population, or will I come up against stochastic problems?”. It is true that sample sizes can be reduced, but saying that sample sizes are reduced below 1 µL is an illusion since, at least for now, a human being cannot handle a sample of less than a microliter, simply because of the size of his hands…

Other questions that have been debated during various discussions while writing papers or abstracts involve what technique is being used for performing the analyses and how can its efficiency be described. For example, in the immunoassay system, are we actually performing affinity chromatography or is it solid-phase extraction? Does it make sense to express a limit of detection when sample preconcentration onto a surface is only limited by the number of available sites which could eventually be filled, if only enough sample is pumped to a chamber, and not the concentration of the sample to be detected? The lines become somewhat difficult to draw between the different techniques since sometimes it is a combination of several methods which are used in order to operate a device. In the end, what will truly matter is not the technique which is used but the application it is used for. The use of “electrokinetically driven microfluidic chips with

surface-modified chambers for heterogeneous immunoassays" would be replaced by "immunoassay sensor". A "microfluidic device for thermal dehybridization of surface-bound DNA for genetic analysis" could be replaced by "DNA melting temperature sensor" or simply, "DNA sensor". It won't really matter what is used inside a device but what the device does. There is already a small library of microfluidic components such as double-T injectors, separation columns and microreaction chambers populating the vocabulary of microfluidics, with which researchers can converse on a daily basis without having to describe them in detail. Why not imagine larger systems which perform a certain function without necessarily having to know what is in it just as in microelectronics? No one calls a microprocessor "microelectronic device consisting of transistors, resistors and capacitors micromachined in silicon for implementation of complex calculus"…

Having asked many such questions, one can conclude that the main advantages of microfluidics with respect to conventional systems, in most cases, remain speed of analysis and multiplexing parallel analyses. Also, they allow more precise control of surface modification and often allow better control in general for observation of chemical and biochemical reactions which perhaps couldn't be observed or implemented before in macroscopic systems. Therefore, precision, speed, parallelism and innovation are all part of the power of this young field of research with which it will continue to forge ahead.

Another interesting point of microfluidics is the multidisciplinary aspect of the whole concept. Teams of researchers coming from various fields such as physics, electrical engineering, chemistry and biology, both theoreticians and practitioners, all joining up to find new solutions to this most varying, fascinating and innovative subject. This is one of

the few fields at the present time which reflects a true vision of the future of science, being a marriage of all existing sciences merging into one melting pot in order to create or discover something new. Scientists are learning how to cross the barriers that have been set for them during their long specialized education. Those who have the courage to seek something new and learn the language of a different science quickly find out that there is always a common ground where they can discuss and work together for improvement and understanding of human lives…

6 ACKNOWLEDGEMENTS

This is probably the most important part which has to be written with the most care, since most of the rest of this document will never make it to the eyes of the people this whole thing is dedicated to… ☺ But this section requires a little prologue before actually starting to thank the people involved:

First of all, I wish to say that I never thought I'd do a PhD because the fields of research I had come across during my college studies didn't seem attractive enough, until one day I met my present group leader (Eli)Sabeth Verpoorte. One early day of spring, when one of my dear friends Gian-Luca Lettieri (with whom I did practically all my scholarity from 2nd primary to the end of my PhD) and I wanted to choose a semester project during our 4th year of college, we decided to visit some of the projects of our present PhD supervisor's group Nico de Rooij. After reading Sabeth's semester project proposal and not truly understanding what it was about (which had nothing to do with the way it was written, but with our lack of comprehension…) we decided to take a chance and meet her for a more extensive explanation. We thought that at the worse case we would have a nice coffee and meet someone new. After about 10 minutes of explaining and waving her hands in the air, Sabeth managed to convince us that this thing called "microfluidics" deserved to be given shot at, even if it was at the time a virtually unheard of field of

research since in 1997, the field was only 7 years old. Even now when we speak of what we do, it is not an easy task for people to understand. “Have you seen the movie Gattaca?” is usually how we start explaining, and if that doesn’t work, the trouble starts and we start waving our hands in the air…

After having completed the semester work with strong interest, the PhD thing still didn’t strike me as a good idea. But the same year, I had dinner with two family friends Samad Hedayat and Ali Hadi, each at different periods of the semester, and somehow, a recursive subject during our various discussions was “what do you want to do after your studies?”. I remember my father wanting me to do a PhD overseas and, as it often happens, kids tend to present a certain deafness when it comes to parents’ advice. But Ali and Samad, after some arguing and me dismissing the idea completely at the end of each discussion, had managed to implant a thought in my brain that evolved during the university year: “What bad can it do you? You won’t regret doing it but you might regret not doing it…”

So having by chance found a field which could actually interest me for a long enough period of time to do a PhD, and having this growing idea of maybe regretting it someday in my head, eventually made me come to Sabeth at the end of my studies asking her for a PhD position. There were just too many things that had happened “by chance” that year to ignore the whole thing altogether…

Almost 4 years later, this story is coming to an end, and if you ask me if I made the right decision, I’ll answer you that time will tell. But what I do know, is that the PhD gave me the time and opportunity to explore parts of my own self. What was truly rewarding, was the story of my everyday life during these 4 years. The people I met, the things I learned

about work, my friends, some colleagues who became good friends, my family and mostly about myself, were the greatest gifts given to me for building the rest of my life… I don't know if I would have discovered all this if I hadn't done a PhD so for the benefit of doubt, I'll say that I did the right thing. ☺

For all these precious presents that were given to me during the time frame of my PhD studies, I wish to thank the following people who have participated in my story from a professional or personal point of view, from close or afar…:

Many thanks to Prof. Nico de Rooij for giving me the opportunity to work in his labs. This was an adventure that has prepared me for the future in a most extraordinary way under dreamlike conditions. Thank you so much…

Thanks to the building blocks of my scholar education, being all the teachers from kindergarten to college. I couldn't have done this without learning how to read and write, to be creative, to analyze, to criticize and to dismiss a lot of what was done in order to keep focus on what is important…

Thanks to Murphy and his wretched law which tends to pursue a researcher throughout his career, making one believe in an unexpected metaphysical aspect of life. I think that by now I have no other choice than believing in some form of heavenly power… ☺

Thanks to the IMT technical staff Gianni (Maestro) Mondin, Pierre-André (Clairon) Clerc, Edith Millote, Nicole, Jose Vaquera, Pierre-André Kuenzi and Sylviane Pochon not only for their technical skills but also for making the yellowness of the cleanroom light, turn into bright pink when it wasn't so much fun being in there…

Thanks to Vincent Auger, Laure Aeschimann, Giovanni Egidi, Luca Berdondini, and all the other people without whom the lunch break wouldn't have been the same…

Special thanks to the Love Boat team: Vincent Auger, Jan Lichtenberg, Gian-Luca Lettieri and Sebastian Gautsch. I will always remember that memorable event… ☺

Thanks to Peter van der Wal for answering many miscellaneous questions going from chemistry to administration, and being pretty patient about it… ☺

Thanks to the people at CSEM who kindly shared their lab with us and didn't mind us turning off the light to perform our experiments all the time: Maria Juvet, Sylvia Guinchard, Caterina Minelli, Isabelle Caelen and especially François Crevoisier.

Thanks to my dear friends Frédéric (Fred) Rossel, Pierre-Yves Cestonaro, Francisco (Chico) Hinojosa, Miguel de Morais; Geraldine Gatto, Cécilia Bandelier, Jose Hinojosa, Fabien Clottu, Astyanax Peca, Vicky Roethlisberger, Yann Gindraux, Antonio (Tony) Rosa, Philippe Heyd and Sergio Taveira, who have always been there in many ways, always supportive and also for giving life all the color and beauty it potentially has…

Special thanks to my dear friends Gian-Luca Lettieri and Sebastien Gautsch who have been with me all the way from primary school to PhD! I couldn't have done this journey without you guys. It seems like yesterday we were still in the schoolyard wondering what we were going to do later on. Things haven't changed so much…

Thanks to Geraldine Dereumaux for her LOVE and support, and for being so patient during the writing of this manuscript…

Thanks to my dear friends who are in various parts of the planet: Arash Arshi, Igor Tulevski, Kaveh Khatami, Azita Hamedani, Leyla Hedayat, Samad and Batoul Hedayat,

Ali Hadi, Natalia Ruiz, Kazem and Nahid Kazempour, John and Fataneh Howe, Jean-Fred Benoît, Joe Whittaker… Thank god for email…

Thanks to my dear friends Sandro de Simeis and Claude Joray for introducing me to the world of fashion, an extraordinary world which is a million light years away from science. Not such a bad place to be on one of those days…

Thanks to the people who tried to come with me along the path of music, a path along which I could seek refuge when science was becoming close to unbearable: Pierre-Yves, Miguel, Thierry, Fabien, Attila, Luca, Vincent, Pietro, Gilles and Joseph, Vincent and Damien, Lucio, Daniele, Marco, Jean-Charles, Georges, Sacha and Georges. I'll produce that album someday…

Thanks to my colleagues who were at some point in time part of the μTAS team: Laura Ceriotti, Antoine Daridon, Rosanne Guijt, Anpan Han, Alexandra Homsey, Sander Koster, Jan Lichtenberg, Vincent Linder, Takayuki Shibata, Anne-Marie Spehar and Sabeth Verpoorte, who became friends along the path to doctorate stardom. Our roads may part for a while but I hope they will come to meet again soon, or else this whole thing wouldn't make much sense…

Thanks to the people sharing my office: Claudio Novelli who has patiently answered to all my computer-related questions and Philippe Dubois who would always see things on the bright side. You guys' positive aura could make a gloomy winter day's fog turn into a bright sunny day. I will invest in stocks someday so we can laugh about it together…

Thanks to all my colleagues in Nico de Rooij's group, past and present who made my stay at IMT so special. Even the smurfs' village can't compete with the atmosphere in this research group… ☺

Special thanks to Gerardo Turcatti from Manteia SA who kept our project alive and without whom half of this thesis would have gone to oblivion…

Special thanks to Sabeth Verpoorte, for about a thousand reasons. As this manuscript progressed in writing, I realized that I couldn't (and apparently still can't) write a sentence without giving a French twist to it, this even if I learned to speak English before French! So thanks for correcting my frenglish and giving it a chic touch. Thanks for answering my million questions a day. Thanks for bearing my impatience when I pushed for something to get done while you would have a thousand other things to take care of. Thanks for being so understanding when the going got tough. Thanks for remaining flexible with your working schedules. Thanks for being a friend and a boss at the same time, (quite a challenge). Thanks for giving me freedom of action and trusting me in my work. Thanks simply for believing in me…

This work is dedicated to my mother (god bless her soul, she was the most extraordinary woman I have ever been granted the chance to know in my life, thank you so much Mom), my father and my brother, who have always been there for me, from the umbilical cord to the end of my PhD… Thank you so much for your love and support…

7 LIST OF PUBLICATIONS

Refereed articles

Thermal Dehybridization of Surface-Bound DNA in a Microfluidic Device for Nucleic Acid Analysis

A. Dodge, G. Turcatti, I. Lawrence, N.F. de Rooij, E. Verpoorte, Submitted to Analytical Chemistry

A Novel Microfluidic Concept for Bioanalysis using Freely Moving Beads Trapped in Recirculating Flows

Gian-Luca Lettieri, Arash Dodge, Gerben Boer, Nico F. de Rooij, Elisabeth Verpoorte, Lab on a Chip, 3, pp. 34-39, 2003.

Chemical and Physical Processes for Integrated Temperature Control in Microfluidic devices

A. Dodge, R.M Guijt, G.W.K. van Dedem, N.F. de Rooij, E. Verpoorte, Lab on a Chip, 3, pp. 1-4, 2003.

Electrokinetically Driven Microfluidic Chips with Surface-Modified Chambers for Heterogeneous Immunoassays

A. Dodge, K. Fluri, E. Verpoorte, N.F. de Rooij, Analytical Chemistry, 73, pp 3400-3409, 2001.

Patents

Microfluidic Heat Exchanger for Localized Temperature Control

A. Dodge, R.M Guijt, G.W.K. van Dedem, N.F. de Rooij, E. Verpoorte, Patent application number 02079584.5, October 31st 2002.

Microfluidic System for the Manipulation and Concentration of Particles Suspended in Liquid

Gian-Luca Lettieri, Arash Dodge, Gerben Boer, Elisabeth Verpoorte, Patent application number 0111503.9, September 5th 2002.

Conference presentations

Integrated Temperature Control System for Microfluidic Devices

A. Dodge, R.M Guijt, G.W.K. van Dedem, N.F. de Rooij, E. Verpoorte, Presented at the μTAS '2002 Conference, Nara, Japan, Proceedings pp. 617-619, Nov. 1-5, 2002.

Development of a Microfluidic Device for Genetic Analysis Based on Hybridization of Surface-Bound DNA

A. Dodge, G. Turcatti, P. Mayer, N.F. de Rooij, E. Verpoorte, Presented at the SmallTalk2002 Conference, San Diego, CA, USA, Jul. 28-31, 2002.

A Microfluidic Chip for Multi-Step, Heterogeneous Immunological Reactions

A. Dodge, E. Verpoorte, N.F. de Rooij, Proceedings of the μTAS '2001 Conference, Monterey, CA, USA, pp.499-500, Oct. 21-25, 2001.

Multi-Inlet Chip for Electrokinetic Immunometric Heterogeneous Immunoassay

A. Dodge, X. Wang, E. Verpoorte, N.F. de Rooij, Proceedings of the Transducers'01-Eurosensors XV Conference, Munich, Germany, pp.1194-1197, June 10-14, 2001.

Valveless, Sealed Microfluidic Device for Automated Heterogeneous Immunoassay: Design and Operational Considerations

A. Dodge, K. Fluri, V. Linder, G.-L. Lettieri, J. Lichtenberg, E. Verpoorte, N.F. de Rooij, Proceedings of the μTAS '2000 Conference, Enschede, the Netherlands, pp.407-410, May 14-18, 2000.

Consequences of Opposing Electrokinetically and Pressure-Induced Flows in Microchannels of Varying Geometries

G.-L. Lettieri, A. Dodge, G. Boer, J. Lichtenberg, E. Verpoorte, N.F. de Rooij, Proceedings of the μTAS '2000 Conference, Enschede, the Netherlands, pp.351-354, May 14-18, 2000.

Studies of Hydrostatic Pressure Effects in Electrokinetically Driven μTAS

G. Boer, A. Dodge, K. Fluri, B.H. van der Schoot, E. Verpoorte, N.F. de Rooij, Proceedings of the μTAS '98 Conference, Banff, Canada, pp.53-56, Oct. 13-16, 1998.

8 REFERENCES

(1) Shchepinov, M. S.; Case-Green, S. C.; Southern, E. M. *Nucleic Acids Research* **1997,** *25*, 1155-1161.

(2) Ngai, P. K. M.; Ackermann, F.; Wendt, H.; Savoca, R.; Bosshard, H. R. *Journal of Immunological Methods* **1993,** *158*, 267-276.

(3) Dubrovsky, T.; Tronin, A.; Dubrovskaya, S.; Vakula, S.; Nicolini, C. *Sensors and Actuators,* **1995,** *B23*, 1-7.

(4) Diamandis, E. P.; Christopoulos, T. K. *Immunoassay*; Academic Press: San Diego, CA, 1996, pp. 228-231.

(5) Levine, I. N. *Physical Chemistry*, 2nd Edition ed.; McGraw-Hill: New York, 1983, 467-468.

(6) Schultz, N. M.; Kennedy, R. T. *Anal Chem* **1993,** *65*, 3161-3165.

(7) Schultz, N. M.; Huang, L.; Kennedy, R. T. *Anal Chem* **1995,** *67*, 924-9.

(8) Schmalzing, D.; Nashabeh, W.; Fuchs, M. *Clin Chem* **1995,** *41*, 1403-6.

(9) Shahdeo, K.; Karnes, H. T. *Mikrochimica Acta* **1998,** *129*, 19-27.

(10) Effenhauser, C. S.; Paulus, A.; Manz, A.; Widmer, H. M. *Analytical Chemistry* **1994,** *66*, 2949-2953.

(11) Schmalzing, D.; Adourian, A.; Koutny, L.; Ziaugra, L.; Matsudaira, P.; Ehrlich, D. *Analytical Chemistry* **1998,** *70*, 2303-2310.

(12) Liu, S. R.; Shi, Y. N.; Ja, W. W.; Mathies, R. A. *Analytical Chemistry* **1999,** *71*, 566-573.

(13) Shi, Y. N.; Simpson, P. C.; Scherer, J. R.; Wexler, D.; Skibola, C.; Smith, M. T.; Mathies, R. A. *Analytical Chemistry* **1999,** *71*, 5354-5361.

(14) Munro, N. J.; Snow, K.; Kant, J. A.; Landers, J. P. *Clinical Chemistry* **1999,** *45*, 1906-1917.

(15) Lazar, I. M.; Ramsey, R. S.; Ramsey, J. M. *Analytical Chemistry* **2001,** *73*, 1733-1739.

(16) Sato, K.; Tokeshi, M.; Odake, T.; Kimura, H.; Ooi, T.; Nakao, M.; Kitamori, T. *Analytical Chemistry* **2000,** *72*, 1144-1147.

(17) Fan, Z. H.; Mangru, S.; Granzow, R.; Heaney, P.; Ho, W.; Dong, Q.; Kumar, R. *Analytical Chemistry* **1999,** *71*, 4851-4859.

(18) Lichtenberg, J.; de Rooij, N. F.; Verpoorte, E. *Talanta* **2002,** *56*, 233-266.

(19) Diamandis, E. P.; Christopoulos, T. K. *Immunoassay*; Academic Press: San Diego, CA, 1996, p. 234.

(20) Bing, D. H.; Boles, C.; Rehman, F. N.; Audeh, M.; Belmarsh, M.; Kelley, B. *7th International Symposium on Human Identification* **1996**, Promega Corp: Madison, WI (www.promega.com/geneticidproc/).

(21) Adessi, C.; Matton, G.; Ayala, G.; Turcatti, G.; Mermod, J. J.; Mayer, P.; Kawashima, E. *Nucleic Acids Research* **2000,** *28*, E87.

(22) Abel, A. P.; Weller, M. G.; Duveneck, G. L.; Ehrat, M.; Widmer, H. M. *Analytical Chemistry* **1996,** *68*, 2905-12.

(23) Ferguson, J. A.; Steemers, F. J.; Walt, D. R. *Analytical Chemistry* **2000,** *72*, 5618-24.

(24) Cantor, C. R.; Smith, C. L. *Genomics The Science and Technology Behind the Human Genome Project*; Wiley, 1999, pp. 99-102.

(25) Oda, R. P.; Strausbauch, M. A.; Huhmer, A. F. R.; Borson, N.; Jurrens, S. R.; Craighead, J.; Wettstein, P. J.; Eckloff, B.; Kline, B.; Landers, J. P. *Analytical Chemistry* **1998**, 4361-4368.

(26) Giordano, B. C.; al., e. *Analytical Biochemistry* **2001,** *291*, 124-132.

(27) White, F. M. *Fluid Mechanics*; McGraw-Hill:, p. 260, 1999.

(28) Kovacs, G. T. A. *Micromachined Transducers Sourcebook*; Mc Graw-Hill.

(29) Daridon, A.; Sequeira, M.; Pennarun-Thomas, G.; Dirac, H.; Krog, J. P.; Gravesen, P.; Lichtenberg, J.; Diamond, D.; Verpoorte, E.; de Rooij, N. F. *Sensors and Actuators B* **2001,** *76*, 235-243.

(30) Grossman *CE: Theory and Practice* **1992**, 18.

(31) Heiger, D. N. *High Performance Capillary Electrophoresis*; Hewlett Packard, 1992, pp. 15-19.

(32) Effenhauser, C. S. *Analytical Chemistry* **1993**.

(33) Fintschenko, Y.; Wilson, G. S. *Mikrochimica Acta* **1998**, 7-18.

(34) Pollema, C. H.; Ruzicka, J. *Analytical Chemistry* **1994,** *66*, 1825-1831.

(35) Cassidy, S. A.; Janis, L. J.; Regnier, F. E. *Analytical Chemistry* **1992,** *64*, 1973-1977.

(36) Hage, D. S.; Thomas, D. H.; Beck, M. S. *Analytical Chemistry* **1993,** *65*, 1622-1630.

(37) Andersson, H.; van der Wijngaart, W.; Stemme, G. *Electrophoresis* **2001,** *22*, 249-257.

(38) Oleschuk, R. D.; Shultz-Lockyear, L. L.; Ning, Y.; Harrison, D. J. *Analytical Chemistry* **2000,** *72*, 585-590.

(39) Fluri, K.; Lettieri, G.; van der Schoot, B. H.; Verpoorte, E.; de Rooij, N. F. In *Micro Total Analysis Systems '98: Proceedings of the μTAS '98 Symposium*; Harrison, D. J., Van den Berg, A., Eds.; Kluwer Academic Publishers: Banff, Alberta, Canada, 1998, pp 347-350.

(40) Fluri, K.; Verpoorte, E.; de Rooij, N. F. In *Digest of Technical Papers 10th Internat. Conf. on Solid-State Sensors and Actuators, Transducers '99*: Sendai, Japan, 1999, pp 1338-1339.

(41) Dodge, A.; Fluri, K.; V., L.; Lettieri, G.; Lichtenberg, J.; Verpoorte, E.; De Rooij, N. F. In *Micro Total Analysis Systems 2000: Proceedings of the μTAS 2000 Symposium*; van den Berg, A., Olthuis, W., Bergveld P., Ed.; Kluwer Academic Publishers: Enschede, Netherlands, 2000, pp 407–410.

(42) Lichtenberg, J.; Verpoorte, E.; de Rooij, N. F. *Electrophoresis* **2001,** *22*, 258-271.

(43) Boer, G.; Dodge, A.; Fluri, K.; van der Schoot, B. H.; Verpoorte, E.; de Rooij, N. F. In *Micro Total Analysis Systems '98: Proceedings of the μTAS'98 Symposium*; Harrison, D. J., van den Berg, A., Eds.; Kluwer Academic Publishers: Banff, Alberta, Canada, 1998, pp 53-56.

(44) Lettieri, G.; Dodge, A.; Boer, G.; Lichtenberg, J.; Verpoorte, E.; de Rooij, N. F. In *Micro Total Analysis Systems 2000: Proceedings of the μTAS 2000 Symposium*; van den Berg, A., Olthuis, W., Bergveld, P., Eds.; Kluwer Academic Publishers: Enschede, The Netherlands, 2000, pp 351-354.

(45) Fletcher, P. D. I.; Haswell, S. J.; Paunov, V. N. *The Analyst* **1999,** *124*, 1273-1282.

(46) Shultz-Lockyear, L. L.; Colyer, C. L.; Fan, Z. H.; Roy, K. I.; Harrison, D. J. *Electrophoresis* **1999,** *20*, 529-536.

(47) Schwab, C.; Bosshard, H. R. *Journal of Immunological Methods* **1992,** *147*, 125-134.

(48) Phillips, T. M. In *Analytical techniques in immunochemistry*; Marcel Dekker Inc.: New York, 1992, pp 262-300.

(49) Effenhauser, C. S.; Bruin, G. J. M.; Paulus, A.; Ehrat, M. *Analytical Chemistry* **1997,** *69*, 3451-3457.

(50) Kutter, J. P.; Jacobson, S. C.; Matsubara, N.; Ramsey, J. M. *Analytical Chemistry* **1998,** *70*, 3291-3297.

(51) Landers, J. P. *Handbook of Capillary electrophoresis*; CRC Press: Boca Raton, 1997.

(52) Huang, X. H.; Gordon, M. J.; Zare, R. N. *Analytical Chemistry* **1988,** *60*, 1837-1838.

(53) Jacobson, S. C.; Hergenröder, R.; Koutny, L. B.; Warmack, R. J.; Ramsey, J. M. *Analytical Chemistry* **1994,** *66*, 1107-1113.

(54) Herr, A. E.; Molho, J. I.; Santiago, J. G.; Mungal, M. G.; Kenny, T. W.; Garguilo, M. G. *Analytical Chemistry* **2000,** *72*, 1053-1057.

(55) Diamandis, E. P.; Christopoulos, T. K. *Immunoassay*; Academic Press: San Diego, CA, 1996, p.91.

(56) Diamandis, E. P.; Christopoulos, T. K. *Immunoassay*; Academic Press: San Diego, CA, 1996, p. 34.

(57) Sportsman, J. R.; Liddil, J. D.; Wilson, G. S. *Anal Chem* **1983,** *55*, 771-5.

(58) Linder, V.; Verpoorte, E.; de Rooij, N. F.; Sigrist, H.; Thormann, W. *Electrophoresis* **2002,** *23*, 740-749.

(59) Diamandis, E. P.; Christopoulos, T. K. *Immunoassay*; Academic Press: San Diego, CA, 1996, p. 37.

(60) Manz, A.; Effenhauser, C. S.; Burggraf, N.; Harrison, D. J.; Seiler, K.; Fluri, K. *Journal of Micromechanics and Microengineering* **1994,** *4*, 257-265.

(61) Ensing, K.; Paulus, A. *Journal of Pharmacy and Biomedical Analysis* **1996,** *14*, 305-315.

(62) Phillips, T. M.; Chmielinska, J. J. *Biomedical Chromatography* **1994,** *8*, 242-246.

(63) Jobs, M.; Fredriksson, S.; Brookes, A. J.; Landegren, U. *Anal Chem* **2002,** *74*, 199-202.

(64) Howell, W. M.; Jobs, M.; Gyllensten, U.; Brookes, A. J. *Nature Biotechnology* **1999,** *17*, 87-88.

(65) Manz, A.; Graber, N.; Widmer, H. M. *Sensors and Actuators B* **1990,** *1*, 244-248.

(66) Jensen, K. F.; Hsing, I.-M.; Srinivasan, R.; Schmidt, M. A. *Proceedings of the First International Conference on Microreaction Technology*, Frankfurt am Main, Germany, February 23-25, 1997. 1997; Springer Verlag; 2-9.

(67) Mullis, K.; Faloona, F.; Scharf, S.; Saiki, R.; Horn, G.; Erlich, H. *Cold Spring Harbor Symposia on Quantitative Biology* **1986,** *51*, 263-273.

(68) Northrup, M. A.; Ching, M. T.; White, R. M.; Watson, R. T. *Technical Digest of Transducers'93: 7th International Conference on Solid State Sensors and Actuators*, Yokohama, Japan 1993; 924-927.

(69) Wilding, P.; Shoffner, M. A.; Kricka, L. J. *Clinical Chemistry* **1994,** *40*, 1815-1818.

(70) Khandurina, J.; McKnight, T. E.; Jacobson, S. C.; Waters, L. C.; Foote, R. S.; Ramsey, J. M. *Analytical Chemistry* **2000,** *72*, 2995-3000.

(71) Srinivasan, R.; Hsing, I. M.; Berger, P. E.; Jensen, K. F.; Firebaugh, S. L.; Schmidt, M. A.; Harold, M. P.; Lerou, J. J.; Ryley, J. F. *American Institute of Chemical Engineers* **1997,** *43*, 3059-3069.

(72) Lee, T. M.; Hsing, I. M.; Lao, A. I.; Carles, M. C. *Analytical Chemistry* **2000,** *72*, 4242-4247.

(73) Kopp, M. U.; de Mello, A. J.; Manz, A. *Science* **1998,** *280*, 1046-1048.

(74) Lagally, E. T.; Simpson, P. C.; Mathies, R. A. *Sensors and Actuators B-Chemical* **2000,** *63*, 138-146.

(75) Fan, X.; Zeng, G.; LaBounty, C.; Bowers, J. E.; Croke, E.; Ahn, C. C.; Huxtable, S.; Majumdar, A.; Shakouri, A. *Applied Physics Letters* **2001,** *78*, 1580-1582.

(76) Pal, D.; Venkataraman, V. *Sensors and Actuators A-Physical* **2002,** *102*, 151-156.

(77) Schütze, J.; Ilgen, H.; Fahrner, W. R. *IEEE Transaction on Industrial Electronics* **2001,** *48*, 281-285.

(78) O'Connor, S. D.; Dantsker, E. In *US patent. Patent application number 20020039280. Filed September 28, 2001, Published April 4, 2002*, 2001.

(79) Swinney, K.; Bornhop, D. J. *Electrophoresis* **2001,** *22*, 2032-6.

(80) Liu, J.; Enzelberger, M.; Quake, S. *Electrophoresis* **2002,** *23*, 1531-1536.

(81) Tyagi, S.; Kramer, F. R. *Nature Biotechnology* **1996,** *14*, 303-8.

(82) Tyagi, S.; Bratu, D. P.; Kramer, F. R. *Nature Biotechnology* **1998,** *16*, 49-53.

(83) Giesendorf, B. A.; Vet, J. A.; Tyagi, S.; Mensink, E. J.; Trijbels, F. J.; Blom, H. J. *Clinical Chemistry* **1998,** *44*, 482-6.

(84) Bonnet, G.; Tyagi, S.; Libchaber, A.; Kramer, F. R. *Proceedings of the National Academy of Sciences of the United States of America* **1999,** *96*, 6171-6.

(85) Bonnet, G.; Krichevsky, O.; Libchaber, A. *Proceedings of the National Academy of Sciences of the United States of America* **1998,** *95*, 8602-6.

(86) Chen, W.; Martinez, G.; Mulchandani, A. *Analytical Biochemistry* **2000,** *280*, 166-72.

(87) Yamamoto, T.; Nojima, T.; Fujii, T. *Lab on a Chip* **2002,** *2*, 197-202.

(88) Dodge, A.; Fluri, K.; Verpoorte, E.; de Rooij, N. F. *Analytical Chemistry* **2001,** *73*, 3400-3409.

(89) Daridon, A.; Fascio, V.; Lichtenberg, J.; Wütrich, R.; Langen, H.; Verpoorte, E.; de Rooij, N. F. *Fresenius Journal of Analytical Chemistry* **2001,** *371*, 261-269.

(90) Ferguson, J. A.; Mau, W.-H. *Australian Journal of Chemistry* **1973,** *26*, 1617-1624.

(91) Sakakibara, J.; Hishida, K.; Maeda, M. *Experiments in Fluids* **1993,** *16*, 82-96.

(92) Slyadnev, M. N.; Tanaka, Y.; Tokeshi, M.; Kitamori, T. *Analytical Chemistry* **2001,** *73*, 4037-4044.

(93) Ross, D.; Gaitan, M.; Locascio, L. E. *Analytical Chemistry* **2001,** *73*, 4117-4132.

(94) Schmalzing, D.; Koutny, L.; Chisholm, D.; Adourian, A.; Matsudaira, P.; Ehrlich, D. *Analytical Biochemistry* **1999,** *270*, 148-52.

(95) Simpson, P. C.; Roach, D.; Woolley, A. T.; Thorsen, T.; Johnston, R.; Sensabaugh, G. F.; Mathies, R. A. *Proceedings of the National Academy of Sciences of the United States of America* **1998,** *95*, 2256-2261.

(96) Huang, Z.; Munro, N.; Huhmer, A. F. R.; Landers, J. P. *Analytical Chemistry* **1999,** *71*, 5309-5314.

(97) Medintz, I.; Wong, W. W.; Sensabaugh, G.; Mathies, R. A. *Electrophoresis* **2000,** *21*, 2352-2358.

(98) Sassi, A. P.; Paulus, A.; Cruzado, I. D.; Bjornson, T.; Hooper, H. H. *Journal of Chromatography A* **2000,** *894*, 203-217.

(99) Medintz, I. L.; Berti, L.; Emrich, C. A.; Tom, J.; Scherer, J. R.; Mathies, R. A. *Clinical Chemistry* **2001,** *47*, 1614-21.

(100) Medintz, I.; Wong, W. W.; Berti, L.; Shiow, L.; Tom, J.; Scherer, J.; Sensabaugh, G.; Mathies, R. A. *Genome Research* **2001,** *11*, 413-421.

(101) Emrich, C. A.; Tian, H. J.; Medintz, I. L.; Mathies, R. A. *Analytical Chemistry* **2002,** *74*, 5076-5083.

(102) Paegel, B. M.; Emrich, C. A.; Weyemayer, G. J.; Scherer, J. R.; Mathies, R. A. *Proceedings of the National Academy of Sciences of the United States of America* **2002,** *99*, 574-579.

(103) Lenigk, R.; Liu, R. H.; Athavale, M.; Chen, Z.; Ganser, D.; Yang, J.; Rauch, C.; Liu, Y.; Chan, B.; Yu, H.; Ray, M.; Marrero, R.; Grodzinski, P. *Analytical Biochemistry* **2002,** *311*, 40-49.

(104) Yuen, P. K.; Li, G.; Bao, Y.; Müller, U. R. *Lab on a Chip* **2003,** *3*, DOI: 10.1039/b210274a.

(105) Schena, M. *Microarray Biochip Technology*; Eaton Publishing: Sunnyvale, CA, pp.87-187, 2000.

(106) Adey, N. B.; Lei, M.; Howard, M. T.; Jensen, J. D.; Mayo, D. A.; Butel, D. L.; Coffin, S. C.; Moyer, T. C.; Slade, D. E.; Spute, M. K.; Hancock, A. M.; Eisenhoffer, G. T.; Dalley, B. K.; McNeely, M. R. *Analytical Chemistry* **2002,** *74*, 6413-6417.

(107) Fan, Z. H.; Mangru, S.; Granzow, R.; Heaney, P.; Ho, W.; Dong, Q.; Kumar, R. *Anal Chem* **1999,** *71*, 4851-4859.

(108) Heller, M. J.; Forster, A. H.; Tu, E. *Electrophoresis* **2000,** *21*, 157-164.

(109) Cheek, B. J.; Steel, A. B.; Torres, M. P.; Yu, Y.-Y.; Yang, H. *Analytical Chemistry* **2001,** *73*, 5777-5783.

(110) Olsen, K. G.; Ross, D. J.; Tarlov, M. J. *Analytical Chemistry* **2002,** *74*, 1436-1441.

(111) Kawashima, E. H.; Farinelli, L.; Mayer, P. In *Patent Application No. WO 98/44152*; GLAXO GROUP LIMITED [GB/GB]; Glaxo Welcome House, Berkeley Avenue, Greenford, Middlesex UB6 0NN (GB), 1998.

(112) Kawashima, E.; Farinelli, L.; Mayer, P. In *Patent Application No. WO 98/44151*; GLAXO WELLCOME PLC; Glaxo Wellcome House, Berkeley Avenue, Greenford, Middlesex UB6 0NN: GB, 1998.

(113) Adessi, C.; Kawashima, E.; Mayer, P.; Mermod, J.-J.; Turcatti, G. In *Patent Application No. WO 00/18957*; Dzieglewska, Hanna, et al; Frank B. Dehn & Co., 179 Queen Victoria Street, London EC4V 4EL: GB, 2000.

(114) Lao, A. I. K.; Lee, T. M. H.; Hsing, I.-M.; Ip, N. Y. *Sensors and Actuators A: Physical* **2000,** *84*, 11-17.

(115) Poser, S.; Schulz, T.; Dillner, U.; Baier, V.; Köhler, J. M.; Schimkat, D.; Mayer, G.; Siebert, A. *Sensors and Actuators A: Physical* **1997,** *62*, 672-675.

(116) Northrup, M. A.; Ching, M. T.; White, R. M.; Watson, R. T. In *Technical Digest of Transducers'93: 7th International Conference on Solid State Sensors and Actuators*: Yokohama, Japan, 1993, pp 924-927.

(117) Northrup, M. A.; Gonzalez, C.; Hadley, D.; Hills, R. F.; Landre, P.; Lehew, S.; Saiki, R.; Sninsky, J. J.; Watson, R.; Watson, R. J. In *Technical Digest of the 8th International Conference on Solid-State Sensors an Actuators*; Middelhoek, S., Cammann, K., Eds.: Stockholm, Sweden, 1995; Vol. 1, pp 764-767.

(118) Prince, J. A.; Feuk, L.; Howell, W. M.; Jobs, M.; Emahazion, T.; Blennow, K.; Brookes, A. J. *Genome Research* **2001,** *11*, 152-162.

(119) Thiel, A. J.; Frutos, A. G.; Jordan, C. E.; Corn, R. M.; Smith, L. M. *Analytical Chemistry* **1997,** *69*, 4948-4956.

(120) Kovacs, G. T. A. In *Micromachined transducers sourcebook*; McGraw-Hill: New York, 1998, pp 792-793.

(121) Beebe, D. J.; Mensing, G. A.; Walker, G. M. *Annual Reviews of Biomedical Engineering* **2002,** *4*, 261-86.

(122) Shultz-Lockyear, L. L.; Colyer, C. L.; Fan, Z. H.; Roy, K. I.; Harrison, D. J. *Electrophoresis* **1999,** *20*, 529-538.

(123) Okahata, Y.; Kawase, M.; Niikura, K.; Ohtake, F.; Furusawa, H.; Ebara, Y. *Analytical Chemistry* **1998,** *70*, 1288-1296.

(124) Cantor, C. R.; Smith, C. L. *Genomics*; John Wiley & Sons: New York, 1999, pp 89-90.

(125) Georgiadis, R.; Peterlinz, K. P.; Peterson, A. W. *Journal of the American Chemical Society* **2000,** *122*, 3166-3173.

(126) Peterson, A. W.; Heaton, R. J.; Georgiadis, R. M. *Nucleic Acids Research* **2001,** *29*, 5163-5168.